UNIVERSITÀ DEGLI STUDI
DI CASSINO E DEL LAZIO MERIDIONALE

Corso di Dottorato in
Metodi, Modelli e Tecnologie per l'Ingegneria

Ingegneria Elettrica

Ciclo XXXIV

Voltage Sags (Dips) Measured in Real Interconnected Systems: Methods and Tools to Detect their Origin, and to Forecast Future Performance

SSD: ING-IND/33

Coordinator
Prof. Fabrizio Marignetti

Ph.D. Student
Leonardo Di Stasio

Supervisors
Prof. Paola Verde
Prof. Pietro Varilone

ACKNOWLEDGEMENTS

This work has been carried out in part in the frame of the grant “Attività di supporto scientifico sulle tematiche di Power Quality nelle reti di distribuzione”; in addition, the activities received in part the financial support from the Italian Ministry of University and Research (MIUR) through the Special Grant “Dipartimenti di eccellenza” Lex. N. 232/31.12.2016 (G.U. n. 297/21.12.2016 S.O. n. 57).

The Ph.D. study was one of the most challenging, because it was the result of a training in which you choose to personally get involved.

I thank my supervisors Paola Verde and Pietro Varilone first for giving me the opportunity to know the fantastic world of the research activity. Also, I express my gratitude for having passed to me their experience and for guiding me on my research journey every day with valuable advice. Thanks especially for having spent some of their time for all the projects carried out during the Ph.D.

I wish to thank my mother and my father, who, with their support both moral and economic, allowed me to achieve one of the most important goals of my life.

My greatest “thank you” goes to Vittoria. Thanks for giving me your immense strength, thanks for all the time you dedicated to me, thanks because you’ve always been there.

I want to thank Eng. Christian Noce, his advices and supports allowed improving the quality and the consistency of all the Ph.D. thesis.

ABSTRACT

The availability of data measured in the field is one of the greatest advances in the last decades for electric power systems planning, management and control. The technological innovations of systems and devices for the measurement of a wide range of quantities allowed their installation at almost all levels of voltages, from distribution to transmission. Increasing number of proposals of new techniques are coming from researchers and system operators for facing the various problems of system operation relying on the availability of measured data in real systems. The data from the field enable data-driven approaches, which can be integrated into traditional model-based methods constructing the so-called digital twin of a system. It is a system digital model whose parameters and linkages are continuously changed and tuned in accordance with the measurements from the actual system in service. New and attractive possibilities for addressing the problems of planning, managing, and controlling the power systems are opening for researchers and system operators.

The studies presented in this thesis used the voltage sags measured in the medium voltage (MV) regional systems of E-Distribuzione for four years. Two main problems were faced by data-driven approaches: the ascertaining the origin of the measured voltage sags, and the forecasting the voltage sags which will occur in the site of the system. The correct ascertaining of the origin of voltage sags is crucial in view of future economic regulation by the national energy Authorities. It gives to the system operator the correct indication if the measured sags were or not due to faults in his own network interconnected with other systems. The possibility of forecasting the future performance in terms of voltage sags per year was a challenge never dealt with in the literature for the absence for field data. The literature, till now, proposed methods, models, and tools to estimate the average performance of a system, derived from model-based approaches.

Regarding the origin of the voltage sags measured at the MV busbars of the High Voltage/Medium Voltage (HV/MV) stations, this thesis analyses and compares two methods which use only the residual voltage, the time the voltage sags occurred, and their duration. The analysis was conducted also studying the effect of the presence of

DG (Distributed Generation). The data from field, moreover, revealed that in some specific cases the sags caused by faults in the MV systems propagated to HV networks. This problem was also studied simulating a portion of a real system, which presents the interconnections between HV and MV network.

Regarding the forecast of voltage sags, the thesis proposed two main methods which use at least three years of measurement. The common choice of these two methods is the selection of the random variable, different from the statistical variable used by all the methods in literature. The random variable used in this study is the time to next event, that is the time intercurred between each couple of sags, instead of the variable number of voltage sags. This choice allows a huge increase of the data sets with the positive consequence of reasonable measurements time to obtain a forecast with acceptable accuracy. The first method, based on Poisson model, is suitable for rare sags, that are the sags occurred with a time to next event of the dimension of hours. The second method, based on Gamma model, is suitable for all the voltage sags, comprehensive of sags occurred close each other as groups. The latter, named clusters, are typically due to exogenous causes from the power systems, like adverse climatic conditions or fires.

Intermittent indices are also proposed introduced for an initial screening of the measured sags to focus if, and how many, clusters are present in the data base of the measured sags. Such analysis drives the successive steps of the statistical analyses for discriminating the adequacy of Poisson and Gamma models.

The studies presented in this thesis are the subjects of the scientific papers listed below.

[1] C. Noce, M. D. Santis, **L. D. Stasio**, P. Varilone and P. Verde, "Detecting the Origin of the Voltage Sags Measured in the Smart Grids," 2019 International Conference on Clean Electrical Power (ICCEP), July 2nd-4th 2019, pp. 129-135, doi: 10.1109/ICCEP.2019.8890121.

[2] C. Noce, **L. Di Stasio**, P. Varilone, P. Verde and M. De Santis, "On the Forecast of the Voltage Sags: First Stages of Analysis on Real Systems," 2020 55th International Universities Power Engineering Conference (UPEC), 1st – 4th September 2020, pp. 1-6, doi: 10.1109/UPEC49904.2020.9209816.

[3] De Santis, M.; **Di Stasio, L.**; Noce, C.; Verde, P.; Varilone, P. Initial Results of an Extensive, Long-Term Study of the Forecasting of Voltage Sags. Energies 2021, 14, 1264. https://doi.org/10.3390/en14051264.

[4] Paola Verde, Pietro Varilone, **Leonardo Di Stasio**, Michele De Santis, Christian Noce, Previsione dei buchi di tensione: sfide aperte dalla regolazione. AEIT - Volume 107 - Numero 1/2 gennaio/febbraio 2021 - ISSN 1825-828X , pp. 46-53.

[5] M. De Santis, **L. Di Stasio**, C. Noce, P. Verde and P. Varilone, "Indices of Intermittence to Improve the Forecasting of the Voltage Sags Measured in Real Systems," in IEEE Transactions on Power Delivery, doi: 10.1109/TPWRD.2021.3082280.
[6] **Leonardo Di Stasio**, Paola Verde, Pietro Varilone, Michele De Santis, Christian Noce, "Stochastic Model to Forecast the Voltage Sags in Real Power Systems", AEIT International Conference, October 4th – 8th 2021.
[7] G. M. Casolino, **L. Di Stasio**, P. Varilone, P. Verde, C. Noce, M. De Santis, "On the Forecast of the Voltage Sags Using the Measurements in Real Power Systems", Accepted for the Conference ICHQP2022, Naples (IT), May 29th- June 1st 2022.

TABLE OF CONTENTS

LIST OF FIGURES

LIST OF TABLES

INTRODUCTION

A voltage sag (dip) is a sudden reduction of the supply voltage to a value between 90% and 5% of the declared voltage followed by a voltage recovery after a short period of time from 10 ms to 1 m [1].The most frequent voltage sags in the electric systems are caused by the short circuits; they could be seen as the natural response of the system to over-currents until protection system feel, recognise and permanently disconnects the fault. Protection systems sense the fault in a period of time up to 50 ms and permanently disconnect the fault in a period of time from 100 ms (typical of HV protection systems) to 500 ms (typical of MV protection systems with intentionally delayed intervention). The main characteristics of a voltage sag are the residual voltage, the duration, the start time, the end time and the depth ((Figure 0)).

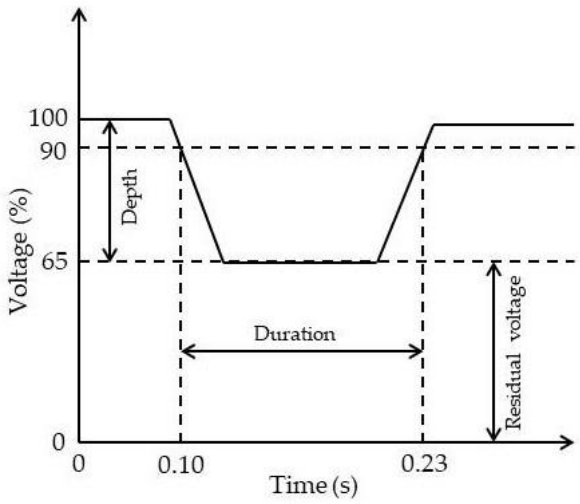

Figure 0 – Main characteristics of a voltage sag; RMS of voltage.

The voltage sag phenomenon is recognized as one of the most significant power quality (PQ) disturbances for modern electric systems. Its effect on the automated industrial plants, on innovative equipment such as those operated by robots and activities managed by computers can result in huge economic damages. [2-5].

In 2009 the National regulation in Europe started [6]. The "3rd Package" Directive 2009/72/EC [6] approved and agreed to by the member states, specifies that the regulatory Authority, together with other competent Authorities, has the duty of setting or approving standards and requirements for the quality of supply or contributing thereto. This important statement pushed the regulatory Authorities to implement a scheme for regulating the quality of voltage.

In Europe the first campaign of measurement regarding voltage quality (VQ) started in 1992 in Norway. Also, in Spain and in France, the regulatory Authorities (Comisión Nacional de Energía – CNE in Spain and Commission de Régulation del'Electricité – CRE in France) issued consultation documents on the procedure of VQ measurement and control.

In Italy the national Authority of Energy, Networks and Environment (ARERA) initiated the PQ regulation with the first consultation document in 2005. In Europe, the Council of European Energy Regulators (CEER) recommended that the quality of voltage must be accounted by regulators due of the economic impact that an inadequate VQ could cause both for customers and for distribution companies. CEER also stressed the need for identify better quality standards and proposed, to ensure levels of guaranteed minimum VQ, economic incentives.

ARERA started the first period of regulation of the quality of voltage in 2011 by the Resolution [7] that was confirmed in 2019 [8]. With the first Resolution, ARERA imposed to all DSO the installation of PQ measurement devices, in respect to CEI EN 61000-4-30 [9], in every MV busbars of all HV/MV substations. These devices must record transitory, short duration and long duration interruptions. About short duration interruptions, i.e. voltage sags, several parameters are recorded, in particular the origin. The registration of the origin of the voltage sag consists in indicating in which system, HV or MV, the fault, which caused that voltage measured sag, occurred.

Thanks to the scientific cooperation with E-Distribuzione, the largest Italian DSO, a very large set of measured voltage sags on real MV busbars were available, which in turn allowed to solve by data-driven approaches two main problems. The assessment of the origin of the measured voltage sags and the forecast of the voltage sags which will occur at the site of the system.

Regarding the origin of the voltage sags measured at the MV busbars of the HV/MV stations, this thesis analyses and compares two methods which use only the residual voltage, the time the voltage sags occurred, and their duration [10]. Two main aspects, typical of distribution systems with DG, were considered: the presence

of on load tap changer (OLTC) of the HV/MV transformers and the action of the DG units in support of the local voltage. The methods were compared on a part of a real HV/MV system. Further, the possible propagation from MV to HV of sags originated n MV system was analysed. The time-domain simulations were used, and short circuits were forced in the nodes of the MV system [11].

Regarding the forecast of voltage sags, as said above, the availability of a huge number of measured sags in the systems opens this appealing option without using simulation methods that are model-based (MB). MB methods require the knowledge of the main characteristics of the system (topology and typology) and the component parameters to perform the simulations. The knowledge of the expected performance is one of the most attractive themes for the system operators, i.e., both distribution system operators (DSOs) and transmission system operators (TSOs). DSOs and TSOs are interested in understanding the future features of their system well enough to implement adequate maintenance and/or effective sag compensation to prevent service interruptions and/or to avoid economic penalties due to regulatory rules. With this aim, a statistical analysis on the measured voltage sags was performed and two models were proposed in literature to characterize:

- rare sags without clusters, i.e. caused by short circuits [12-15];
- rare sags with clusters that could be caused by atmospheric phenomena, i.e. wind, storms, fires [12], [16].

Rare voltage sags meet the conditions of a Poisson process. The presence of clusters brings the phenomenon far from the conditions of Poisson model. If the clusters are included into all the measured sags, the Gamma distribution is the most adequate model. In fact, the clusters introduce a time dependence of the events, which requires to pass to a stochastic model, which is achievable by means of a Gamma distribution.

The need to characterize only rare voltage sags, excluding sags clusters, allowed to introduce in literature new intermittent indices that furnish an initial screening of the measured sags to focus if, and how many, clusters are present in the data base of the measured sags [15]. The proposed models were statistically validated by means of good-ness of fitting indices and after used to forecast future performances of the sites of the same regional electric power system.

The common choice of these two methods is the choice of the random variable, different from the statistical variable used by all the methods in literature. The random variable used in this study is the time to next event, that is the time intercurred between each couple of sags, instead of the variable number of voltage

sags. This choice allows very larger data sets with the positive consequence of reasonable measurements time required for obtaining acceptable confidence of the forecast.

CHAPTER 1.

REGULATING THE VOLTAGE QUALITY

This chapter illustrates the main aspects of the energy regulation in Europe and in Italy. It gives the scenario of reference for the research activities conducted during the PhD.

1.1 Introduction

In Italy, the national Authority ARERA established by the lex 481 in 1995, determined an improvement in the energy supply service dealing with different aspects of energy supply service quality: commercial quality, energy supply continuity and VQ [7].

The regulation of the continuity of the energy supply forced economic investments to improve protection systems performance, remote control, and grid automation. ARERA established specific continuity energy supply indicators. Exceeding the minimum values of continuity indicators imposed by ARERA results in penalties for the DSOs or TSOs. The interruptions can be caused by many reasons:

- originated by HV faults;
- originated by MV faults;
- external causes or "exogenous causes" i.e. wind, storm, fire, …., etc.

For regulatory purposes, the interruptions can be divided into two groups:

- with notification;
- without notification.

The interruptions without notification are classified in:

- long i.e. 3 minutes of maximum duration;
- short i.e. duration from 1 second up to 3 minutes;
- transitory i.e. up to 1 second.

Every year, the DSOs and the TSOs must communicate to ARERA the service continuity data relating to the previous year, essentially the number of interruptions and their duration. The objectives of the first continuity period of regulation were to reduce the regional gaps between the regions of the Centre-North and those of the South, and to bring the (average) Italian level of continuity close to that of other member states of the European Community.

The regulation of VQ is the most difficult subject of any regulatory action. The problem is characterised by several phenomena occurring in a wide range of time from the transitory to the long duration Examples of transitory phenomena are the frequency variation caused by lightning strikes, examples of short duration phenomena are voltage sags, swell, examples of long duration phenomena are interruptions, overvoltage, distortions due to harmonics, inter-harmonics, noise and voltage fluctuations.

The standard EN 50160 is a standard of reference of the VQ of public networks [1]. The standard considers electrical energy as a product and defines specific limits and maximum values within which users can expect that the characteristics of the voltage are contained. The standard also clarifies that the customers must make robust their plants to disturbs normally present in distribution power systems. The disturbances are classified in events and variations. Events are sudden and significate deviations from the ideal voltage waveform, instead variations are continuous time deviations with limited amplitude.

The standard's purpose is to define and describe voltage supply characteristics regarding:

- frequency;
- amplitude;
- voltage waveform;
- symmetry.

The nominal value of the frequency of the supply voltage must be equal to 50 Hz. Under nominal operating condition[1], the average value of the fundamental frequency measured in a 10 s time interval must be between 52 Hz – 47 Hz. Under nominal operating condition, the variation of the voltage supply value must not exceed ± 10% of the declared value. Under nominal operating condition, at every site the 95% of the values of every harmonic voltage must be less than the values indicated in Table 1.1.

Table 1.1 – Harmonic voltages at the power supply terminals, up to the 25th order, expressed as a percentage of the fundamental voltage V1

Odd harmonics				**Even harmonics**	
Not multiple of 3		**Multiple of 3**			
h Order	**Amplitude**	**h Order**	**Related Amplitude**	**h Order**	**Related Amplitude**
5	6.0%	3	5.0%	2	2.0%
7	5.0%	9	1.5%	4	1.0%
11	3.5%	15	0.5%	6 …. 24	0.5%
13	3.0%	21	0.5%		
17	2.0%				
19	1.5%				
23	1.5%				
25	1.5%				

[1] The nominal operating conditions guarantee the correct operation of the devices connected to the electrical system. In Italy, at each connection point of the electrical system, the frequency and the voltage supply must be kept at values close to the nominal ones. The nominal value of the supply voltage depends on the considered network (HV, MV or Low Voltage (LV)). The nominal value of the frequency, in Italy, is equal to 50 Hz.

Under nominal operating conditions, considering one-week period, the 95% of the RMS[2] values of the inverse sequence component of the voltage power supply, averaged over 10 min, must be in the range between 0 % and 2 % of the direct sequence component of the voltage power supply.

Over-voltages and voltage sags are random phenomena that impact on the on the voltage waveform. The over-voltages are usually caused by load disconnections or lightning strikes, most of the voltage sags in transmission and distribution networks are originated by power systems faults.

Relating to recorded voltage sags, the standard gives a summary table (Table 1.2) of reference to be used for reporting the voltage sags.

Table 1.2 – Voltage sag classification in terms of duration and residual voltage Vr.

Residual Voltage V_r [%]	**Duration "t" [ms]**				
	10 ≤t≤ 200	**200 <t≤ 500**	**500 <t≤ 1000**	**1000 <t≤ 5000**	**5000 <t≤ 60000**
90 >V_r≥ 80	A1	A2	A3	A4	A5
80 >V_r≥ 70	B1	B2	B3	B4	B5
70 >V_r≥ 40	C1	C2	C3	C4	C5
40 >V_r≥ 5	D1	D2	D3	D4	D5
V_r > 5	X1	X2	X3	X4	X5

Voltage sags can affect the operation of equipment. The standards EN 61000-4-11 [17] and EN 61000-4-34 [18] defined two classes of equipment in function of their susceptibility to the voltage sags; they are:

- "Class 2 equipment" those that don't stop their operation in presence of voltage sags belonging to the cells A1, B1, A2, B2 of Table 1.2;
- "Class 3 equipment" those that don't stop their operation in presence of voltage sags belonging to the cells A1, B1, A2, B2, A3, A4 of Table 1.2.

1.2 Overview of Regulatory Activities in Europe

[2] The root mean square value (RMS) of the voltage supply is equal to $\frac{V_{max}}{\sqrt{2}}$, where V_{max} is the maximum value of the voltage waveform.

Since the 1st Council of European Energy Regulators (CEER) Benchmarking Report on Quality of Electricity Supply (QoS) in 2001 [19], the role of National regulation Authorities continuously facilitated the development and setting of standards and economic incentives for VQ.

During the 3rd CEER Benchmarking Report on QoS in 2005 [20] only 6 European countries reported the presence of VQ monitoring systems (VQM). During the 5th CEER Benchmarking Report on QoS in 2011, 18 European countries reported to have an operational VQM system. The reduction in the cost of VQMs and the increase in their performance has led to a significant growth in the number of VQMs installed in the distribution and transmission networks. Also the issue of EN 50160 and EN61000-4-30 contributed to obtain comparable results from different monitoring devices..

The "Guidelines of Good Practice on the Implementation and Use of Voltage Quality Monitoring Systems for Regulatory Purposes" published in December 2012 [21], give an overview of possible applications of the results from VQM programmes including recommendations on the number and location of the monitors. Different kinds of disturbances were discussed and some monitoring data were delivered.

In [22] CEER addresses the current goals and regulatory approaches for DSOs, elaborated on changing needs given by market developments. The document [22] considers the changing aims in regulation which are driven by the energy transition. The main common targets are:

- ensuring a non-discriminatory network access;
- promoting cost efficiency;
- ensuring financial viability;
- facilitating innovation;
- ensuring security of supply;
- improving quality of service, i.e. DSOs offer the right services, with a service quality level that is satisfactory for network users, and contributes to security of supply for the whole network system.

The design of a regulatory system can incentivise DSOs to reach those targets. The Regulator will have to keep this in mind and strike a balance between the tools considering the desired outcomes. Every tool has certain advantages and disadvantages. CEER emphasises that for the design of the regulatory system there is not an equal approach across Europe. In Netherlands regulatory incentives for energy losses allowed a reduction of the costs of energy losses.

The European Directive 2019/944 of the "European Parliament and of the Council of 5th June 2019 on common rules for the internal market for electricity", imposed to all electricity supplier to establish with the final clients a contract in which are specified:

- the services provided;
- the quality levels of the service offered;
- the compensation and the methods of reimbursement applicable if the stipulated service quality levels are not reached, even in the case of inaccurate or late billing.

The article 59, instead, concerns tasks and skills of all European Authorities. In particular, regarding the quality levels of the energy supply service, the Authorities can:

- establish or approve standards and requirements relating to the quality of service and supply or contribute to them together with other competent Authorities;
- monitor compliance with the rules relating to the safety and reliability of the network;
- review past performance.

Since 1992, by invitation of the Norway Authority (Norges Vassdrags Energidirektorat - NVE), the main players in the electricity sector have participated in a program to measure the quality of voltage with the aim of characterizing the Norwegian electricity grid through the measurement of all the parameters required by the EN 50160 standard. In 2001, the Norwegian system detected that ¼ of the recorded voltage sags were originated in the HV network. More than 50% of the voltage sags measured in Norway do not exceed 30% of depth. The average value is very variable from place to place, and the distribution of the voltage sags during the year is very irregular, having peaks on the days of greatest atmospheric perturbation. At the conclusion of this campaign, NVE proposed and introduced a new directive relating the VQ which provides the extension of some parameters (rapid variations of the voltage, flicker, voltage imbalance, harmonic distortion) to the networks distribution of electricity with a nominal voltage greater than 35 kV. Furthermore NVE has introduced precise reference limits, both regarding to distribution networks with nominal voltage lower than 35 kV or higher.

The Spanish regulatory Authority (Comisión Nacional de Energía - CNE), in implementing the Royal Decree 1955/2000, issued a consultation document on the

procedures of PQ measurement and control. CNE intends to develop zonal indexes of the power quality, for the purposes of possible future regulations, with particular reference to short interruptions, voltage sags, value effective of the power supply voltage, voltage unbalance and distortion total harmonic [23].

In France [23], the regulatory Authority (Commission de Régulation del'Electricité - CRE) has defined for all MV and HV customers, annual maximum thresholds according to the population density of the Municipalities, due to short and long interruptions. For short interruptions, the maximum thresholds are equal to 30 interruptions/year due to low concentration (municipalities with less than 10,000 inhabitants) and 10 interruptions/year for the average concentration (common between 10,000 and 100,000 inhabitants). In case of exceeding the maximum thresholds, the DSO or TSO must compensate the damage suffered by the customer. As for the voltage sags, the access conditions standards to MV networks do not provide for maximum thresholds; however, a contractual form is envisaged, with payment by the customer for the definition of contractual thresholds on the maximum number of voltage sags with residual voltage less than 70% and duration greater than 600 ms. For the transmission systems, there is a maximum threshold of 5 voltage sags per year, upon payment of an annual premium by the customer.

1.3 National Regulation in Italy

With the Resolution [7], ARERA required the DSOs to install a voltage monitoring system on every MV busbars of all HV/MV substations of the Italian power system (Figure 1.1).

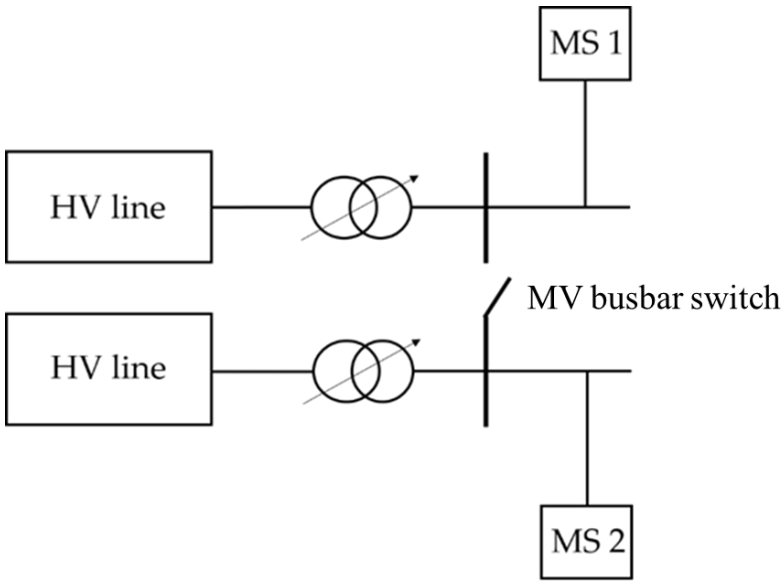

Figure 1.1 Simplified scheme of an example of an HV/MV (High Voltage/Medium Voltage) substation equipped with two measuring systems, i.e., MS1 (Measurement System 1) and MS2 (Measurement System 2), installed at the MV (Medium Voltage) busbars.

In the intention of ARERA, this monitoring system could allow to:

1. ensure an adequate VQ level on distribution system and reduce differences of performance in all Italian regions;
2. dispose of comparable and verifiable quality indices, to allow an adequate information to all customers interested to VQ disturbances;
3. build a starting point for the availability of data finalized to a future introduction of regulation.

Further, ARERA in 2012 instituted a working table focusing the attention on voltage sags measurement in according to the initiatives of the European Directive and the initiatives of the CEER to improve the quality of the electricity supply service All Italian DSOs and TSO, participated at the working table under the coordination of RSE (Ricerca Sistema Elettrico). The activities of the working table related the definition of the functional and technical features of the monitoring system. The technical specifies related:

1. data format regarding voltage sags measured by the national monitoring system;
2. data availability;
3. false voltage sags detecting criterion;
4. origin of voltage sags detecting criterion shared by all the working table's participants.

The working table's activities began in 2011 and continued until 2013 to:

1. validate the criterion for ascertaining the origin of voltage sags initially shared by all the working table's participants;
2. improve the criterion for detecting the origin of voltage sags;
3. define data management mode related to voltage sags occurred in specific operating condition (maintenance, bus coupler status).

In the first phase of the work table's activities, all DSOs must allow access to the VQ monitoring data to the Authority as superuser. In the second phase, RSE has created a national data monitoring system, as a super-partes entity. The national data monitoring system is called MonNaLiSA (in Italian Monitoraggio Nazionale a Livello di Stazioni AT/MT); it is also a website to which the Authority and DSOs have access.

Every year all DSOs must communicate to the Authority trough RSE the data related to the national monitoring VQ system. In particular, data related to the year 20XX must be communicated to RSE by email until April the 30th of the year 20(XX+1) for uploading to MonNaLiSA web site.The summing table related to the data of the national monitoring VQ system will be available for consultation from July the 1st of the year 20(XX+1) and only TRUE[3] voltage sags will be considered. Furthermore, all TRUE voltage sags will be characterized according to their origin (MV or HV). Appendix A of [24] contains a brief description of the MonNaLiSA web site and the access criteria.

MonNaLiSA required a data process to guarantee adequate uniformity. The format of the file containing all VQ events is .csv (comma separated values), and its name must comply with the rules of Figure 1.2.

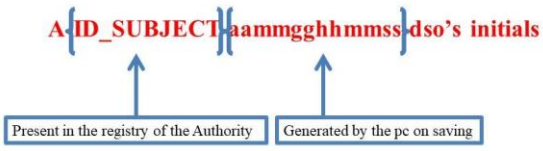

Figure 1.2 Syntax for naming the event file

[3] TRUE voltage sags are the voltage sags selected by a proper procedure as those really occurred at a site. They are distinguished from the false voltage sags caused by the voltage transformer saturation used in the measurement systems.

The registered data were composed of several parameters of the measured voltage sags in every MV busbar of every HV/MV substation. All the data were collected in a format table [24], such as in Table 1.3.

Table 1.3 – Format of recorded data relating to voltage sags measured at MV busbars.

#	ID Sub	ID Bus	RS	ST	TR	T_{occ}	D	V_n	V_r	V_r	DP	$MaxI_{TR}$	Type	Origin
1	Id Sub Code	Id Bus Code	X	X	X	gg/mm/aaaa hh:mm:ss.cc	hh:mm:ss.cc	kV	kV	%	Yes	Yes	T	HV
											No	No	F	MV
													NA	
2	Id Sub Code	Id Bus Code	X			gg/mm/aaaa hh:mm:ss.cc	hh:mm:ss.cc	kV	kV	%	Yes	Yes	T	HV
											No	No	F	MV
													NA	
3	Id Sub Code	Id Bus Code		X		gg/mm/aaaa hh:mm:ss.cc	hh:mm:ss.cc	kV	kV	%	Yes	Yes	T	HV
											No	No	F	MV
													NA	
4	Id Sub Code	Id Bus Code			X	gg/mm/aaaa hh:mm:ss.cc	hh:mm:ss.cc	kV	kV	%	Yes	Yes	T	HV
											No	No	F	MV
													NA	
5	Id Sub Code	Id Bus Code	X	X		gg/mm/aaaa hh:mm:ss.cc)	hh:mm:ss.cc	kV	kV	%	Yes	Yes	T	HV
											No	No	F	MV
													NA	
6	Id Sub Code	Id Bus Code	X		X	gg/mm/aaaa hh:mm:ss.cc)	hh:mm:ss.cc	kV	kV	%	Yes	Yes	T	HV
											No	No	F	MV
													NA	
7	Id Sub Code	Id Bus Code		X	X	gg/mm/aaaa hh:mm:ss.cc)	hh:mm:ss.cc	kV	kV	%	Yes	Yes	T	HV
											No	No	F	MV
													NA	
.	…	…	…	…	…	…	…	…	…	…	…	…	…	…
.	…	…	…	…	…	…	…	…	…	…	…	…	…	…
.	…	…	…	…	…	…	…	…	…	…	…	…	…	…
.	…	…	…	…	…	…	…	…	…	…	…	…	…	…
M	…	…	…	…	…	…	…	…	…	…	…	…	…	…

With reference to Table 1.3, the data are:

- the sequential number of the sag (#);
- the code that identifies the HV/MV substation (ID Sub);
- the code that identifies the MV busbar (ID Bus);
- the phase involved (RS and/or ST and/or TR);
- the start time of the sag in terms of day, month, year, hour, minute, second with a least a resolution of hundredths of a second (Tocc);
- the duration of the sag with at least resolution of hundredths of a second (D);
- the nominal voltage in kV (Vn) ;
- the residual voltage both in kV and in percentage of Vn (Vr);
- the intervention of the distance protection (DP);
- the intervention of the maximum current protection of the transformer (MaxITr);
- the type of voltage sag if true (T), false (F), not available (NA);
- the system, HV or MV, where the sag was originated (Origin).

The classification true-false-not available refers to the possible effects of the voltage transformer saturation used in the MSs, which can result in false voltage sags. The Resolution of ARERA [7] required DSOs to install a proper algorithm in the MSs for identifying the true voltage sags, i.e. T, distinguishing them from false sags, i.e. F, and from those whose identification is not unique, i.e. not available (NA). The algorithm is based on the measurement of the asymmetry of the voltage waveform during the sag [25]. The RMS value of the 2^{nd} voltage harmonic is calculated for the three phases. The RMS values were calculated on a time period equal to 20ms and updated every 10 ms. The RMS value in percentage related to the RMS value of the nominal voltage was calculated and it was compared to a threshold equal to 10% of the nominal RMS value of the voltage. The criterion is resumed in Table 1.4.

Table 1.4– Table for classification of voltage sag's type.

Type	Description	RS	ST	TR
F	False	F	F	F
T	True	T	T	T
NA	Not available	Every combination different from the preceding's.		

The condition NA corresponds to the inability of the MS of communicating with the central system. In [24] it was specified that during long term campaign of measurement, malfunction cases of the measuring systems can occur due to the input circuit of measurement equipment. In these cases, elevate number of events measured in one hour at day can be recorded. In [24], a measuring system installed on MV busbars, registered about one hundred events per year when malfunctions cases occurred, and this can be taken as a reference.

The activities of ARERA in the field of VQ were focused on the voltage sags concerning the MV network and slow voltage variations concerning the low voltage network. In the field of the regulation of voltage sags, ARERA means to deepen the following areas:

1. introduction of an individual standard on the maximum number of voltage sags for MV customers and automatic repayments in the case of overcoming of the standard;
2. incentives for reducing the number of voltage sags and their severity for voltage sags originated in MV network;
3. study of a special contract for MV costumers particularly sensitive to voltage sags.

With the Resolution [26], the Authority established that, from 2016, MV users will receive, in addition to the annual information on the service continuity levels recorded at their delivery point, also information on the voltage sags recorded from the VQM equipment in service at the MV busbar that supplies their systems according to the CEI EN 50160 standard.

In 2019, ARERA asked TSO for the data relating from 2017 to 2018 for setting the standard on the maximum number of voltage sags. HV end customers must make the data recorded available for the TSO. ARERA postpones to a future the automatic refunds. In 2020, the Resolution of ARERA n.524/2020 [27], in updating the Resolution 567/2019 [8], introduced the individual regulation regarding the so-called micro interruptions for HV customers participating to this regulation on voluntary basis. The micro interruptions are defined in [27] as the sum of transient interruptions and voltage sags. The transient interruptions are interruptions with duration not exceeding 1 s, and amplitude lower than 5% of the declared nominal voltage. Five HV customers participated at micro interruptions monitoring period from the 1st July 2017 to 30th June 2019. With reference to Table 1.2, the micro interruptions under this regulation were the sum of:

1. the voltage sags belonging to the cells: A5, B3, B4, B5, C2, C3, D2, D3, D4, D5, X2, X3, X4 and X5;
2. the transient interruptions originated in HV network occurred in normal operating conditions, that is not occurred in demonstrable emergency conditions during temporary network assets, ad depicted in Figure 1.3.

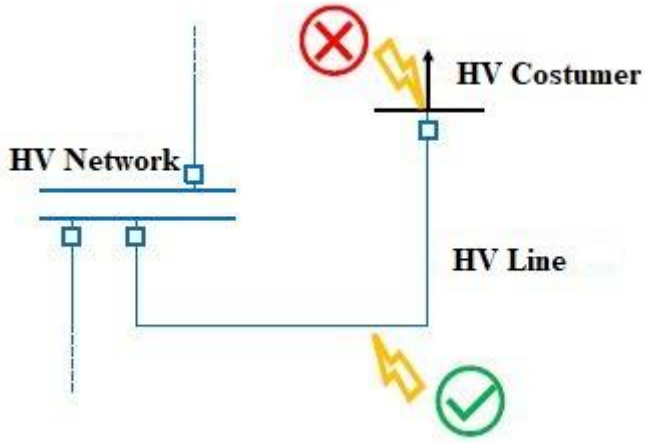

Figure 1.3 Transient interruptions responsibility of TERNA originated in HV network or HV line

After the monitoring period, the individual indicator was proposed as the number of micro interruptions yearly recorded. In the case that the number of micro interruptions are greater than the maximum level, TERNA is required to provide an automatic refund computed by:

$$I = \frac{\min(n;w)-s}{n} * \sum_{i=1}^{n} V_p * PEI_i \quad (1.2)$$

where:

- n is the number of regulated micro interruptions;
- s is the specific level of micro interruptions;
- w is the parameter that fixed the maximum value of refundable micro interruptions equal to 3 times the value of s;
- PEI_i is the interrupted power in kW measured 15 minutes earlier the ith micro interruption;
- V_p is a parameter equal to 0.65 € for 1 kW of interrupted power.

The maximum value of the automatic refund to the same HV costumer is 97500 €/year. A new monitoring period was issued by the article 23 bis of the Resolution of

ARERA n.524/2020 from the 1st January 2022 to 31st December 2022. Figure 1.4 shows the conceptual steps of the Resolution n.524/2020.

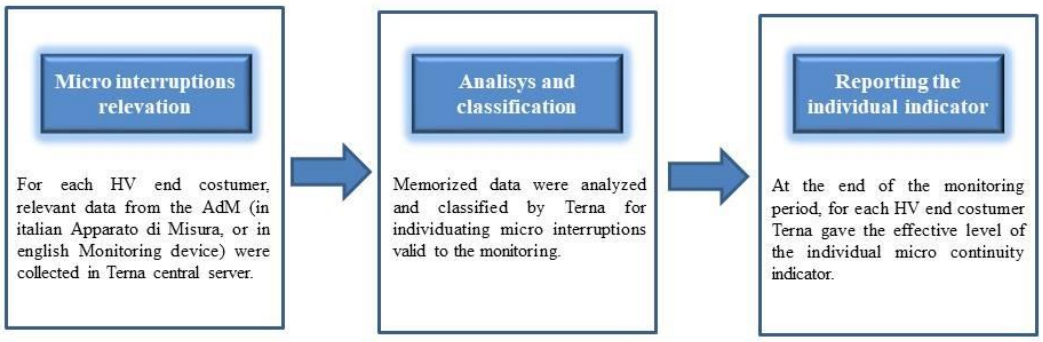

Figure 1.4 Flow chart of the operative aspects of the new monitoring period

CHAPTER 2.

DETECTING THE ORIGIN OF MEASURED VOLTAGE SAGS

Voltage sags measured in the actual networks are mostly due to faults. Establishing where the fault originating a voltage sag occurred is not straightforward in case of interconnected networks operating at different voltage levels. The different methods proposed in the literature and in the Italian regulation by the National Energy Agency are shown. The effects of DG units on the results obtainable applying the methods of the Italian regulation are analysed and compared. A case of propagation of sags originated in the distribution network up to the transmission network is studied and discussed.

2.1 Introduction

The interconnections among the MV systems and the HV systems introduce difficulties in ascertaining the origins of the voltage sags measured at a given busbar. In fact, voltage sags pass across the HV/MV transformer of the HV/MV substations and propagate through the interconnected networks. The types and the characteristics of voltage sags can change depending:

- the connections between the primary winding and the secondary winding of the transformer;
- the loads.

Due to the propagation of voltage sags, even one single node in which a fault current occurred, can be the origin of several voltage sags. A short circuit occurred on the MV busbar of the HV/MV substation or along a MV line connected to the MV busbar of the HV/MV substation can cause a voltage sag that can be measured on:

- the HV side of the HV/MV substation where the fault occurred;
- the MV side of the HV/MV substation where the fault occurred;
- the HV side of HV/MV substation electrically close to the one where the fault occurred;
- the MV side of HV/MV substation electrically close to the one where the fault occurred.

The occurrence of a voltage sag, in the previous cases, depends on several factors; the most important are:

- the short circuit power of the equivalent HV system;
- the distance of the fault from the point of measurement;
- the topology of the considered system;
- the position of the bus-coupler.

The methods proposed in the relevant literature to ascertain the origin of voltage sags can be grouped in three main categories, i.e., Single Monitor-based (SM-based) methods, Multi Monitor-based (MM-based) methods, and Hybrid Method (HyM).

Generally, SMs-based use only one point of measurement to identify whether a measured voltage sag originated in the upstream system or in downstream system from the measurement point; MMs-based methods use several points of measurements in different busses; the HyMs identifies the part of the system,

downstream or upstream where the sag was originated as an SM-based does, but uses several points of measurements, as an MM-based does.

The scheme of reference is shown in Figure 2.1, where only the data measured by the PQ recorder installed at point M of the system are used [28]. The point M corresponds to a busbar of the HV/MV station (not displayed in Figure 2.1), usually it is on the MV busbar. Unlike the SM-based methods,

Most of the SM-based require measurements of both the voltages and the currents.

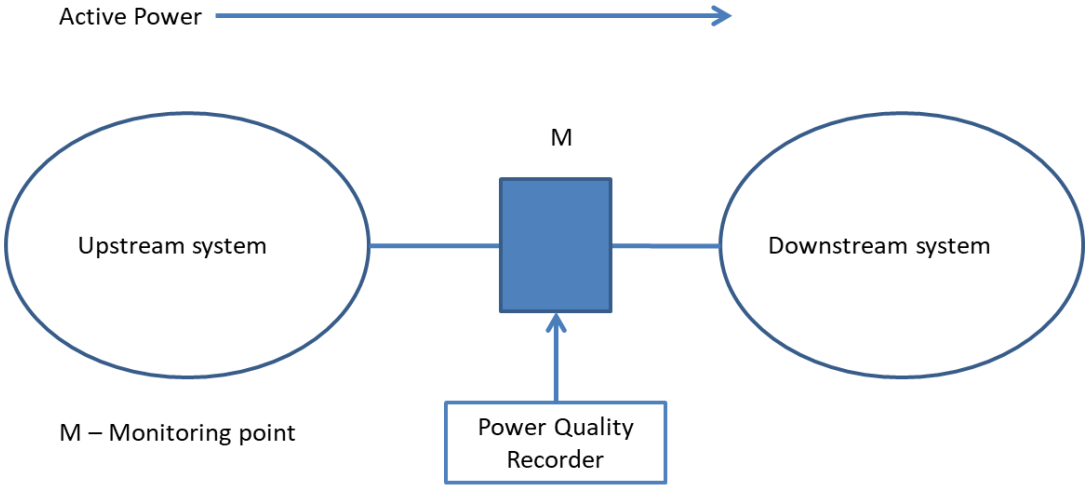

Figure 2.1 Scheme of reference for single-monitor methods

The so-called Voltage Magnitude-based method [29] is the only method that uses just the measurements of voltages, but it requires both the pre-fault voltages and the post-fault voltages measured at both sides of the transformer, which interconnects HV and MV systems.

Most of the MMs-based require the measurement of several data or the acquisition of further information about the system [30-32].

In Italy, the Resolution of ARERA 198/2011 [7] proposed a SM-based method, called M1, that uses only the measurements of the voltage sags measured in the same HV/MV substation (MS_1, MS_2 in Figure 2.2). The paper [33] proposed an HyM, named M2. This method uses the data derived from a number of MSs; MS_1, MS_2, MS_3 and MS_4 in Figure 2.2, that are installed in different HV/MV substations, but furnishes only the part of the system (HV or MV) where the sag was originated, like a SM does.

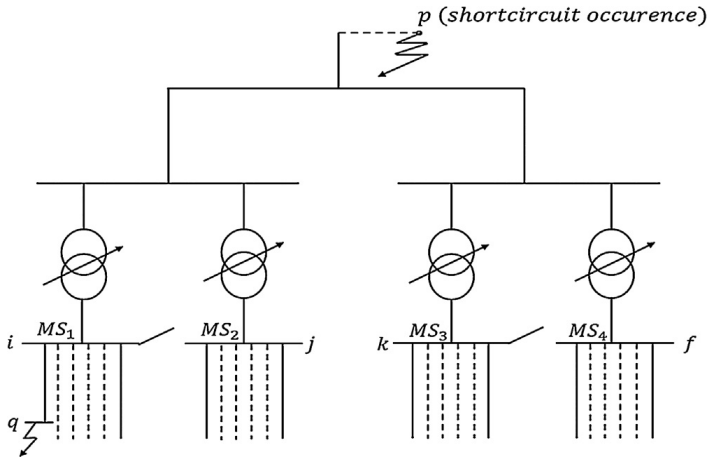

Figure 2.2 Scheme of reference for M2

In modern distribution systems, like smart grids are, to establish the system where the fault originating a measured sag occurred is complicated by the presence of added units for making active the networks. The presence of DG and OLTCs could affect the results of the SM-based, in particular M1. The OLTCs are used to compensate the increasing of the voltage at the extreme of the MV line (negative voltage drop) caused by the current flowing through the line from to the DG units. Any HV/MV substation, in which one of the two HV/MV transformers feeds a line connecting a DG unit, can operate with two different values of the transformer ratio. This operating condition can affect the results of the method M1 since the different ratio of the two transformers can result in different values of the residual voltages measured at each MV busbar of the HV/MV substation, independently from the system (downstream or upstream) where it originated. The DG unit, in short circuit condition, could sustain the voltage during the sag. The action of the DG depends on the type of connection of the DG to the network (direct or by means of a power converter), the type of the control adopted at the DG terminal, the ratings of the current protections.

The methods applied in the Italian regulation, that is M1 and M2, are presented and discussed together in the same section, even if M1 is a SM and M2 is an HyM.

Finally, the data from field revealed that in some specific cases the sags caused by faults in the MV systems propagated to HV networks. This problem was studied simulating a portion of a real system, which presents the interconnections between HV and MV network. The simulation results proved that this condition could occur.

2.2 Analysis of the Literature

The assessment of the origin of voltage sags was addressed in literature, even before the extensive measurement campaigns on the networks. It is significant that most of the methods proposed in literature have been applied on simulated networks and not on data measured on real networks. The methodologies proposed in the literature can be classified into three categories:

1. Single Monitor (SM-methods);
2. Multi Monitor (MM-methods;
3. Hybrid Method (HyM).

SM-methods apply to a single node, typically a transformer station or a node where a transformer is present. The goal of a SM-method is to identify the cause of a voltage sag in this node by discriminating between two positions: upstream section (Up-stream) and downstream section (Down-stream).

MM-methods apply to multiple nodes of a network where the equipment which measures the voltage sags is installed. Unlike the SM-methods, the MM-methods use several points of measurements in different busses. Then, the data that are obtained are processed to identify the exact origin of the voltage sag rather than analysing the part of the system where the voltage sag originated.

A HyM identifies the part of the system, downstream or upstream where the sag was originated as an SM-based does, but uses several points of measurements, as an MM-based does. Only one method, named M2, belongs to this category; it will be presented and discussed in Section 2.2.3.

2.2.1 SM-methods

The principal SM-methods are:

- Disturbance power and disturbance energy method;
- Slope of system trajectory method;
- Resistance sign method;
- Real current component method;
- Distance relay method;
- Voltage magnitude-based method;
- Instantaneous voltage and current vectors;

- Superimposed quantities and negative sequence
- S-transform disturbance power;
- Wavelet multi-resolution.
- Dg-component.

In the following, the main properties of each method are recalled; all the details of the method can be derived from the bibliography references.

- ***Disturbance power and disturbance energy method*** [28]

It was the first method to be published, and it aims to identify the location of the fault that generated the sag (downstream or upstream of the observation node) using the pre-fault power flow as an indicator. With reference to Figure 2.3, the disturbing power (2.1) is defined as the difference between the power recorded during the event, P_f, and the power recorded in steady state, P_{ss}, at the observation node.

$$\Delta P = P_f - P_{ss} \tag{2.1}$$

The final sign of the disturbing power defines the position of the fault, upstream of the observation node if negative, downstream if positive.

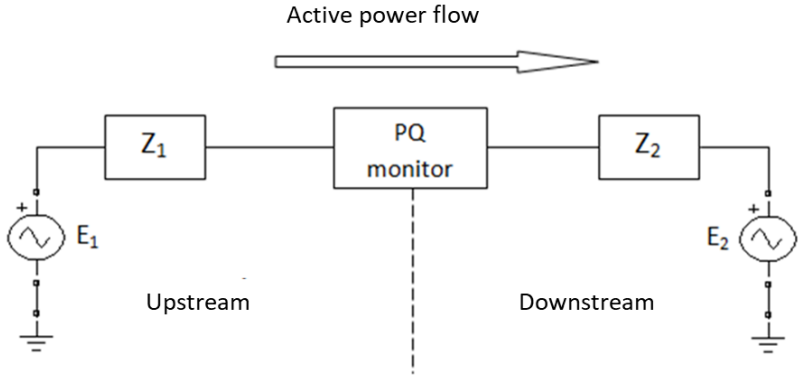

Figure 2.3 Reference circuit for ascertaining of the origin of the voltage sag

- ***Slope of system trajectory method*** [28]

The method considers the relationship (2.2) between voltage and current at the observation node to identify the location of the fault (Figure 2.3).

$$VI\cos\theta = -R_1 I^2 + E_1 I\cos\theta_1 \tag{2.2}$$

Where E_1 is the supply voltage, R_1 is the real part of Z_1, V and I are respectively the RMS value of the voltage and current measured by the PQ-monitor in the observation node, θ is the angle between the current and the voltage in the observation node and $\theta 1$ is the angle between the current and the voltage in the generation node.

During the voltage sag, *I* and *V* were recorded in the observation node and a least squares linearization is applied. The method states that, if the slope (2.3) of the straight line is positive, the fault is upstream, if it is negative the fault is downstream (2.4). If during the event there is an inversion of the power flow, the fault is still upstream. The method has been extensively tested with satisfactory results for symmetrical faults.

$$|V\cos\theta| = -R_1 I + E_1 \cos\theta \tag{2.3}$$

$$|V\cos\theta| = +R_1 I + E_1 \cos\theta \tag{2.4}$$

- ***Resistance sign method*** [28]

The method has the advantage of using only the direct sequence currents and voltages. Collecting a set of *n* values of currents and voltages at the observation node before and during the voltage sag, the following matrices shown in relations (2.5) and (2.6) are constructed. From each matrix the value of the resistance *R* is calculated; the test is considered discriminating if the two resulting *R* have the same sign.

$$\begin{bmatrix} R \\ X \\ E_{RE} \end{bmatrix} = \begin{bmatrix} I_{RE}(1) & I_{IM}(1) & 1 \\ . & . & . \\ . & . & . \\ . & . & . \\ I_{RE}(n) & I_{IM}(n) & 1 \end{bmatrix}^{-1} \begin{bmatrix} V_{RE}(1) \\ . \\ . \\ . \\ V_{RE}(n) \end{bmatrix} \tag{2.5}$$

$$\begin{bmatrix} R \\ X \\ E_{IM} \end{bmatrix} = \begin{bmatrix} I_{IM}(1) & I_{RE}(1) & 1 \\ . & . & . \\ . & . & . \\ . & . & . \\ I_{IM}(n) & I_{RE}(n) & 1 \end{bmatrix}^{-1} \begin{bmatrix} V_{IM}(1) \\ . \\ . \\ . \\ V_{IM}(n) \end{bmatrix} \tag{2.6}$$

With reference to the matrix relations (2.5) and (2.6), the subscript *RE* and *IM* denote the real and imaginary part respectively. The positive sign of the two resistance values indicates a fault upstream of the observation node, negative for downstream.

- ***Real current component method*** [28]

The method states that if the value of $Icos\theta$, where I is the RMS value of the current recorded in the observation node at the beginning of the sag, is negative, the fault is upstream of it; downstream if positive. Obviously, in case of polarity inversion, the analysis must be carried out during the variation of the current and on the phase quantities..

- ***Distance relay method*** [28]

The method considers the impedance $\dot{Z}_s$ (2.7) from the observation node before and after the sag, determined by means of the voltage and current phasors $\bar{V}$ and $\bar{I}$.

$$\dot{Z}_s = \frac{\bar{V}}{\bar{I}} \tag{2.7}$$

If the absolute value of the impedance during the sag is less than that of the impedance before the sag, and if the phase of the impedance during the sag is positive, the fault is downstream of the observation node; upstream otherwise. Based on numerous comparative studies effected in [28], it can be concluded that the reliability of the above-mentioned methods is better than the Distance relay method in case of symmetrical faults on transmission networks.

- ***Voltage magnitude-based method*** **[28]**

The method only uses the voltage sag amplitude and the pre-fault voltage. With reference to the diagram shown in Figure 2.4, the idea is to compare the voltage during the sag ($V_{i\text{-}sag}$) on the two sides of the transformer and pre-fault voltage ($V_{i\text{-}prefault}$), as expressed by relations (2.8) and (2.9).

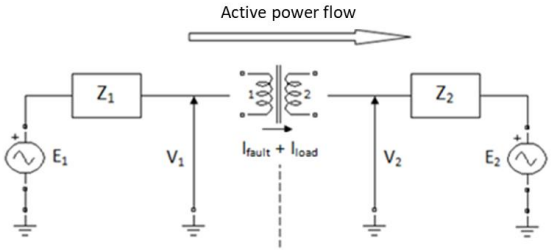

Figure 2.4 Reference circuit for locating the origin of the voltage sag

$$V_1 = \frac{V_{1-sag}}{V_{1-prefault}} \tag{2.8}$$

$$V_2 = \frac{V_{2-sag}}{V_{2-prefault}} \tag{2.9}$$

If V_1 is greater than V_2 the fault is downstream of the transformer, upstream otherwise. If there are no generation units downstream of the transformer, it is expected that V_1 and V_2 will be the same in case of a fault upstream.

Similar conclusions are reached by considering the voltage variations on the two sides of the transformer, as expressed in relations (2.10) and (2.11):

$$\Delta V_1 = Z_1 (I_{fault} + I_{load}) \tag{2.10}$$

$$\Delta V_2 = (Z_1 + Z_{TRAFO})(I_{fault} + I_{load}) \tag{2.11}$$

where, with reference to Figure 2.4, I_{fault} is the fault current, I_{load} is the load, Z_{TRAFO} is the impedance of the transformer. If $\Delta V2$ is greater than $\Delta V1$ it is concluded that the fault is downstream of the transformer, otherwise upstream.

- ***Instantaneous voltage and current vectors*** [28]

The Instantaneous Voltage and Current Vectors (IVCV) technique uses instantaneous voltage and current vectors. Let's consider that voltages and currents during voltage sags usually contain a heavy content of harmonics at a frequency higher than the fundamental. The use of conventional phasor-based techniques, could be inappropriate. In these cases, it is valuable to use the instantaneous values of the voltage and current.

This technique computes the instantaneous norm of the voltage and current quantities to obtain, in addition to the instantaneous active power, also the instantaneous apparent power; the ratio between these two quantities gives the instantaneous power factor [34]:

$$p(t) = v(t)^T \cdot i(t), \quad \|v(t)\| = \sqrt{v(t)^T \cdot v(t)}, \quad \|i(t)\| = \sqrt{i(t)^T \cdot i(t)}, s(t) = \|v(t)\| \cdot \|i(t)\| \tag{2.12}$$

$$PF(t) = \frac{p(t)}{s(t)} \tag{2.13}$$

Let us consider a phase-to-phase fault in the system reported in Figure 2.5.

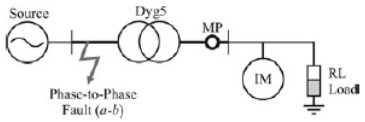

Figure 2.5 Phase to phase fault in radial system.

It is possible to compute two main figures, that is the slope of the waveform of $i(t)$ against the modules of $\frac{p(t)}{i(t)}$ and the first peak of the quantity $\frac{p(t)}{\|v(t)\|}$; their values discriminate the origin of the sag as shown in (2.14) and (2.15). These figures are calculated for different cycles before and during the voltage sag.

$$slope\left(\|i(t)\|, \frac{|p(t)|}{\|i(t)\|}\right)\begin{cases} > 0, upstream \\ < 0, downstream \end{cases} \tag{2.14}$$

$$first\ peak\left(\frac{p(t)}{\|v(t)\|}\right)\begin{cases} < 0, upstream \\ > 0, downstream \end{cases} \tag{2.15}$$

- ***Superimposed quantities and negative sequence*** [28]

This method uses the principle of superposition to determine the voltages and currents of the circuit where a fault has occurred. The voltages and currents during the fault are expressed by their respective values before the fault:

$$V_{i-sag} = V_{prefault} + \Delta V, \qquad I_{fault} = I_{prefault} + \Delta I \tag{2.16}$$

The terms ΔV and ΔI represent the difference between voltage and current before and during the fault. The concept is like that used for directional relays. If a fault occurs in the direct direction, ΔV will assume a negative sign, consequently the origin of the voltage sag is downstream; if the fault is in the reverse direction, the ΔV will assume a positive value, consequently the origin of the variation is upstream. [35].

- ***S-transform disturbance power*** [28]

This method is based on the transform *S* (*ST)* with a window whose amplitude varies with the frequency. The *ST* of a signal over time *x (t)* is defined as:

$$s(\tau, f) = \frac{|f|}{\sqrt{2\pi}} \int_{-\infty}^{+\infty} x(t) e^{\frac{-(t-\tau)^2 f^2}{2}} e^{-i2\pi f t} dt \tag{2.17}$$

where t e τ are time variable and the window function $w(t,f) = \frac{|f|}{\sqrt{2\pi}} e^{-\frac{f^2 t^2}{2}}$ is a Gaussian function with variance $\sigma^2 = \frac{1}{f^2}$ depending on frequency.

If a voltage sag occurs on the network, the voltage quality measurement device (*VQM*) will record the event. The origin of the voltage sag could be upstream or downstream of the control point (Figure 2.1, here presented again as Figure 2.6 for clarity). The part on the left of the observation point (upstream) is the one that feeds the power flow recorded by *VQM* while the part on the right concerns the part of the network that sees the power flow coming from the *VQM*.

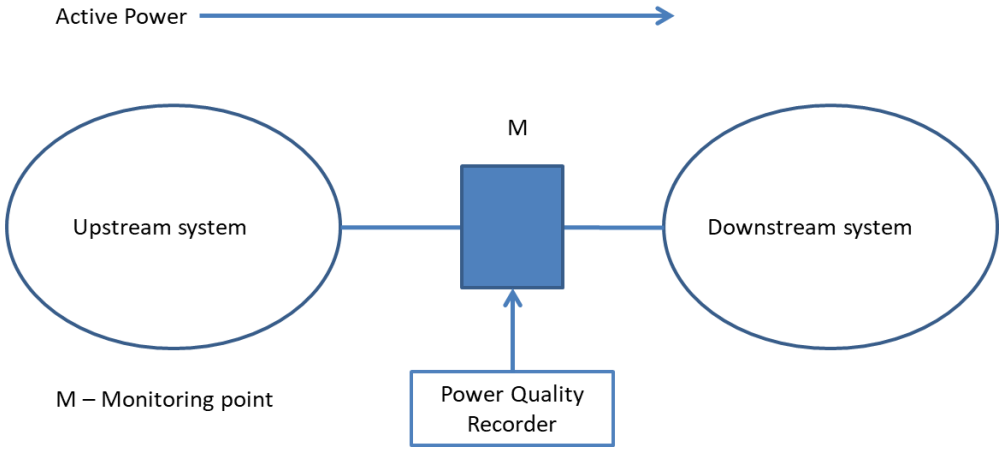

Figure 2.6. Measuring point between upstream and downstream system.

Different methods that use the *ST* are proposed to determine the origin of the voltage sags. One of these involves transforming the instantaneous electrical quantities of voltage and current and determining the maximum value of their product. It is assumed that the power flow to the VQM increases during a downstream type of event and decreases during an upstream event.

To determine the origin of the sag, the disturbance power indicated with the expression $\Delta p\ (t)$ is taken into consideration; it is defined as:

$$\Delta p(t) = p(t)_{sag} - p(t)_{presag} \begin{cases} < 0, upstream \\ > 0, downstream \end{cases}, \quad (2.18)$$

where $p(t)_{sag}$ is the instantaneous power during the voltage sag and $p(t)_{presag}$ is the instantaneous power before the voltage sag in steady state conditions.

It is possible to relate the instantaneous power in the time domain to the value in *ST*, by first calculating the voltage and current transformations and after making the product:

$$p_{st}(t) = \max|S|_v(t) \times \max|S|_i(t)' \quad (2.19)$$

Where $p_{st}(t)$ is the *ST* of the instantaneous power, $|S|_v(t)$ is the matrix of the absolute values of the transform *S* of the voltage and $|S|_i(t)'$ is the transposed matrix of the absolute values of the transform *S* of the current.

The disturbing power in *ST* is defined by the difference between $p_{st}(t)$ during the sag and $p_{st}(t)$ before the sag which respectively represent the transforms according to *ST* of the instantaneous power during the voltage sag and of the instantaneous power before the occurrence of the sag [36].

$$\Delta p_{st}(t) = p_{st}(t)_{sag} - p_{st}(t)_{presag} \begin{cases} < 0, upstream \\ > 0, downstream \end{cases}, \quad (2.20)$$

- ***Wavelet multi-resolution*** [28]

This method is based on the concept of multi-resolution, which allows the representation of a signal on different scales. This method takes advantage of multi-resolution and considers the energy flow recorded at a control point (M) during a voltage sag (Figure 2.7).

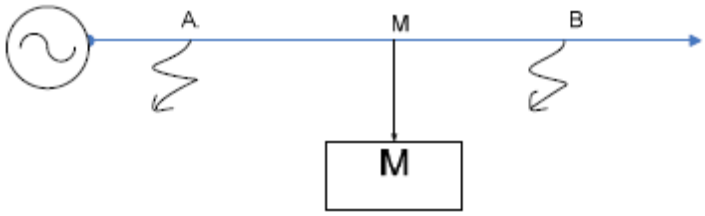

Figure 2.7 Control point M used for determining the origin of the voltage sag

The power variation on the three phases due to the presence of the voltage sag is initially computed. After the use of the wavelet transform, the energy difference of the power signals previously computed is analysed for locating the origin of the sag. An arbitrary signal *x(t)* can be decomposed using the multi-resolution formula as follows:

$$x(t) = \sum_k c_J(k)\phi_{J,k}(t) + \sum_{j=1}^{J}\sum_k d_j(k)\psi_{j,k}(t) \quad (2.21)$$

The first part of the expression on the right is the projection of the *x(t)* signal in space with change of scale; it is a smooth approximation of the starting signal. The term $c_J(k)$ takes the name of discrete smoothed approximation while $\phi_{J,k}(t)$, represents the scale function. The second part is the projection of the signal into the

wavelet space, the term $d_j(k)$ is the coefficient of the wavelet transform, and $\psi_{j,k}(t)$ is the wavelet function that acts as a link between the wavelet transform and the classification multi-resolution type.

According to the Parseval theorem, the energy of the original signal can be obtained as the sum of the energies contained in each frequency sub-band; these contributions can be obtained starting from the low and high frequency coefficients for each space with change of scale.

$$\int |f(t)|^2 dt = \sum \left|C_j(t)\right|^2 + \sum_j \sum_k \left|d_j(k)\right|^2 \quad (2.22)$$

If we consider the previous formula while the voltage sag occurs, we obtain the energy contained by the signal following the sag, this value can be indicated with *E*. If we suppose that we have computed the energy content of the signal in stationary conditions and indicate it with E_0, we can calculate the energy variation as $\Delta E = E - E_0$. The decision criterion considers the value of ΔE during the voltage sag as shown in (2.23) [37]:

$$\begin{cases} if\ \Delta E < 0, downstream\ M \\ if\ \Delta E > 0, upstream\ M \end{cases} \quad (2.23)$$

- ***Dg-component*** [28]

The method is based on the measurement of impedance in the coordinates system {dq0}. The impedance is defined as the relationship between voltage and current of a generic phase at the control point (M), the ratio is calculated both in module and in phase during the occurrence of a voltage sag.

$$|Z| = \frac{V_a}{I_a}\ , \angle \bar{Z} = \angle \bar{V}_a - \angle \bar{I}_a \quad (2.24)$$

A possible scenario of the proposed measurement system can be the one shown in Figure 2.8, where the different values of *Z* indicate the impedances of the relative lines, M is the observation point of phase voltage and current.

As a cause of change in the electrical parameters of the circuit, an induction motor was introduced. The starting current of the induction motor could cause a voltage sag in the power supply line. A transient in the operation of the motor can lead to a change in the impedance measured at the observation point [38].

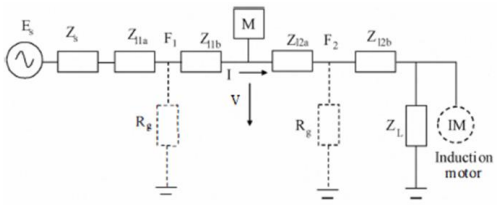

Figure 2.8 Equivalent single-phase circuit with induction motor connected

In according to the definition of instantaneous power, the measurement of the instantaneous impedance of a three-phase system results from the following relationship:

$$Z(t) = \frac{V(t)}{I(t)} = \frac{\|V(t)\|^2}{p(t)} = \frac{V_a(t)^2 + V_b(t)^2 + V_c(t)^2}{V_a(t)I_a(t) + V_b(t)I_b(t) + V_c(t)I_c(t)} \tag{2.25}$$

Considering the instantaneous impedance, a transformation in the coordinate system $\{dq0\}$ is applied. It is necessary to filter the harmonic components associated with the voltage sag, for example by means of a Butterworth-type low-pass filter. The impedance measurement in the new coordinate system can be expressed as:

$$Z(t) = \frac{\|V(t)\|^2}{p(t)} = \frac{{V_d}^2(t) + {V_q}^2(t) + {V_0}^2(t)}{V_d(t)I_d(t) + V_q(t)I_q(t) + V_0(t)I_0(t)} \tag{2.26}$$

The impedance during the occurrence of a voltage sag and the impedance in stationary conditions are calculated, If the condition $0 < Z_{sag} < Z_{steady}$ is verified, the disturbance source originates from the right side of the control point, otherwise from the left.

2.2.2 MM-methods

The main MM methods are:

- Direction and event cause-based method (DEC);
- Topological locating algorithm-based method (TLA);
- Coefficient matrix-based method (CM);
- Branch current deviation-based method (BCD);
- Multivariable regression-based method (MVR).

In the following, the main properties of each method are recalled.

- ***Direction and event cause-based method (DEC Method)*** [39]

DEC-Method is a technique that refers to the cause that generated the event to determine the origin of the voltage sag. First, it is necessary to define at least one observation point able to identify the relative position of the origin of the event.

Basically, the measuring point has the task of determining the up area or down area; an example of this configuration is shown in Figure 2.9

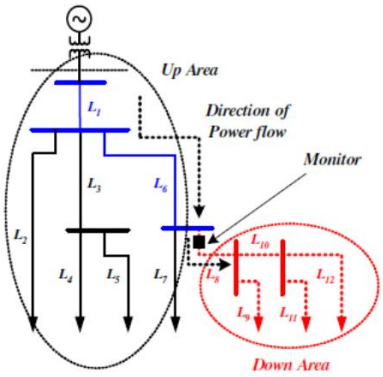

Figure 2.9 Electrical network with a single monitor for discriminating down area or up area.

From an electrical and traditional point of view, in case of passive system the power flows from a source towards the loads, passing through meters. Therefore the "down area" can be defined as that area to which the power flow arrives after passing through the measurement point; the "up area" is the one not included to the previous "down area".

The relative position of the origin of the event (a fault) can be determined as follows:

$$down\ area\ \ if\ \frac{I^1{}_{sag}}{I^1{}_{bf}} \geq Thr_{LF} \qquad (2.27)$$

$$up\ area\ \ if\ \frac{I^1{}_{sag}}{I^1{}_{bf}} < Thr_{LF}$$

where:

- $I^1{}_{sag}$ is the fundamental component of the current during the voltage sag;
- $I^1{}_{bf}$ is the fundamental component of the pre fault current;
- Thr_{LF} is a threshold value equal to $\frac{I^1{}_{sag}}{I^1{}_{bf}}$ appropriately fixed.

- ***Topological locating algorithm-based method (TLA Method)*** [40]

The TLA Method is based on the topological location of the origin of the sag. The algorithm that allows to locate the position uses several concepts, that is: "up-area" and "down-area", defined as for the previous method, the graph theory, the position of the measurement points and the relative position of the origin of the event; all this information is useful for determining the topological coverage matrix and the direction matrix. The product of the coverage matrix and the direction matrix yields the candidate matrix.

$$M_c = \frac{1}{M} \cdot M_{co} \cdot M_D \tag{2.28}$$

where M_c is the candidate matrix, M_{co} the coverage matrix and M_D the direction matrix. Being a MM method, their number can vary according to needs. The area where the fault originated is determined by means of the candidate matrix. Clearly, the greater the number of measurement components, the greater the accuracy of the area determination.

- ***Coefficient matrix method (CM Method)*** [41]

The CM Method uses the coefficients of the system matrix and those of the matrix of the measured voltages to estimate the voltages of the nodes that are not being measured. The studies were conducted in stationary conditions. In a different formulation of this method the node voltages measured on the network represent the stationary conditions, while the variation of the node voltages due to a variation of the network loads represent the voltage sag.

A voltage change index is used to identify the source node of the voltage sag, considering the largest change from the stationary value. The following coefficient is introduced:

$$V\% = \frac{(V_{bf} - V_{sag})}{V_{bf}} \times 100 \tag{2.29}$$

It is possible to compute the maximum value between the different terms:

$$V_{sag,k} = max|V_{\%1}, V_{\%2}, V_{\%3}, \dots\dots\dots\dots V_{\%n}| \tag{2.30}$$

In the previous expressions V_{bf} is the node voltage in stationary conditions while V_{sag} is the minimum voltage sag value.

The origin node of a voltage sag can be considered as that node with the maximum value of *V%* with respect to the other nodes. If the number and position of the measuring points and the coefficients of the system matrix are known, the method can estimate the voltage at not measured nodes.

- ***Branch current deviation-based method (BCD Method)*** [42]

The BCD Method identifies the origin of a voltage sag using a limited number of measuring instruments installed in a large transmission network The first step in the BCD method is to determine where positioning the measuring instruments in such a way that it is possible to locate the origin of the voltage sag by calculating, at each

measuring point, the variations of the currents on the branches of the network before and after the fault. The position of the measurement points can be determined using the following equation:

$$\frac{\partial f}{\partial V^k{}_f} = \sum_{\substack{i=1 \\ i\neq j}}^{m} \sum_{\substack{j=1 \\ j\neq i}}^{m} \frac{(z_{ik} - z_{jk})/(z_{kk} + z^k{}_f)}{z_{b,ij}}, k = 1,2,\dots,m \tag{2.31}$$

In (2.31) z_{ik} is the transfer impedance between node *i* and node *k*, z_{jk} is the transfer matrix between node j and node k, z_{kk} is the Thevenin impedance at node *k*, $z^k{}_f$ is the fault impedance, $z_{b,ij}$ is the branch impedance between node *i* and node *j*, *m* is the number of nodes in the network and *n* is the number of branches in the network .Equation (2.31) represents the sensitivity of the variation of the fault current in relation to the fault voltage at node *k*.

By putting the equation values for all nodes in descending order, the node that has suffered a fault with the highest value is given priority for the positioning of the measurement system. The current variation is then measured from time to time, using the formula:

$$BCD_i = \frac{I_f - I_s}{I_s} \tag{2.32}$$

where I_s and I_f are the currents before and during the voltage sag respectively.

When a fault occurs, the values of the branch currents which are connected to the fault location node will increase significantly, and such large current variations are easily detected by the measurement systems. The localization of the origin of a voltage sag can be determined by establishing a priority between the variations of the branch currents, recorded at each measurement point, before and after the fault.

- ***Multivariable regression-based method (MVR Method)*** [43-46]

The number and positioning of the measurement systems are initially determined by a genetic algorithm and by the Mallow *Cp* index. Considering the nodes under measurement as independent variables in the MVR model, adequate regression coefficients are obtained from the test data to estimate the stresses of the nodes not under measurement. Once tested, regression models are used to determine the maximum voltage variation (*VD*) and the minimum standard deviation (*SD*) which

allow to identify the exact location of the origin of the voltage sag. After an evaluation of the positioning of the measurement points, if a fault occurs in each node of the network, the MVR model estimates all the voltages of the nodes not subjected to measurement by means of the *VD* and *SD* indices and therefore identifies the exact position of the source that causes the voltage sag.

The method is formulated by the following equations:

$$B = (X'X)^{-1}X'Y, \tilde{V} = B_0 + \sum_{j=1}^{k} B_j V_{ij}, i = 1, \dots, n \quad (2.33)$$

$$E = V - \tilde{V} \quad (2.34)$$

$$VD = \Delta V = (V_{bf} - V_{sag})/V_{sag} \quad (2.35)$$

$$SD = \sqrt{\frac{\sum_{i=1}^{n}(V_i - \bar{V})^2}{n-1}} \quad (2.36)$$

Where *B, X, Y, E, V* and $\tilde{V}$ are respectively the regression coefficient, the independent variables, the dependent variables, the measurement error, the measured voltage and the estimated voltage.

2.2.3. Methods Applied in Italian Regulation

The methods applied in the Italian regulation [7-8, 26, 27], are named M1 and M2; they use only the measurements of the main characteristics of the voltage sags, i.e., the amplitudes of the residual voltages that are under the limit of 90%, the time they occurred, and their duration. The objective of M1 and M2 is to establish where the voltage sags originated, i.e., in the HV network or in the MV network. Neither method detects the exact node where the sag originated; rather, they identify the network in which the sag originated. With reference to the categories of methods already available in the literature, M1 and M2 fall in the categories of SM and HyM, respectively M1 is a SM because it has the aim of identifying whether the sag originated in the HV upstream system or in the MV downstream system MV interconnected by HV/MV substation. However, M1 presents some differences if compared with any SM in the fact that it performs a pair-to-pair analysis of the voltage sags that are measured almost contemporaneously on the MV busbars of the same HV/MV substation.

M2 is a HyM since it uses data that come from several MS that are installed in different nodes, and identifies the part of the system in which the voltage sags originated rather than detecting their exact origins, as done by a MM method.

M1 attributes the origin of all single voltage sags that occur only at one of the MV busses from the same HV busbar to the down-stream system, i.e., the MV network. For voltage sags that occur at all of the MV busbars from the same HV busbar, these voltage sags originate in the upstream system, i.e., the HV network, if all of the following conditions are met:

a) the residual voltages of the voltage sags differ by no more than 3%;

b) the voltage sags occur within 60 ms of each other;

c) the durations of the voltage sags are within 20 ms of each other.

M2 was developed from the following considerations.

A voltage sag originated at higher voltage levels can involve portion of the lower voltage network, including both busses of the same HV/MV substations and busses of different HV/MV substations. As a result of these observations, all the voltage sags that occurred almost contemporaneously in a given portion of the interconnected system were analysed by M2. Regarding the amplitude of the voltage sags caused by the same fault, the same per unit value of the short circuit current in the generic node *p*, can cause a wide range of values of the residual voltages associated with voltage sags. The presence of the OLTCs of the HV/MV transformers must be considered. Also, in the same HV/MV stations, these devices can operate at different positions so that the difference of the residual voltages can exceed the 3% limit imposed by M1. This is particularly true when, for a high penetration of GD, the power flow of the transformers can be very intermittent. Summarising, voltage sags measured at the MV busbars from different HV/MV substations were originated in the upstream system, i.e., the HV network, if all of the following conditions are met:

a) the time of occurrence of the analysed voltage sags is inside a time range of 60 ms;

b) the HV/MV substations are electrically close each other;

In 2018, for all the Italian MV network managed by E-Distribuzione, the distribution of the measured voltage sags according to the method M1 and M2 is reported in Table 2.1.

Table 2.1 Percentage distribution of the origin of the voltage sags measured in Italy in 2018

Method	***MV [%]***	***HV [%]***
M1	64.39	35.61
M2	57.69	42.31

The total number of voltage sags measured in Italy in 2018 was equal to 403531 and the percentage values in Table 2.1, 2.2, 2.3, 2.4, 2.5 and 2.6 are calculated according to the total number of sags. M1 method assigned to the MV network 259831 voltage sags, instead M2 assigned to the MV network 232816 voltage sags.

Table 2.2 and 2.3 reported the percentage distribution of the voltage sags assigned by M1 and M2 to the MV network according to EN 50160. Table 2.4 and 2.5 reported the percentage distribution of the voltage sags assigned by M1 and M2 to the HV network according to EN 50160. From the results reported in Table 2.2 and 2.3, the most critical value is inside cell C1 of the voltage sags assigned to the MV network (duration from 10 ms to 200 ms and residual voltage from 40% to 70% of the nominal value).

Table 2.2 Percentage distribution of the MV voltage sags measured in Italy in 2018 assigned by M1

	Duration [ms]						
Residual Voltage [%]	10÷200	200÷500	500÷1000	1000÷5000	5000÷60000	60000÷180000	180000
90÷80	20.12	4.05	0.80	0.39	0.17	0.02	0.01
80÷70	9.07	2.92	0.29	0.09	0.08	0.00	0.01
70÷40	15.21	4.23	0.25	0.09	0.17	0.01	0.02
40÷5	4.71	1.40	0.10	0.02	0.07	0.01	0.01
5÷0	0.01	0.00	0.00	0.00	0.00	0.00	0.00

Table 2.3 Percentage distribution of the MV voltage sags measured in Italy in 2018 assigned by M2

	Duration [ms]						
Residual Voltage [%]	10÷200	200÷500	500÷1000	1000÷5000	5000÷60000	60000÷180000	180000
90÷80	15.00	3.97	0.79	0.40	0.17	0.02	0.02
80÷70	7.98	2.98	0.27	0.09	0.07	0.00	0.01
70÷40	14.88	4.31	0.23	0.09	0.17	0.01	0.02
40÷5	4.59	1.40	0.10	0.02	0.07	0.01	0.01
5÷0	0.01	0.00	0.00	0.00	0.00	0.00	0.00

Table 2.4 Percentage distribution of the HV voltage sags measured in Italy in 2018 assigned by M1

	Duration [ms]						
Residual Voltage [%]	10÷200	200÷500	500÷1000	1000÷5000	5000÷60000	60000÷180000	180000
90÷80	18.85	1.29	0.19	0.07	0.01	0.00	0.01
80÷70	6.81	0.69	0.11	0.04	0.00	0.00	0.00
70÷40	5.15	0.82	0.13	0.03	0.00	0.00	0.00
40÷5	1.11	0.28	0.07	0.01	0.00	0.00	0.00
5÷0	0.00	0.00	0.00	0.00	0.00	0.00	0.00

Table 2.5 Percentage distribution of the HV voltage sags measured in Italy in 2018 assigned by M2

	Duration [ms]						
Residual Voltage[%]	10÷200	200÷500	500÷1000	1000÷5000	5000÷60000	60000÷180000	180000
90÷80	23.98	1.37	0.20	0.06	0.01	0.00	0.00
80÷70	7.90	0.63	0.12	0.04	0.00	0.00	0.00
70÷40	5.48	0.74	0.15	0.04	0.00	0.00	0.00
40÷5	1.23	0.29	0.07	0.01	0.00	0.00	0.00
5÷0	0.01	0.00	0.00	0.00	0.00	0.00	0.00

Figure 2.10 reported the monthly distribution of the voltage sags measured in Italy and assigned to the MV and HV network by M1. It is possible to highlight how the months with a higher percentage distribution of voltage sags are August and October 2018. According to Table 2.1, on 64% of the voltage sags are assigned to the MV network, 20% of the voltage sags were recorded in the months of June, July and August 2018. This could be due to summer thunderstorms but also to the failure of the joints of underground MV cables due to high temperatures and high load.

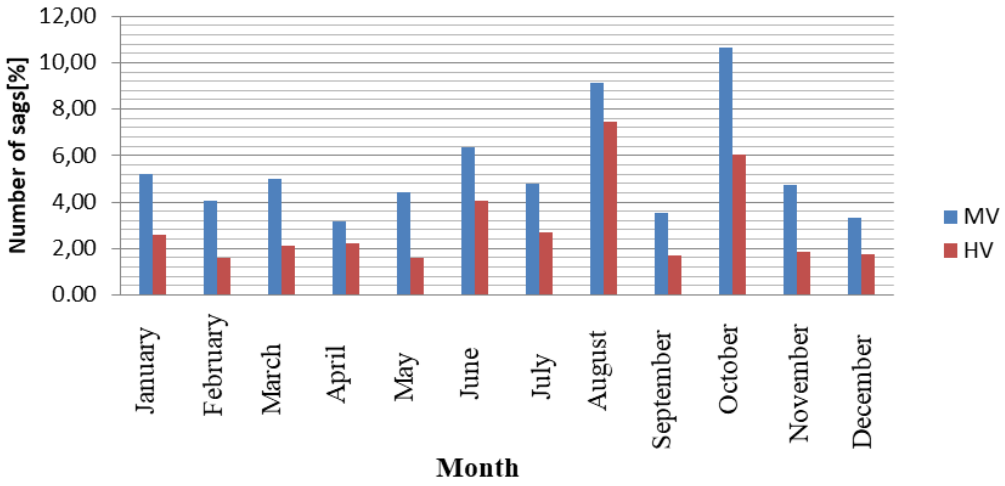

Figure 2.10 Monthly distribution of measured voltage sags – M1

Correlations studies have been carried out in accordance with the available data of MV protection systems and the MV busbar switch state. The data are from 01-01-2018 to 30-06-2018, and in that period the total number of voltage sags measured was equal to 171063.

The study was aimed to ascertain if the voltage sags originated in the MV network by one of the used criteria were correlated with the intervention of the protection system installed on the same network. In the absence of the correlation, two main causes are reasonable for the voltage sags wrongly attributed to the MV:

a) the fault that originated the voltage sag was inside the customer plant fed by the MV network

b) the voltage sag was originated by exogenous events such as wind, fires or thunderstorms.

Regarding protections data, two types of time are available, i.e. the so called time of system and the time of the apparatus. The time of system is the time of the intervention of protection as measured by the data acquisition system; the time of apparatus is the time of the intervention as directly derived from the protection system. The correlation was analysed only for the time of apparatus as suggested by the DSO. In the Italian distribution system, the total number of the recorded interventions of the protection systems was 225686, after the filtering actions it was 199,883 for the time of apparatus. The information regarding the time of apparatus is not available for all the data. Data without this information were discarded by the filtering action. The correlation between every voltage sag and the protection intervention was in the domain, named local, of the protection systems installed on the same MV busbar in which the voltage sag was recorded.

The distribution of the origin of the measured voltage sags according with the method M1 and M2 is reported in Table 2.6. M1 method assigned to the MV network 113785 voltage sags, instead M2 assigned to the MV network 104807 voltage sags. The values of the percentages are expressed in terms of the total number of the voltage sags.

Table 2.6 Percentage distribution of the origin of the voltage sags measured in Italy from 01-01-2018 to 30-06-2018

Method	MV [%]	HV [%]
M1	66.51	33.48
M2	61.27	38.83

Table 2.7 shows the percentage distribution of the voltage sags assigned to MV in Italy correlated with only one intervention of the protection system, considering the time of apparatus in the local domain. The values of the percentages are expressed in terms of the total number of the voltage sags assigned to the MV network by the different criteria (113785 voltage sags assigned to MV network by M1 and 104807 voltage sags assigned to MV network by M2).

Table 2.7 Percentage distribution of the MV voltage sags correlated with only one intervention of the protection system, considering the time of apparatus in the local domain [%]

Method	MV sags correlated [%]
M1	31.30%
M2	34.32%

According to the results in Table 2.7, only 31.30% and 34.32% of the voltage sags assigned to the MV network by M1 and M2 respectively, were correlated with the

intervention of the protection system. Data were deeply analysed and the correlation between the voltage sag and the protection system was verified in a time window from 0 s to 1 m delay. The results were reported in Table 2.8.

Table. 2.8 – Percentage distribution of the voltage sags assigned to the MV in Italy - year 2018 correlated with only one intervention of the protection system, considering the time of apparatus in the local domain [%]

	Range [s]										
Criterion	**0-0.1**	**0.1-0.2**	**0.2-0.5**	**0.5-1**	**1-2**	**2-3**	**3-4**	**4-5**	**5-10**	**10-30**	**30-60**
M1	3.79	5.27	7.54	1.24	0.92	0.24	0.15	0.07	0.26	0.69	0.94
M2	3.89	5.26	7.57	1.27	0.94	0.24	0.15	0.08	0.27	0.71	0.96

2.3 Detailed Analyses on the Origin of the Sags Measured in Italy

The results of Table 2.7 and Table 2.8 suggested performing further analyses for detecting false attributions of the origin to the MV network, and evaluating intermittent voltage sags caused by:

i) the automation of the protection systems;
ii) atmospherically phenomena.

The analyses studied:

- the correlation of the origin with MV protection systems;
- the correlation of the origin with the state of the MV busbar switch;
- the correlation of the origin with the protections of the MV lines equipped with an automatic reclosing device.

- Correlation analysis of the origin with MV protection

The number of voltage sags assigned to the MV network by M1 and not correlated with the intervention of one protection system was equal to 78142 voltage sags. The number of voltage sags assigned to the MV network by M2 and not correlated with the intervention of one protection system was equal to 68812 voltage sags.

The values of the percentages in Table 2.9 are expressed in terms of the total number of the voltage sags assigned to the MV network by the different criteria (113785 voltage sags assigned to MV network by M1 and 104807 voltage sags assigned to MV network by M2).

Table 2.9 Percentage distribution of the MV voltage sags not correlated with only one intervention of the protection system, considering the time of apparatus in the local domain [%]

Method	MV sags not correlated [%]
M1	68.70%
M2	65.68%

The correlated and not correlated voltage sags were analysed according to EN 50160 and the results were reported respectively in Table 2.12, Table 2.13 and Table 2.10, Table 2.11.

The percentage values are computed according to the total number of MV voltage sags measured in Italy from 01-01-2018 to 30-06-2018 (113785 voltage sags assigned to MV network by M1 and 104807 voltage sags assigned to MV network by M2).

A high percentage of not correlated voltage sags belong to cells A1, A2, B1 and B2. However, this high percentage of not correlated events with the intervention of one protection system could not cause major problems in terms of future economic regulations because these events fall into immunity classes 2 and 3. Instead, the high percentage of not correlated voltage sags belonging to class C1 requires particular attention.

According to the results reported in Table 2.12 and 2.13, a high percentage of MV voltage sags correlated with the intervention of the protection system present these characteristics:

- residual voltage between 70-40% of the nominal value;
- duration in the range 10 - 200 ms.

Table 2.10 Percentage distribution of the MV voltage sags measured in Italy in 2018 assigned by M1 not correlated with only one intervention of the protection system, considering the time of apparatus in the local domain [%]

	Duration [ms]						
Residual Voltage [%]	10÷200	200÷500	500÷1000	1000÷5000	5000÷60000	60000÷180000	180000
90÷80	24.95	3.25	1.12	0.34	0.20	0.03	0.04
80÷70	10.21	2.11	0.47	0.11	0.08	0.01	0.02
70÷40	16.60	3.01	0.27	0.12	0.08	0.01	0.02
40÷5	4.19	1.06	0.09	0.02	0.02	0.01	0.02
5÷0	0.01	0.00	0.00	0.00	0.00	0.00	0.00

Table 2.11 Percentage distribution of the MV voltage sags measured in Italy in 2018 assigned by M2 not correlated with only one intervention of the protection system, considering the time of apparatus in the local domain [%]

	Duration [ms]						
Residual Voltage [%]	10÷200	200÷500	500÷1000	1000÷5000	5000÷60000	60000÷180000	180000
90÷80	20.40	3.28	1.21	0.39	0.21	0.04	0.05
80÷70	9.75	2.28	0.49	0.12	0.09	0.01	0.02
70÷40	17.65	3.31	0.25	0.12	0.09	0.01	0.03
40÷5	4.38	1.18	0.10	0.03	0.03	0.02	0.02
5÷0	0.01	0.00	0.00	0.00	0.00	0.00	0.00

Table 2.12 Percentage distribution of the MV voltage sags measured in Italy in 2018 assigned by M1 correlated with only one intervention of the protection system, considering the time of apparatus in the local domain [%]

	Duration [ms]						
Residual Voltage [%]	10÷200	200÷500	500÷1000	1000÷5000	5000÷60000	60000÷180000	180000
90÷80	3.80	2.87	0.29	0.37	0.01	0.00	0.00
80÷70	3.07	2.27	0.06	0.07	0.01	0.00	0.00
70÷40	9.03	4.03	0.15	0.05	0.02	0.00	0.00
40÷5	3.65	1.42	0.09	0.02	0.01	0.00	0.00
5÷0	0.00	0.00	0.00	0.00	0.00	0.00	0.00

Table 2.13 Percentage distribution of the MV voltage sags measured in Italy in 2018 assigned by M2 correlated with only one intervention of the protection system, considering the time of apparatus in the local domain [%]

	Duration [ms]						
Residual Voltage [%]	10÷200	200÷500	500÷1000	1000÷5000	5000÷60000	60000÷180000	180000
90÷80	4.20	3.15	0.32	0.41	0.01	0.00	0.00
80÷70	3.40	2.53	0.07	0.08	0.01	0.00	0.00
70÷40	9.96	4.37	0.16	0.06	0.02	0.00	0.00
40÷5	3.89	1.53	0.11	0.02	0.02	0.00	0.00
5÷0	0.00	0.00	0.00	0.00	0.00	0.00	0.00

- Correlation analysis of the origin with the state of the MV busbar switch

The analyses were conducted on the same data set considering the state of the MV busbar switch in Figure 2.11.

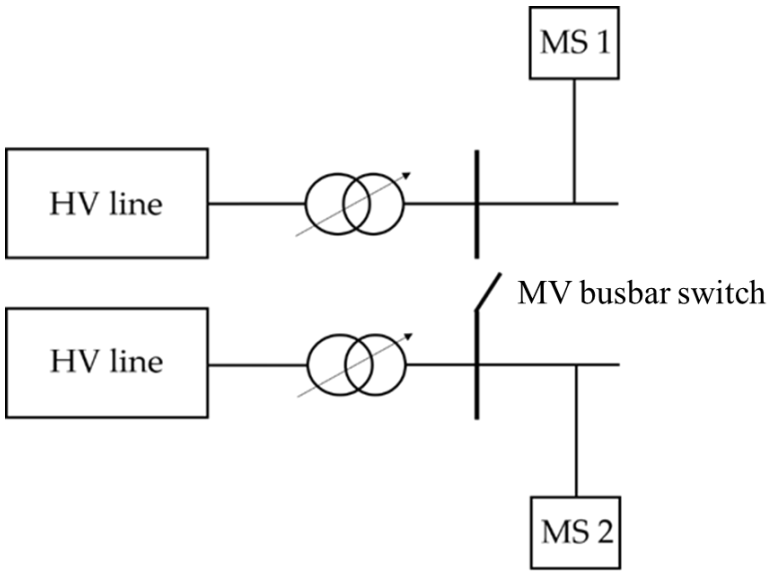

Figure 2.11 Simplified scheme of a HV/MV station: MV busbar switch in open position

The goal of the analysis was to detect the pairs of the voltage sags assigned to the MV network which occurred at any HV/MV station in the same date, the same time and with equal residual voltage, in the respect of the accuracy of the installed instruments. Considering the accuracy of the instruments, two voltage sags are considered identical if the difference between the residual voltages is less than 3% and the difference between the times of occurrence is less than 60 ms. Once identified these identical voltage sags, the position of the MV busbar switch was verified.

In open position, two identical faults in the MV network could cause identical voltage sags. This is a very improbable condition in a real network If the MV busbar switch is in the open position and two identical voltage sags assigned to the MV system are recorded, it is possible that:

- the criterion applied to establish the origin failed;
- the recorded state of the MV busbar switch was incorrect.

In close position, a fault in the MV network could cause identical voltage sags.

The analysis was performed on the voltage sags in the Italian network whose origin was assigned by each of the criteria M1 and M2. The analysis of the records of

the state of the MV busbar switch is extended to one year before the date of occurrence of the identical voltage sags, if possible, in function of the availability of the recorded data. The available data start from 01-01-2017 to 30-06-2018.

Tables 2.14 and 2.15 show the results of the correlation between the state of the MV busbar switch and the identical voltage sags assigned to the MV and to HV by the different criteria registered in the considered system. The table shows both the absolute number and the percentage value of the identical voltage sags correlated to the state of the MV busbar switch; the open state corresponds to the code S1O; the close state to the code S1C.

Table 2.14 - Identical voltage sags originating in the MV network correlated with the actual state of the MV busbar switch – Italy – Method M1 and M2.

Method	Total number of voltage sags	Percentage S1O [%]	Percentage S1C [%]	Number of identical voltage sags correlated to the S1C	Number of identical voltage sags correlated to the S1O
M1	171063	0.08	0.11	138	204
M2	171063	2.12	0.70	3636	1204

The obtained results show that the identical voltage sags originated in the MV and correlated with the S1O are very few in the considered systems and for the considered year.

Table 2.15 - Identical voltage sags originating in the HV network correlated with the actual state of the MV busbar switch – Italy – Criteria M1 and M2.

Criterion	Total number of voltage sags	Percentage S1O [%]	Percentage S1C [%]	Number of identical voltage sags correlated to the S1C	Number of identical voltage sags correlated to the S1O
M1	171063	9.69	19.68	16571	33665
M2	171063	7.64	19.20	13073	32665

In the presence of an intervention of the protection system installed at the MV busbars, the attribution of the origin to the HV network was wrong if identical voltage sags were correlated with the close state of the MV busbar switch.

In any case whether the identical pairs of sags were assigned to the MV or HV network correlated with the closed state of the MV busbar switch, it is not possible to accurately determine the origin of the voltage sags. It is possible to determine with absolute certainty the origin of these events only if both the intervention of the MV and HV protections are available.

- Correlation analysis of the origin with protections of the MV lines equipped with an automatic reclosing device.

In cooperation with the DSO, it was possible to consider the characteristic time intervals of the protections of the MV lines equipped with an automatic reclosing device, known as DRA (Dispositivo di Richiusura Automatica, in Italian, or Automatic Reclosure Device, in English). Figure 2.12 shows that the protection system acts with four consecutive snaps and three reclosures after a fault: a first rapid reclosure (1RR in Figure 2.12) and two successive slow reclosures (1RS and 2RS in Figure 2.12).

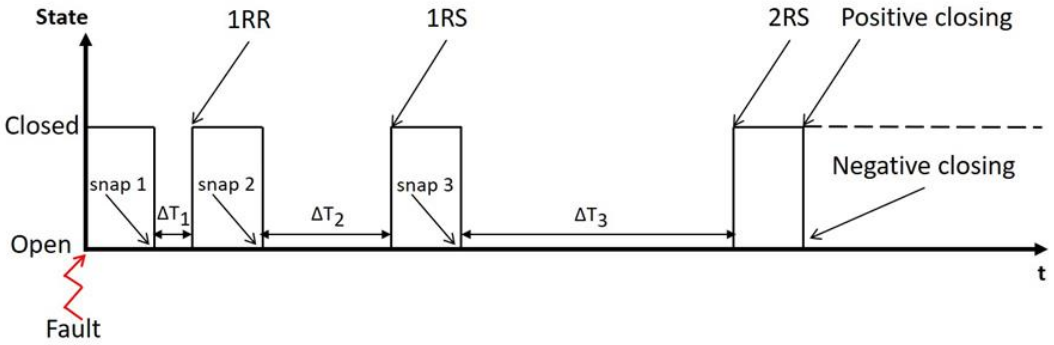

Figure 2.12 Automatic reclosing cycle of a DRA (Dispositivo di Richiusura Automatica, in Italian, or Automatic Reclosure Device, in English).

The typical delays of each reclosure after the preceding opening (*ΔT1*, *ΔT2* and *ΔT3* in Figure 2.12) are in the following time ranges:

0.4 s ≤ *ΔT1* ≤ 3 s;

30 s ≤ *ΔT2* ≤ 90 s;

30 s ≤ *ΔT3* ≤ 120 s.

The voltage sags correlated with the interventions of the protection system, considering the time of apparatus in the local domain [%] and the time ranges reported in Figure 2.12, were analysed according to EN 50160 and the results were reported in Table 2.16 and 2.17.

The percentage values are calculated according to the total number of MV voltage sags measured in Italy from 01-01-2018 to 30-06-2018(113785 voltage sags assigned to MV network by M1 and 104807 voltage sags assigned to MV network by M2).

11.37% of the voltage sags assigned to the MV network by M1 were caused by automatic reclosing devices, instead 12.38% of the voltage sags assigned to the MV network by M2 were caused by automatic reclosing devices. Summing up, about 30% of the MV voltage sags assigned by M1 and M2 correlated with protection systems, were caused by automatic reclosing devices and the highest percentage belongs to C1 class.

Table 2.16 Percentage distribution of the MV voltage sags measured in Italy in 2018 assigned by M1 correlated with the interventions of the protection system, considering the time of apparatus in the local domain [%] and the time ranges reported in Figure 2.10

	Duration [ms]						
Residual Voltage [%]	10÷200	200÷500	500÷1000	1000÷5000	5000÷60000	60000÷180000	180000
90÷80	1.40	1.06	0.10	0.14	0.00	0.00	0.00
80÷70	1.07	0.83	0.01	0.01	0.00	0.00	0.00
70÷40	3.40	1.48	0.06	0.01	0.00	0.00	0.00
40÷5	1.29	0.46	0.03	0.01	0.00	0.00	0.00
5÷0	0.00	0.00	0.00	0.00	0.00	0.00	0.00

Table 2.17 Percentage distribution of the MV voltage sags measured in Italy in 2018 assigned by M2 correlated with the interventions of the protection system, considering the time of apparatus in the local domain [%] and the time ranges reported in Figure 2.10

	Duration [ms]						
Residual Voltage [%]	10÷200	200÷500	500÷1000	1000÷5000	5000÷60000	60000÷180000	180000
90÷80	1.53	1.16	0.11	0.15	0.00	0.00	0.00
80÷70	1.18	0.93	0.02	0.02	0.00	0.00	0.00
70÷40	3.70	1.61	0.06	0.01	0.00	0.00	0.00
40÷5	1.37	0.49	0.03	0.01	0.00	0.00	0.00
5÷0	0.00	0.00	0.00	0.00	0.00	0.00	0.00

2.3.1 Accounting for the Presence of GD

The spread of GD on a large scale has radically changed the flow of energy that became bidirectional. In the presence of GD, the HV/MV transformers equipped with OLTCs were used to compensate the voltage increase at the end of the MV line (negative voltage drop) caused by the current flowing through the line from to the DG units; furthermore the OLTCs were used to counteract voltage fluctuations due to the variation of the power produced by the GD units caused, for example, by the variation of irradiation and temperature of the panels in the case of photovoltaic systems. This operational condition can adversely affect the results of the methods for the discrimination of the origin of voltage sags since the different relationship between the two transformers can determine different values of the residual voltages measured on each MV busbar of the HV/MV substation. Another aspect that can negatively impact the methods for ascertaining the origin of the voltage sags concerns the possible action of the GD unit in sustaining the voltage during the voltage sag caused by a short circuit.

The action of the GD depends on:

1. type of connection of the GD to the network (direct or through a power converter);
2. the type of control adopted.

Considering the GD units connected to the distribution network via power converters, in the presence of a voltage sag registered on the MV busbar, the GD may have a sufficient low voltage crossing capability to stay connected to the grid [47-49]. Figure 2.13 presents the LVRT and Over voltage ride through characteristics for static generators provided by the CEI 0-16 standard [50].

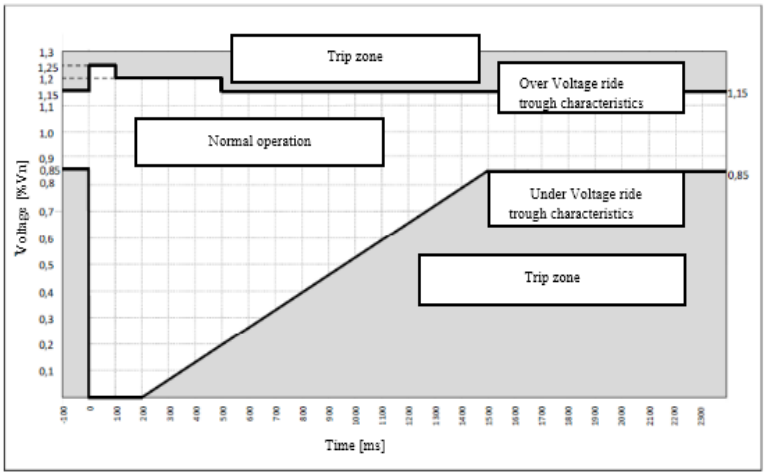

Figure 2.13 Low voltage ride through and Over voltage ride through characteristics for static generators.

The generators of a generation park must not disconnect from the grid in the area beyond and along the points of the characteristic (*V*-*t*) indicated in Figure 2.13, where *V* is the phase-to-phase voltage at the common connection point. These values

are expressed in percentage of MV rated voltage (linked). In the minimum conditions of voltage and time (ie below the LVRT characteristic) is allowed temporarily interrupt the active and reactive power supplied. In the area below (in grey) the generators of a generation park can disconnect from the network. The behaviour indicated by the curve in figure 2.13 must be guaranteed against lowering of one or more voltages; i.e it can be activated both for asymmetrical faults when one of the three voltage measurements exceeds the voltage sag in depth and duration admitted.

In compliance with the maximum limit of the output current, the GD unit can sustain the voltage according to the control on the power converter [49]. If the control also acts to regulate the reactive power during the voltage sag, the presence of GD can affect the results of the different methods for ascertaining the origin of voltage sags presented in the previous sections of this thesis. The capability of both methods M1 and M2, of attributing the exact origin of voltage sags, was compared by means of the time domain simulations of the HV/MV system, reported in Figure 2.14. The time domain simulations were performed by means of tool Simscape Electrical of Matlab©®.

As Figure 2.14 shows, the system is composed of 9 HV/MV substations and two customer substations (at #9 and #10); in Figure 2.14 the HV/MV substations are indicated as vertical black bars with the corresponding number on the top of it. The system is a part of a real network in service in Italy.

The electrical parameters of the main components of the system, in Figure 2.14, are in Table 2.18. The main electrical characteristics of the transformers and of the lines are reported in Table 2.19.

All the HV/MV substations were connected to the busbars of the system in Figure 2.14 via HV/MV transformers, which were equipped with OLTC.

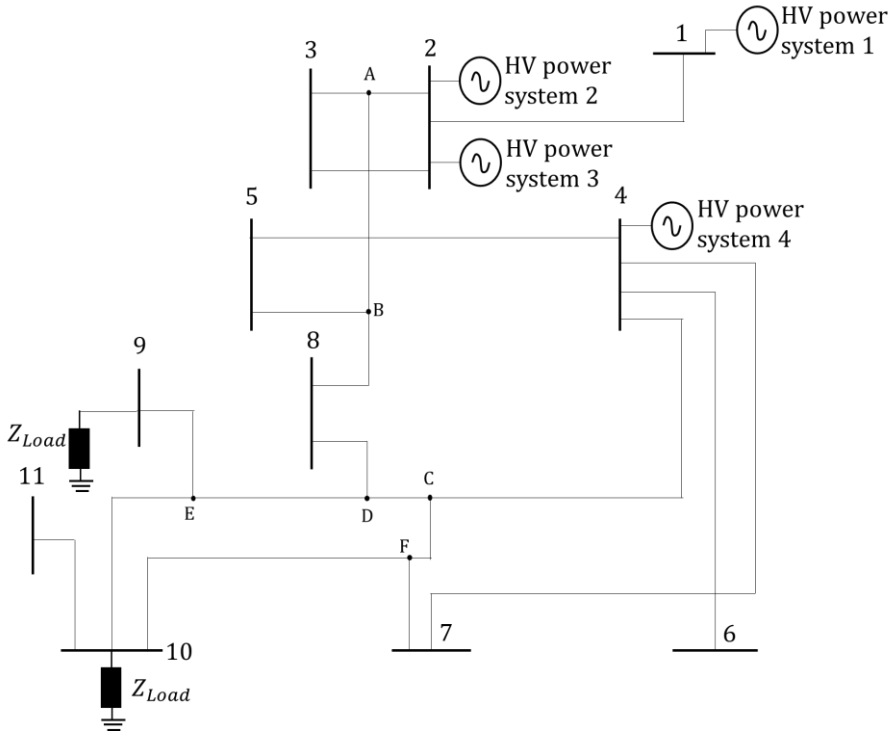

Figure 2.14 Scheme of the studied system.

Table 2.18 Parameters of the equivalent systems

#	Component	Details
1	Equivalent HV system1	6679MVA, 220kV, 50Hz
2	Equivalent HV system2	6993MVA, 220kV, 50Hz
3	Equivalent HV system3	2462MVA, 150kV, 50Hz
4	Equivalent HV system4	2649MVA, 150kV, 50Hz

The data of the equivalent HV systems are derived from the website of Terna.

Table 2.19 Main characteristics of the HV lines and HV/MV transformers of the system in Figure 2

#	Component	Details
1	HV/MV Transformer	25MVA, 60kV-20kV, 50Hz
2	HV/MV Transformer	63MVA, 220kV-60kV, 50Hz
3	HV/MV Transformer	63MVA, 150-60kV, 50Hz
4	HV Line from #1 to #2	10.2 km
5	HV Line from #2 to A	0.35 km
6	HV Line from #3 to A	1.19 km
7	HV Line from #2 to #3	1.69 km
8	HV Line from A to B	2.42 km
9	HV Line from #4 to #5	7.1 km
10	HV Line from B to #5	0.55 km
11	HV Line from B to #8	5 km
12	HV Line from #8 to D	3 km
13	HV Line from D to C	0.75 km
14	HV Line from #4 to C	5.89 km
15	HV Line from C to F	9.23 km
16	HV Line from #7 to F	0.15 km
17	HV Line from #4 to #7	16.51 km
18	HV Line from #4 to #6	12 km
19	HV Line from D to E	2.8 km
20	HV Line from #10 to E	10.97 km
21	HV Line from #9 to E	2.33 km
22	HV Line from #10 to F	2.92 km
23	HV Line from #10 to #11	2 km

The characteristics of the HV lines are reported in Table 2.20.

Table 2.20 Characteristics of the HV lines

f	R_{line}	L_{line}	C_{line}	l
[Hz]	**[Ohm/km]**	**[H/km]**	**[F/km]**	**[km]**
50	0.133	0.0014	$9e^{-9}$	-

The schematic diagram of the HV/MV substation is shown in Figure 2.15. Two transformers composed it: the transformer RED (RE) and the transformer GREEN (GR). The MV busbars of the RE and GR transformer were separated by the MV busbar switch in the open position.

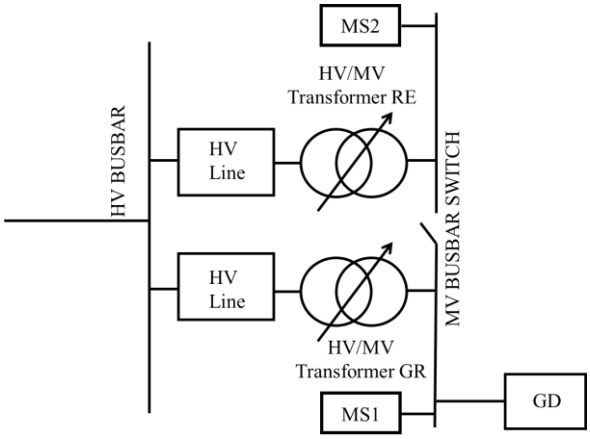

Figure 2.15 Schematics of a HV/MV substation

The DG units were photovoltaic systems (PV); they were modelled as reported in [47-49]. We assumed that the DG was able to provide, at the PCC (point of common connection) with the network, constant values of active and reactive powers in the normal operating conditions.

The methods M1 and M2 were used to identify the origin of the measured voltage sags in the case when a fault in the HV network occurred with the DG unit connected, and the ratio of the transformer equal to the nominal value.

For all the three previous cases, the short-circuit fault starts at 0.2 s and stops at 0.5 s. The voltage waveforms on the busbars are expressed through their RMS voltage values in p.u. Since it was impossible to show all the results, in the following we analysed and compared M1 and M2 applied to the voltage sags measured at the busbar 7. Both measurement devices MS1 and MS2 recorded voltage sags of different residual voltage as the fault position varied, as reported in Table VI. In this case, a PV system of active power equal to 6.3 MW was considered, assuming $cos\varphi$ = 0.9, constant irradiation and temperature, such as to guarantee constant the maximum output power from the PV panels.

Figure 2.16 shows the difference between the residual voltages, ΔV, measured at the two busbars, RE and GR, of the substation connected to the busbar #7 versus the value of the residual voltage at the GR busbar where the DG was connected. The obtained points were presented also with the interpolating curve.

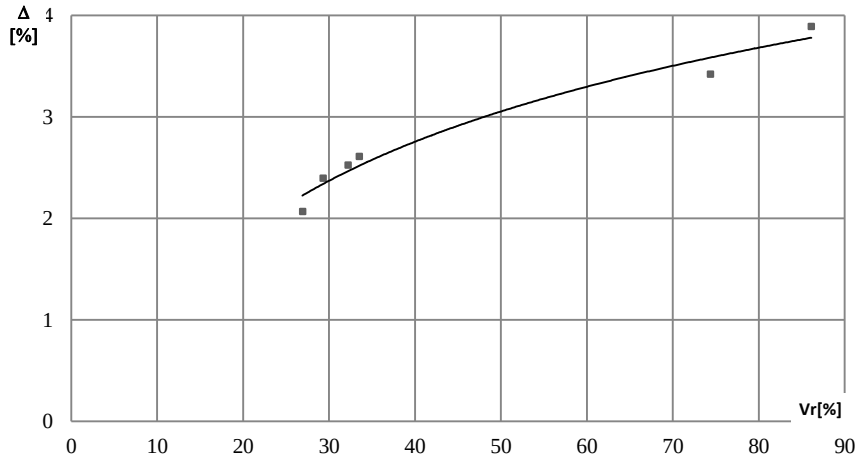

Figure 2.16 Difference between the residual voltages ΔV, measured at the two busbars, RE and GR, of the substation connected to #7 versus the value of the residual voltage, Vr, at the GR busbar

The ride through capability against low voltage of the PV units was considered following the standard [50].

For the short-circuits which did not cause the output current to go over the limits of protection of the coupling inverter, the PV delivered active and reactive powers to the PCC close to the reference values and, so doing, it sustained the voltage. For the short-circuits which, instead, caused the output current to go over the protection limit, the PV did not guarantee, at the PCC, the pre-assigned value of active and reactive powers; hence, the effect of sustaining the voltage was minor. Finally, for such short circuits, that caused the reduction of the voltage, at the terminals of the PV system, for a duration such that the PV was out of the normal operation zone, shown in Figure 13, the PV was disconnected.

Figure 2.17 shows the plots of the residual voltages of the sags recorded on both busbars RE and GR of substation 7; the voltage sags were caused by short-circuits at the HV windings of substation connected to the busbar #1.

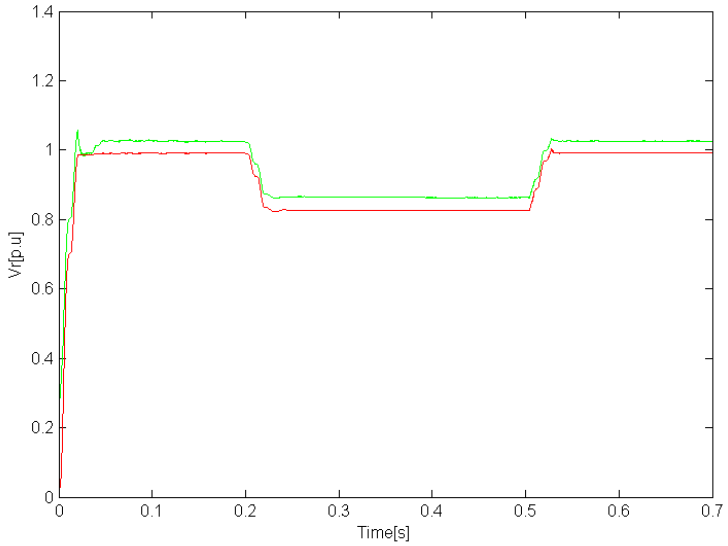

Figure 2.17 Residual voltage profiles of sags recorded on both #7RE and #7GR for fault position #1

Figure 2.18 reports the residual voltage profiles of sags recorded on both busbars RE and GR of substation 7 due to the short circuits at the HV windings of substation connected to the busbar #11.

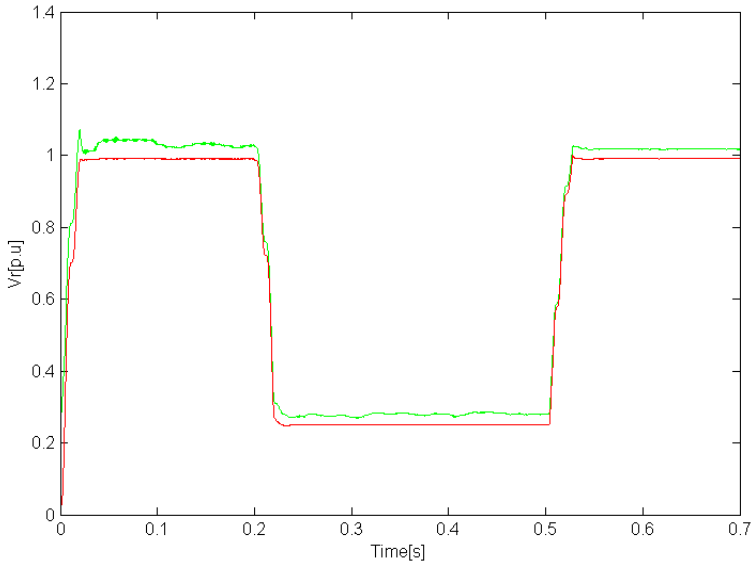

Figure 2.18 Residual voltage profiles of sags recorded on both #7RE and #7 GR for fault position #11

Figures 2.17 and 2.18 evidence the appreciable difference of the voltage on the two busbars (RE and GR) of the same substation in #7 due to the action of the PV

unit installed at the GR7. It is important to evidence that some fault positions (#4, #5, #8, and #10) caused the disconnection of the PV. These cases were obviously excluded in the analysis.

Table 2.22 shows the corresponding results of M1 and M2; it was evident that M1 failed in attributing the correct origin in the case of fault positions #1 and #6.

Table 2.21 Residual voltages measured at the MV busbars of the substation HV/MV #7 expressed as percentage of the nominal value

	1	**2**	**3**	**6**	**9**	**11**
#7RE	82.22	26.91	29.69	70.94	30.89	24.83
#7GR	86.11	29.31	32.22	74.36	33.50	26.90

Table 2.22 Results of M1 and M2

fault position #						
	1	**2**	**3**	**6**	**9**	**11**
Results of M1						
#7RE	MV	HV	HV	MV	HV	HV
#7GR	MV	HV	HV	MV	HV	HV
Results of M2						
#7RE	HV	HV	HV	HV	HV	HV
#7GR	HV	HV	HV	HV	HV	HV

In the presence of PV units, the accuracy of M2 appreciably improved the results of M1. This was primary due to the absence in M2 of the maximum limit on the difference of the residual voltages of the measured voltage sags. Moreover, M2 ascertained the common origin of the sags in the HV network by also analysing the voltage sags measured in other electrically close HV/MV substations.

2.3.2 Propagation of Sags Originated in the MV Network toward the HV Network

Figure 2.19 shows the scheme of a HV/MV substation assumed as reference for evaluating the voltage sags due to short circuits in the MV system (fault position, FP). The scheme comprises:

- the HV system supplying the HV/MV substation;
- two HV/MV transformers with OLTC identified in Figure 2.18 as HV/MV transformer RE and HV/MV transformer GR;
- two MV lines, each fed by one of the two HV/MV transformers;

- four points of reference for detecting the voltage sags (VB1, VB2, VB3 VB4) with the following correspondence:
  - VB1 for the detection of a voltage sag on the HV busbar on the primary windings of the HV/MV transformer RE;
  - VB2 for the detection of a voltage sag on the MV busbar on the secondary windings of the HV/MV transformer RE;
  - VB3 for the detection of a voltage sag on the HV busbar on the primary windings of the HV/MV transformer GR;
  - VB4 for the detection of a voltage sag on the MV busbar on the secondary windings of the HV/MV transformer GR.

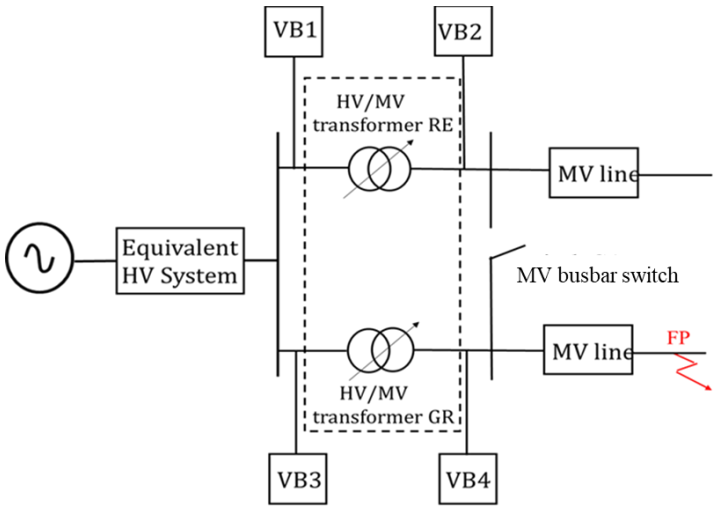

Figure 2.19 Scheme of the considered system

Assuming normal operating conditions before the faults, symmetrical short circuits were simulated with open state of the switch on the MV busbars. The system of Figure 2.19 can be modelled by means of direct sequence single-phase circuit, as shown in Figure 2.20.

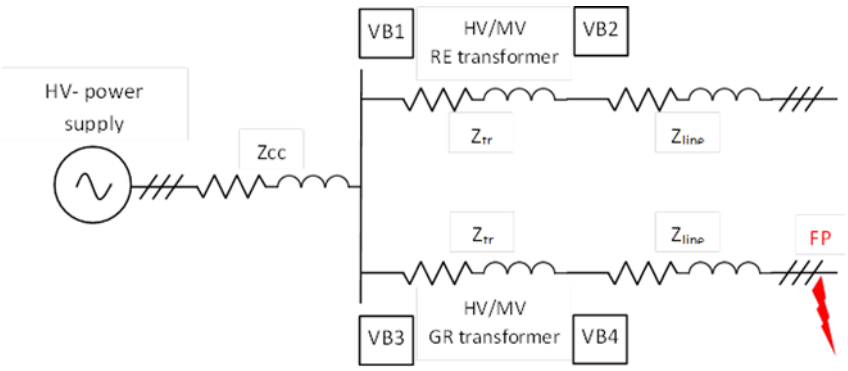

Figure 2.20 Single phase equivalent circuit of the considered system

According to the Method of Critical Distance, the voltage V_A, in any point A of the system during the fault occurred at any point *X* distant from *A* by the impedance ZL_X can be evaluated according to Figure 2.19 as:

$$V_A = V_{A1} + V_{A2} \tag{2.37}$$

where V_{A1} is the pre-fault voltage at the point A, and V_{A2} is the voltage at the point A due to the fault, given by:

$$V_{A1} = E_{pg} \tag{2.38}$$

$$V_{A2} = -\frac{E_{pg}}{Z_s + zL_x} * Z_s \tag{2.39}$$

with:

- *Zs*: sum of the equivalent short-circuit impedance of the HV system (*Zcc*) and the equivalent short-circuit impedance (*Ztr*) of the two transformers;
- $zL_x = R_{line} + jX_{line}$ [Ohm/km]: equivalent short circuit impedance of the MV line;
- $I_{cc} = -E_{pg}/(Z_s + zL_x)$: short circuit current injected in the node A calculated as following:
- E_{pg}: pre-fault voltage.

Considering the equations from (2.37) to (2.39), we evaluate the during fault voltages at the four points of interest VB1, VB2, VB3 and VB4. Neglecting the voltage drop on the impedance *Zcc*, according to Figure 2.20, we obtain:

$$\mathrm{VB1} = \mathrm{VB3} = \frac{E_{pg}}{Zcc + Z_{\mathrm{tr}} + zL_x} * (Z_{\mathrm{tr}} + zL_x) \tag{2.40}$$

$$\mathrm{VB2}\,[p.u] = \mathrm{VB1} - \frac{E_{pg}}{Zcc + Z_{\mathrm{tr}} + zL_x} * \frac{Zcc}{Zcc + Z_{\mathrm{tr}}} * Z_{\mathrm{tr}} \tag{2.41}$$

$$\mathrm{VB4} = \frac{VB1}{Zcc + Z_{\mathrm{tr}} + zL_x} * zL_x \tag{2.42}$$

The equations from (2.40) to (2.42) allows computing the during fault voltage in the points of interest for different values of short circuit power of the HV equivalent system (varying Zcc), and for different distance of the fault (varying zLX).

Several cases were simulated varying the short circuit power of the HV system and the distance of the fault from the point of interest (MV busbar of the transformer GR or VB4).

The data of each component are listed below. The characteristics of the two transformers are reported in Table 2.23 and Table 2.24; those of the MV line are reported in Table 2.25.

Table 2.23 Characteristics of the transformer RE

V1 **[kV]**	***V2*** **[kV]**	***S*** **[MVA]**	***IO*** **[%]**	***Pfe*** **[%]**	***Vcc*** **[%]**	R_{tr1} **[p.u]**	R_{tr2} **[p.u]**
60	21.60	12	1	0.13	12.240	0.004	0.004

Table 2.24 Characteristics of the transformer GR

V_1 **[kV]**	V_2 **[kV]**	***S*** **[MVA]**	I_O **[%]**	P_{fe} **[%]**	V_{cc} **[%]**	R_{tr1} **[p.u]**	R_{tr2} **[p.u]**
60	21.60	12	1	0.14	12.140	0.004	0.004

Table 2.25 Characteristics of the MV Line

f **[Hz]**	R_{line} **[Ohm/km]**	L_{line} **[H/km]**	C_{line} **[F/km]**	***l*** **[km]**
50	0.117	0.0010	12.74e-9	Variable

The characteristics of the equivalent HV system are reported in Table 2.26, moreover the equivalent short-circuit impedance (Zcc) of the HV system has been calculated assuming $\frac{\mathrm{Xcc}}{\mathrm{Rcc}}$ equal to 10.

Table 2.26 Characteristics of the equivalent HV System

Vn **[kV]**	***Pcc*** **[MVA]**
60	1000

Figure 2.21 shows the voltage in p.u of VB1 and of VB3 (HV busbars of the primary of the transformers RE and GR) as a function of the distance of VB4 from the fault. The curves are parametrized according to the short circuit power of the equivalent HV system seen from the observation node which is always VB4.

For example, for a short circuit at the end of a MV line (30km) and for a short circuit power of the equivalent HV system equal to 1000 MVA, the voltage in p.u. measured is equal to 0.97 p.u. In this case there is no voltage sag in the HV system. For the same distance (30 Km), a lower short circuit power of the equivalent HV system seen from the points VB4 can register a voltage sag with a minimum residual voltage of 0.76 p.u. for Pcc = 100 MVA. For different distances, for example in the case of a short circuit on the MV line at 5 Km far from VB4, and for a short circuit power of the equivalent HV system equal to 600 MVA, the voltage in p.u. measured in VB1 and in VB3 is equal to 0.89 p.u. In this case there is a light voltage sag in the HV system.

In the case of a short circuit on the MV line at 3 Km far from VB4, and for a short circuit power of the equivalent HV system equal to 1000 MVA, the voltage in p.u measured in VB1 and in VB3 is equal to 0.93 p.u. In this case there is no voltage sag in the HV system.

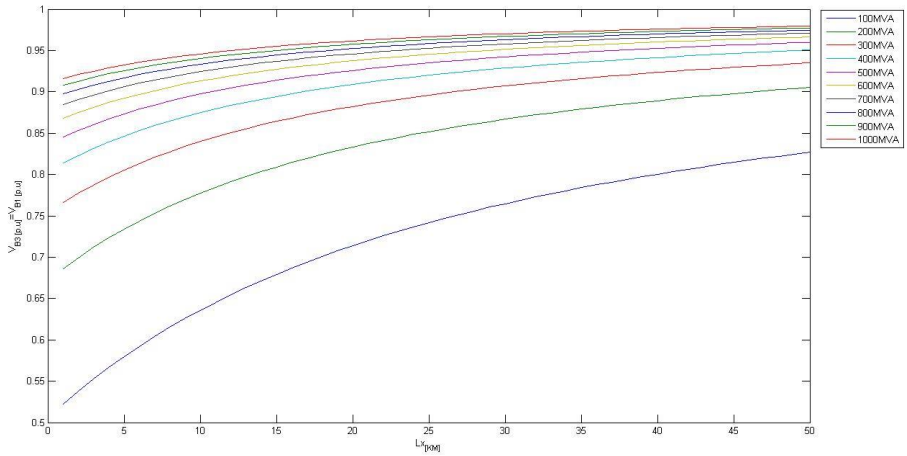

Figure 2.21 Plot of the voltage at the busbars VB1 and VB3 versus the distance of VB4 to the fault

Figure 2.22 shows the voltage in p.u of VB2 (MV busbar of the secondary of the transformer RE) as a function of the distance of VB4 to the fault. The curves are parametrized according to the short circuit power of the equivalent HV system seen from the observation node which is VB2. In particular for a short circuit at the end of a MV line (30km) and for a short circuit power of the equivalent HV system equal to 1000 MVA, the voltage is equal to 0.95 p.u. In this case, no voltage sag was measured on the other MV busbars of transformer RE. For the same distance (30 Km), a lower short circuit power of the equivalent HV system seen from the points VB2 can experience a voltage sag with a minimum residual voltage of 0.71 p.u. for Pcc = 100 MVA.

For different distances, for example in the case of a short circuit on the MV line at 5 Km far from VB4, and for a short circuit power of the equivalent HV system equal to 600 MVA, the voltage in p.u. measured in VB2 is equal to 0.87 p.u. In this case there is a light voltage sag in the HV system. In the case of a short circuit on the MV line at 3 Km far from VB4, and for a short circuit power of the equivalent HV system equal to 1000 MVA, the voltage in p.u measured in VB2 is equal to 0.91 p.u.

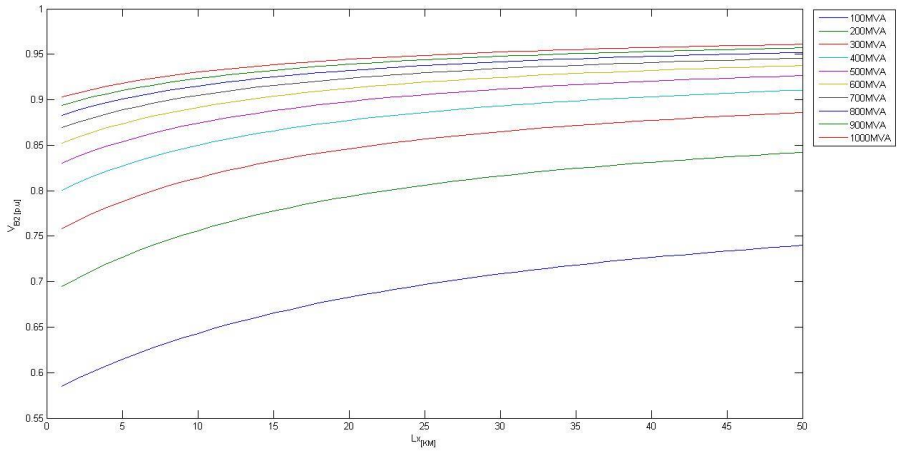

Figure 2.22 Plot of the voltage at the busbar VB2 versus the distance of VB4 to the fault

Figure 2.23 shows the voltage of VB4 (MV busbar of the secondary of the transformer GR) connected to the MV line where the fault occurred as a function of the distance from the fault. The curves are parametrized according to the short circuit power of the equivalent HV system. For a short circuit at the end of a MV line (30 km) and for a short circuit power of the equivalent HV system equal to 1000 MVA, the voltage in p.u measured is equal to 0.66 p.u. For the same distance (30 Km), a

lower short circuit power of the equivalent HV system, VB4 can experience a voltage sag with a minimum residual voltage of 0.44 p.u. for Pcc= 100 MVA

For different distances, for example in the case of a short circuit on the MV line at 5 Km far from VB4, and for a short circuit power of the equivalent HV system equal to 600 MVA, the voltage in p.u measured in VB4 is equal to 0.23 p.u. In this case there is a deep voltage sag in the HV system. In the case of a short circuit on the MV line at 3 Km far from VB4, and for a short circuit power of the equivalent HV system equal to 1000 MVA, the voltage in p.u. measured in VB4 is equal to 0.16 p.u.

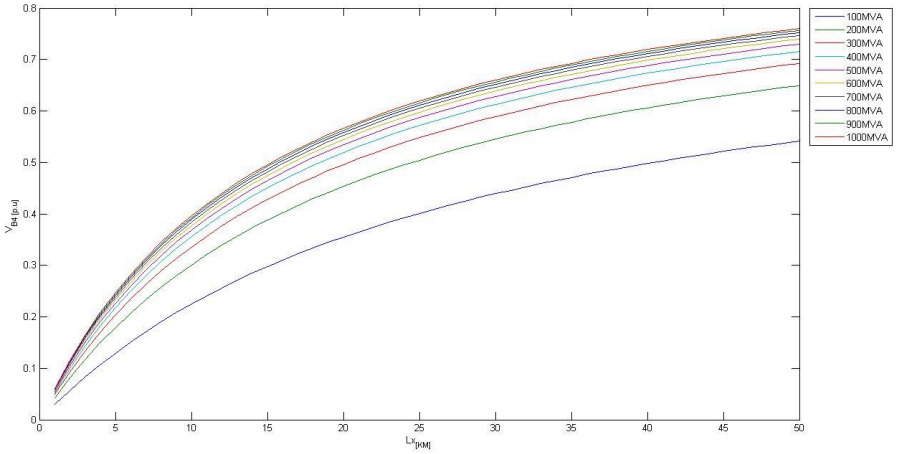

Figure 2.23 Plot of the voltage of VB4 versus the distance of VB4 to the fault

Assuming that:

- the short circuits are symmetrical;
- the MV busbar switch is closed,

VB2 is equal to VB4 and:

$$Z_{\text{tr\_p}} = \frac{Z_{\text{tr\_RE}} * Z_{\text{tr}_{\text{GR}}}}{Z_{\text{tr\_RE}} + Z_{\text{tr}_{\text{GR}}}} \tag{2.46}$$

Considering the previous equations from (2.36) to (2.38), we obtain the following equations for evaluating the during fault voltages (in p.u.) at the four points of interest VB1, VB2, VB3 and VB4. Neglecting the voltage drop on the impedance *Zcc*, according to Figure 2.19, we obtain:

$$\mathrm{VB1} = \mathrm{VB3} = \frac{E_{pg}}{Zcc + Z_{\mathrm{tr}} + zL_x} * (Z_{\mathrm{tr}} + zL_x) \tag{2.47}$$

$$\mathrm{VB2} = \mathrm{VB4} = \frac{\mathrm{VB1} = \mathrm{VB3}}{Zcc + Z_{\mathrm{tr}} + zL_x} * zL_x \tag{2.48}$$

Figure 2.24 shows the voltage in p.u of VB1 and of VB3 (HV busbars of the primary of the transformers RE and GR) as a function of the distance of VB4 from the fault. The curves are parametrized according to the short circuit power of the equivalent HV system seen from the observation node which is always VB4. For example, for a short circuit at the end of a MV line (30km) and for a short circuit power of the equivalent HV system equal to 1000 MVA, the voltage in p.u measured is equal to 0.96 p.u. In this case there is no voltage sag in the HV system. For the same distance (30 Km), a lower short circuit power of the equivalent HV system seen from the points VB4 can register a voltage sag with a minimum residual voltage of 0.73 p.u. for Pcc = 100 MVA.

For different distances, for example in the case of a short circuit on the MV line at 5 Km far from VB4, and for a short circuit power of the equivalent HV system equal to 600 MVA, the voltage in p.u measured in VB1 and in VB3 is equal to 0.84 p.u. In this case there is a light voltage sag in the HV system. In the case of a short circuit on the MV line at 3 Km far from VB4, and for a short circuit power of the equivalent HV system equal to 1000 MVA, the voltage in p.u measured in VB1 and in VB3 is equal to 0.88 p.u. In this case a voltage sag originated in the MV system was measured also in the HV network.

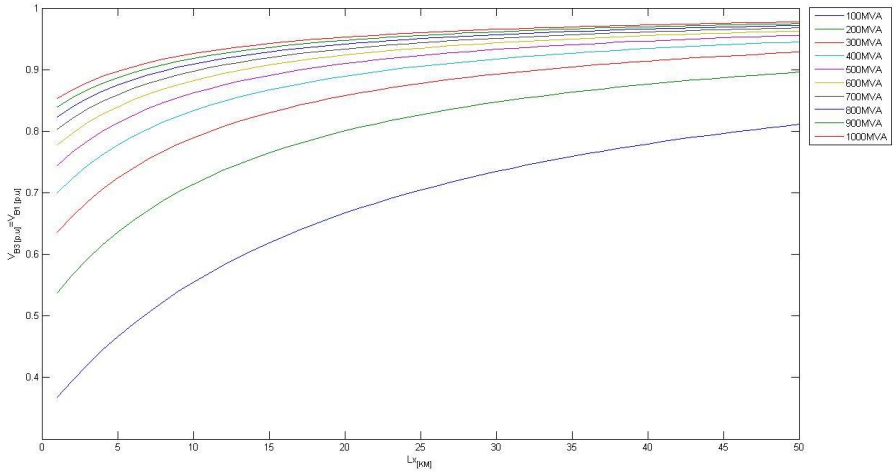

Figure 2.24 Plot of the voltage at the busbars VB1 and VB3 versus the distance of VB4 to the fault

Figure 2.25 shows the voltage in p.u of VB2 (MV busbar of the secondary of the transformer RE) and of VB4 (MV busbar of the secondary of the transformer GR) as a function of the distance of VB4 to the fault. The curves are parametrized according to the short circuit power of the equivalent HV system seen from the observation node which is VB2. For a short circuit at the end of a MV line (30 km) and for a short circuit power of the equivalent HV system equal to 1000 MVA, the voltage is equal to 0.77 p.u. In this case, two voltage sags were measured on the two MV busbars of transformer RE and GR. For the same distance (30 Km), a lower short circuit power of the equivalent HV system seen from the points VB2 and VB4 can experience two voltage sags with minimum residual voltages of 0.50 p.u. for Pcc= 100 MVA.

For different distances, for example in the case of a short circuit on the MV line at 5 Km far from VB4, and for a short circuit power of the equivalent HV system equal to 600 MVA, the voltage in p.u measured in VB2 and VB4 is equal to 0.35 p.u. In the case of a short circuit on the MV line at 3 Km far from VB4, and for a short circuit power of the equivalent HV system equal to 1000 MVA, the voltage in p.u measured in VB2 is equal to 0.27 p.u.

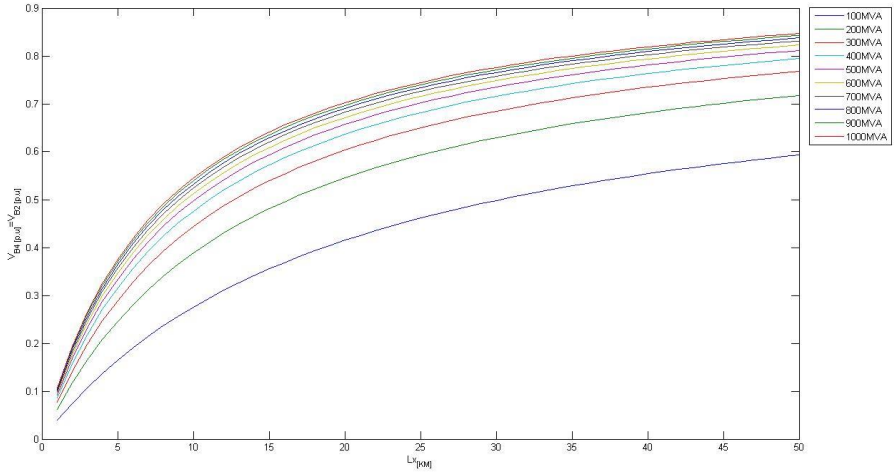

Figure 2.25 Plot of the voltage at the busbars VB2 and VB4 versus the distance of VB4 to the fault

Table 2.27 shows the relevant results obtained by simulations. For the cases B and C, when the MV busbar switch is open, two different voltage sags are measured on the MV busbars. Figure 2.26 reported the value of ΔV equal to $|VB4 - VB2|$, in p.u. as a function of the distance of VB4 to the fault. The value of ΔV is never less than 0.2 p.u for every value of P_{cc} and L_x when the MV busbar switch is open. For the cases B and C, a voltage sag originated in the MV network (the fault occurred along the MV line) was measured also in the HV network and on the other MV busbar of the same HV/MV substation. For the case A, when the MV busbar switch is open, a voltage sag originated in the MV network (the fault occurred along the MV line) was measured only on the MV busbar where the MV faulted line is connected.

For the cases B and C, when the MV busbar switch is close, two equal voltage sags are measured on the MV busbars. In this case, the value of ΔV is always equal to 0.0 p.u for every value of P_{cc} and L_x. For the cases B and C, a voltage sag originated in the MV network (the fault occurred along the MV line) was measured also in the HV network and on the other MV busbar of the same HV/MV substation. The measured voltage sags are deeper than those measured for the cases B and C when the MV busbar switch is open. For the case A, when the MV busbar switch is close, two voltage sags were measured on the two MV busbars of the same HV/MV substation. For the case D, when the MV busbar switch is open a voltage sag originated in the MV network was measured only on the MV busbar where the MV faulted line is connected; instead, when MV busbar switch is close, a voltage sag

originated in the MV network was measured also in the HV network and on the other MV busbar of the same HV/MV substation.

Table 2.27 Summing table of different cases

Case	MV busbar switch	VB1	VB2	VB3	VB4
A	**Open**	0.97	0.95	0.97	0.66
B		**0.76**	**0.71**	**0.76**	**0.44**
C		**0.89**	**0.87**	**0.89**	**0.23**
D		0.93	0.91	0.93	0.16
A	**Close**	0.96	**0.77**	0.96	**0.77**
B		**0.73**	**0.50**	**0.73**	**0.50**
C		**0.84**	**0.35**	**0.84**	**0.35**
D		**0.88**	**0.27**	**0.88**	**0.27**

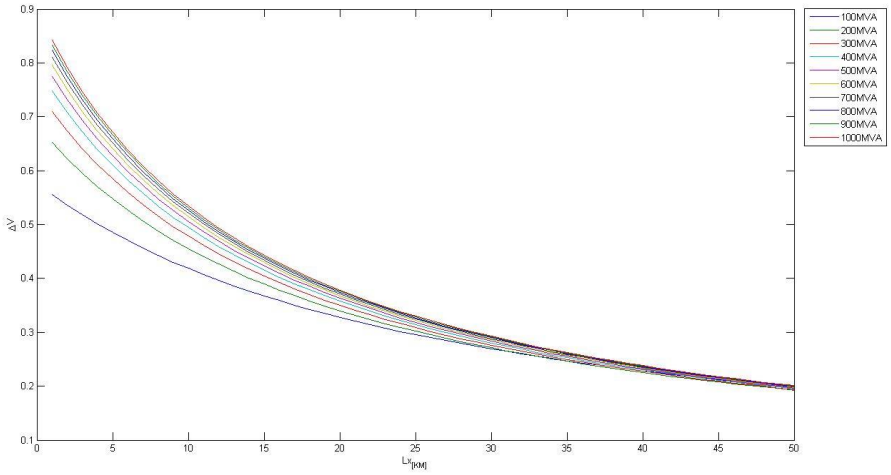

Figure 2.26 Plot of ΔV *versus the distance of VB4 to the fault*

In conclusion, the occurrence of a voltage sag, depends on several factors; the most important are:

2. the short circuit power of the equivalent HV system;
3. the distance of the fault from the point of measurement;
4. the topology of the considered system;
5. the position of the MV busbar switch.

The portion of a real system of Figure 2.13 was used for verifying the real possibility that a voltage sag originated in MV network could be measured also in the HV network. The analysis was performed by simulating the system in Matlab/Simulink. The Simulink model is reported in Figure 2.27.

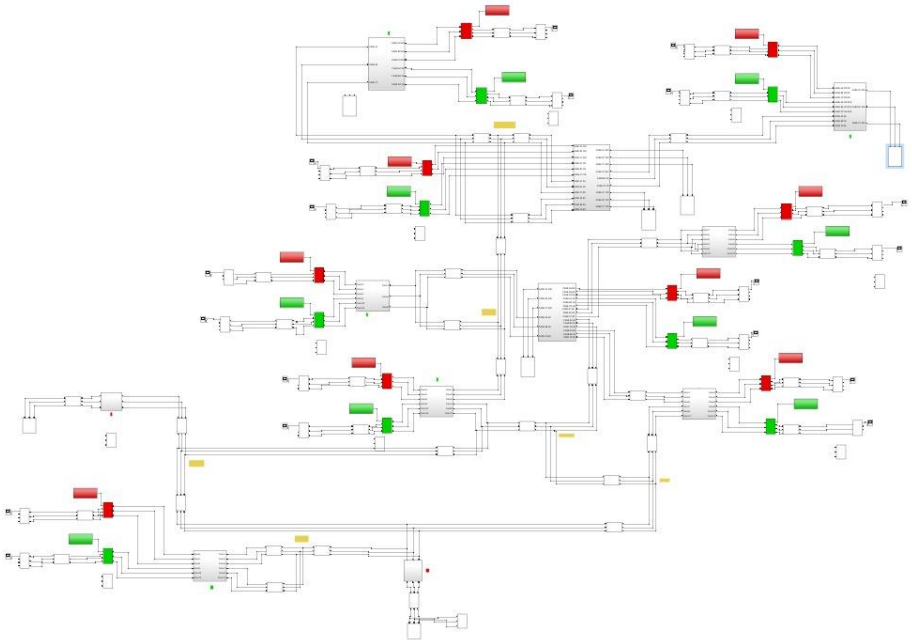

Figure 2.27 Simulink model

For evaluating whether a voltage sag due to a fault in the MV network can appear on a busbar of the HV network, the during fault voltages were measured both on the primary and on the secondary windings of the two HV/MV transformers (transformer RE and transformer GR) of each HV/MV substations.

The during fault matrix was derived in several cases in function of the chosen fault positions. In particular, the fault positions are the MV busbars of the transformer GR of every substation. The resulting matrix of the during fault voltages for these cases has 18 rows (points of observations) and 11 columns (fault positions). Further cases considered the faults along the MV lines. In particular, the fault position was varied along the lines fed by the node 2 and the node 8. Moreover, a further matrix of the during fault voltages considered the fault position fixed at a distance from the MV busbar of every HV/MV substations at 2,5 Km.

Table 2.28 shows the during fault voltages in percentage of the nominal voltage at the secondary windings of all HV/MV substations for fault positions corresponding to the MV busbar of HV/MV transformers. In this table and in the successive tables, the empty cells correspond to the absence of a voltage sag (residual voltage not lower than 90%).

Table 2.28 Residual voltage measured on the secondary winding of all HV/MV subtations; the fault positions correspond to the MV busbars of all the HV/MV transformers (transformer GR).

		# Fault position										
		1GR	**2GR**	**3GR**	**4GR**	**5GR**	**6GR**	**7GR**	**8GR**	**9GR**	**10GR**	**11GR**
# Observation node	**1RE**											
	1GR	0.11										
	2RE	8.,55	89.02									
	2GR											
	3RE		62.12	0.18					89.18			
	3GR		62.12	0.18					89.18			
	4RE		76.98		85.51		88.32	89.08	85.26			
	4GR		76.98		0.05		88.32	89.08	85.26			
	5RE		67.07		89.43				84.95			
	5GR		67.06		89.42	0.02			84.93			
	6RE		76.97		85.49		65.91	89.06	85.24			
	6GR		72.57	87.63	80.61	88.77	0.28	83.98	80.37	86.93	86.75	84.97
	7RE		74.21		86.16		88.75	71.70	81.30	89.59	87.12	83.69
	7GR		74.21		86.16		88.75	0.15	81.30	89.59	87.12	83.69
	8RE		71.09		87.45		89.76	87.44	76.75	88.29	88.91	86.11
	8GR		71.09		87.45		89.76	87.44	0.06	88.29	88.91	86.11
	11RE		71.86		86.60		89.00	82.65	77.99	86.95	81.10	72.88
	11GR		71.86		86.60		89.00	82.65	77.99	86.96	81.10	0.13

The substations 6, 7, 8, 11 are the nodes of the system with the widest exposed area. They are the nodes of the system more sensitive to voltage sags for faults originating in the other nodes. The explanation of this behaviour could be attributed to the fact that they are nodes far from HV equivalent system.

The substation 2 is the node of the system that presents the widest affected area that is the node of the system that causes deeper voltage sags because its short circuit is the highest one.

Table 2.29 shows voltages measured on the primary windings of all HV/MV substations for fault positions corresponding to the MV busbar of HV/MV transformers.

Table 2.29 Residual voltages [%] measured on the primary winding of all the HV/MV transformers

		# Fault position										
		1GR	**2GR**	**3GR**	**4GR**	**5GR**	**6GR**	**7GR**	**8GR**	**9**	**10**	**11GR**
# Observation node	**1HV**	65.23										
	2HV		64.60	87.46					89.89			
	3HV		62.16	86.60					89.23			
	4HV		77.05		85.58		88.40	88.40	85.33			
	5HV		67.10		89.48				84.99			
	6HV		76.99		85.52		65.94	65.94	85.27			
	7HV		74.26		86.21		88.80	88.80	81.35	89.64	87.17	83.69
	8HV		71.14		87.50		89.81	89.81	76.80	88.34	88.96	86.11
	11HV		71.91		86.66		89.06	89.06	78.04	87.01	81.15	72.48

The nodes of the system that have the widest exposed area are highlighted in yellow; the fault positions “2GR” and “8GR” that presents the most affected area are highlighted in red.

Further cases were simulated considering the substation 2. Several faults were forced along the MV line fed by the transformer GR; the results are reported in Table 2.30.

Table 2.30 Residual voltages [%] measured on the primary winding of all transformers of Tab.7 for short circuit forced on several positions (varying the distance of the fault from the MV busbar) along the MV line fed by the substation 2 .

Fault position #2						
		Distance of the fault [km]				
		0	**0.5**	**1**	**1.5**	**2**
# Observation node	**1HV**					
	2HV	64.60	79.92	86.68	89.93	
	3HV	62.16	78.49	85.71	89.19	
	4HV	77.05	87.03			
	5HV	67.10	81.19	87.43		
	6HV	76.99	86.97			
	7HV	74.26	85.21	89.95		
	8HV	71.14	83.38	88.76		
	11HV	71.91	83.65	88.78		

The results are very significant since they evidence the effect of the distance of the fault from the point where the voltage sag can be measured also in more complex systems than the simplified system showed previously.

Similar simulations were performed for the substation 8; the results are reported in Table 2.31. The results are close to the ones of Table 2.30 even if the voltage sags are characterised by a greater residual voltage.

Table 2.31 Residual voltages [%] measured on the primary winding of all transformers for short circuit forced on several positions (varying the distance of the fault from the MV busbar) along the MV line fed by the substation 8 .

		Fault position #8 Distance of the fault [km]										
		0	**0.5**	**1**	**1.5**	**2**	**2.5**	**3**	**3.5**	**4**	**4.5**	**5**
# Observation node	**1HV**											
	2HV	89.89										
	3HV	89.23										
	4HV	85.33	86.79	88.09	89.25							
	5HV	84.99	86.45	87.74	88.90	89.90						
	6HV	85.27	86.73	88.03	89.19							
	7HV	81.35	83.26	84.84	86.28	87.52	88.57	89.45				
	8HV	76.80	79.22	81.21	83.00	84.55	85.88	87.00	87.96	88.78	89.48	
	11HV	78.04	80.29	82.11	83.77	85.21	86.43	87.47	88.35	89.10	89.75	

Table 2.32 and Table 2.33 show the matrix of the during fault voltages due to the fault positions fixed at a distance from the MV busbar of every HV/MV substations at 2.5 Km. The MV lines of the substations are fed by the transformers GR. Table 2.32 refers to the MV busbars, and Table 2.33 refers to the HV busbars.

Table 2.32 Residual voltages measured on the secondary windings of all HV/MV substations; the fault positions are along the MV lines at a fixed distance of 2,5 Km from the MV busbars of the substations.

		# Fault position										
		1GR	**2GR**	**3GR**	**4GR**	**5GR**	**6GR**	**7GR**	**8GR**	**9**	**10**	**11GR**
# Observation node	**1RE**											
	1GR	62.18										
	2RE											
	2GR		83.38									
	3RE			76.05								
	3GR			76.05								
	4RE											
	4GR				44.29							
	5RE											
	5GR					23.04						
	6RE						76.21					
	6GR		89.65		85.23	89.49	35.18		85.80	88.46	88.33	
	7RE								88.51		89.94	
	7GR							72.44	88.51		89.94	
	8RE								85.83			
	8GR								48.07			
	11RE								86.38	89.70	85.31	89.26
	11GR								86.38	89.70	85.31	69.83

Table 2.33 Residual voltages measured on the primary windings of all HV/MV substations; the fault positions are along the MV lines at a fixed distance of 2,5 Km from the MV busbars of the substations

		Fault position #										
		1GR	**2GR**	**3GR**	**4GR**	**5GR**	**6GR**	**7GR**	**8GR**	**9**	**10**	**11GR**
# Observation node	**1HV**	85,54										
	2HV											
	3HV											
	4HV											
	5HV											
	6HV						76.24					
	7HV								88.57		90.00	
	8HV								85.88			
	11HV								86.43	89.75	85.36	89.32

CHAPTER 3

CHARACTERIZING CLUSTERS OF SAGS

The sags measured in real systems consist of both rare voltage sags and grouped voltage sags (clusters); clusters are stochastic events, defined as group of voltage sags which occur close each other with a time between from some seconds to some hours. To detect and analyse the clusters, new site indices of intermittence are proposed. These indices were measured in every site at which clusters were present, and the measurements included the frequency, time of grouping, and the large number of sags that constituted them.

3.1 Introduction

Clusters of sags are important for reflecting the severity of the voltage sag of nodes in the power system. It is important to highlight that all of the related references in the literature, as well as the popular recommended practices [51], estimate the average performance of a system in terms of the number of voltage sags (or indices related to them) by simulating the system in short circuit conditions and using the fault rate of the components to derive the expected yearly frequency of voltage sags. This means that the relevant literature always has focused on voltage sags due to faults, which are the rare voltage sags. Thus, simulated voltage sags generally are used rather than measured voltage sags, and this is the approach taken in this thesis work.

No study in the literature has dealt with the problem of estimating the average performance of a system in terms of clusters of sags. The causes of intermittent sags have not been analysed thoroughly and reported in the literature, but, generally, they can be due to adverse weather, cascading failure, reclosing events, incorrect registration, and recurring faults. Also, they could be linked to incipient faults in some critical components of the lines, such as the cable joints. In the literature, indices aimed specifically to characterize multiple sags are not available. In [51] the authors proposed a voltage-sag severity index, which was specifically intended for evaluating the severity of multiple voltage sags on sensitive loads. For ascertaining and filtering the voltage sags grouped in clusters, in this chapter new site indices are proposed.

The data from the field proved that the measured sags, in MV networks, can be divided into two main categories, i.e., the rare voltage sags and the clusters. Clusters appear as grouped events with the intervals of the adjacent voltage sags concentrated in $1\text{-}10^4$ s [52-54]. Thanks to the cooperation with E-Distribuzione, data from field were available during the studies of this thesis. The regional system, whose measured data were analysed and processed, has 83 HV/MV Substations with 152 MV busbars that represents the points of measurement of the voltage sags. They corresponded to 17 substations with 1 HV/MV transformer (1 measurement point), 63 substations with 2 HV/MV transformers (2 measurement points for each substation), and 3 substations with 3 HV/MV transformers (3 measurement points for each substation).

The available data start from 1 January 2015 to 31 December 2018. Table 3.1 shows the synthesis of the main data used in the study.

Table 3.1 Number of voltage sags measured in 4 years of measurements.

	Number of voltage sags
Voltage sags measured in 2015	12371
Voltage sags measured in 2016	9633
Voltage sags measured in 2017	17107
Voltage sags measured in 2018	19664

The one-dimensional scatterplot in Figure 3.1 highlights the stochastic nature of voltage sag occurrences, as these appear randomly in time, with periods of absences and others when sags appear as clusters, typically caused by severe weather events and other natural causes such as fires. However, from 0.4 s to 120 s, grouping of events defined as multiple events, that belong to the category of clusters, could be caused by:

- incorrect registration;
- the effect of the MV lines protection equipped by an automatic reclosing device.

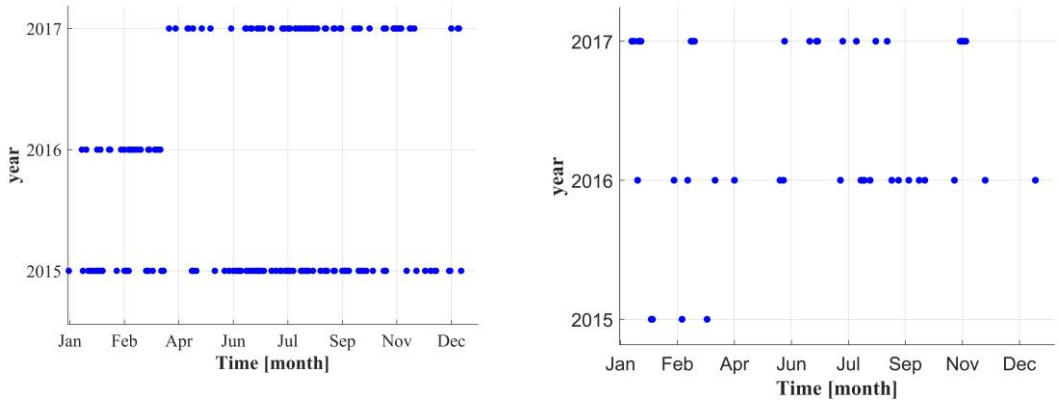

a) b)

Figure 3.1. Scatter plot of voltage sags(dots) recorded at the site #39 a) and #92 b) during three years of measurements.

All the events that belong to this category were aggregated as a single event performing the procedure of time aggregation. Time aggregation defined an equivalent voltage sag in the case of multiple voltage sags occurred in a short period of time. Multiple voltage sags occurred in a time window were considered as a single event. The choice of the time window depends on the reasoning to perform the time

aggregation. If the time aggregation was used to remove multiple events from the statistical analysis a time window of few seconds would be sufficient.

The main reasons to aggregate multiple sags are:

1) the effect on the operation of equipment and processes;
2) the possibility of incorrect registration;
3) the common cause that originated them.

Regarding the effect on the operation of equipment and processes, if the first voltage sag of the group will trip the equipment, causing the process to stop, the second and the successive sags will find the equipment still down. Consequently, it is reasonable to aggregate the events, separated from each other by a time that is less than the recovery time of the equipment and/or process them as a single event.

Regarding the possibility of the incorrect registration of multiple sags, the algorithm used in the measurement systems may register the end of a sag before the event is over. In fact, the voltage in real cases could recover above the threshold of sag-ending for some cycles and, afterwards, drop below the threshold again.

Regarding the common causes originating in all the sags that belong to the same group, one of the most frequent events is the unsuccessful reclosing after a permanent fault. For all the customers supplied by nodes that are electrically close to the permanent fault, this operation will cause a sequence of sags with their numbers and durations linked to the characteristics of the breaker.

The time aggregation of the multiple sags discussed in points 1) and 2) was performed using a time interval of 2 s, in according with the previous considerations. All the successive sags in time up to 2 s were considered as a single event, with a beneficial effect also on the mass of the data to be processed later.

The time aggregation of the multiple sags discussed in point (3) was conducted appropriately by selecting the time intervals in the function of the actual protection characteristics installed in the analysed MV networks recalled in § 2.3.

Therefore, a sequence of consecutive voltage sags registered in the above time ranges were grouped, and, afterwards, the sequence was used as a single sag represented by the first sag of the sequence; each group could be formed by two sags, if the first reclosure (1RR) was unsuccessful, by three sags, if the first slow reclosure (1SR) also was unsuccessful, and by four sags if the second slow reclosure (2SR) also was unsuccessful.

Figure 3.2 and Figure 3.3 presented the cumulative density functions of the duration and residual voltages of the measured voltage sags in busbar #39, before the time aggregation and after time aggregation with time window equal to 2 seconds. In

both a time window of 2 s presented a cumulative probability function of the duration and residual voltage that don't deviate from the cumulative density function of the duration and residual voltage before time aggregation. Similar results reported in Figure 3.4 and Figure 3.5 have been obtained for the site #92.

Further verifications of the acceptability of the effects of the time aggregation were performed also on the plane amplitude, duration in Figure 3.6 and Figure 3.7. Figures 3.6 and 3.7, showed these plots for the sites #39 and #92 before time aggregation (a) and after time aggregation with time window of 2 seconds (b). The distribution of the sags in the plane {amplitude, duration} appeared unchanged after time aggregation with time window equal to 2 seconds (b).

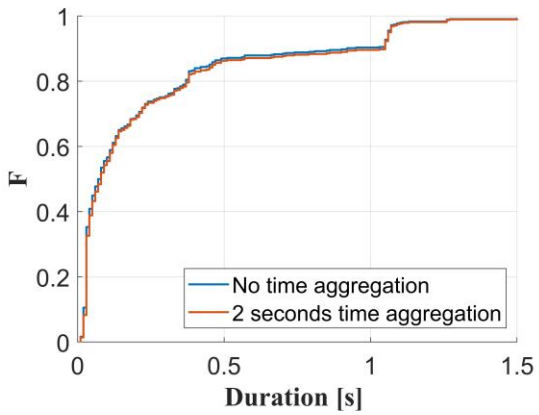

Figure 3.2 Cumulative density function of the duration of voltage sags measured in the site #39

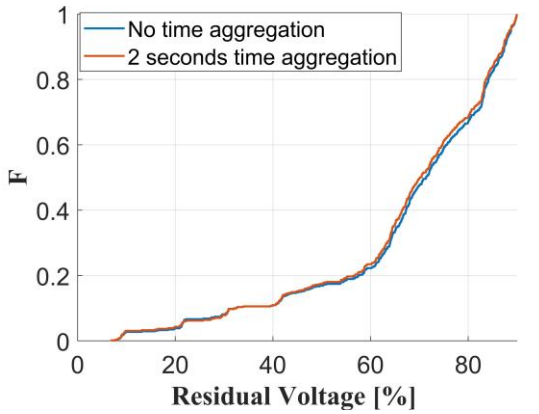

Figure 3.3 Cumulative density function of the residual voltage of voltage sags measured in the site #39

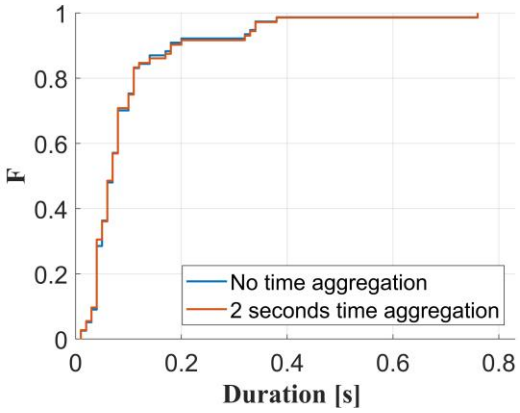

Figure 3.4 Cumulative density function of the duration of voltage sags measured in the site #92

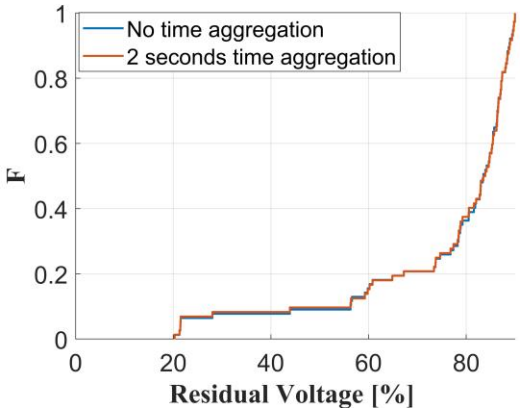

Figure 3.5 Cumulative density function of the residual voltage of voltage sags measured in the site #92

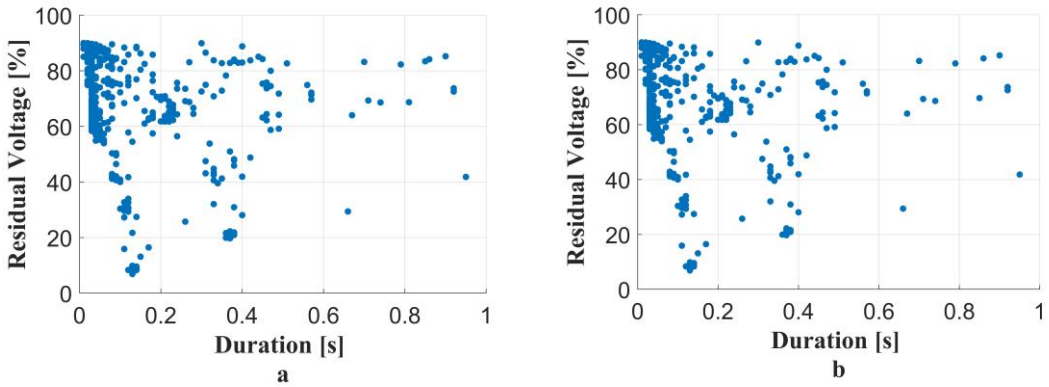

Figure 3.6 Scatter plots (Residual Voltage, Duration) of the voltage sags measured in 2015, 2016 and 2017 at the site #39 before time aggregation(a), and after time aggregation with time window of 2 seconds (b).

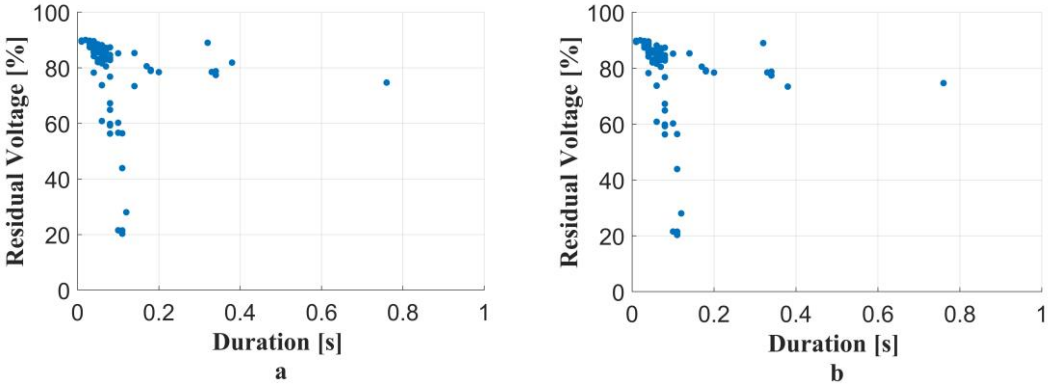

Figure 3.7 Scatter plots (Residual Voltage, Duration) of the voltage sags measured in 2015, 2016 and 2017 at the site #92before time aggregation(a), and after time aggregation with time window of 2 seconds (b).

Figures 3.8 and 3.9 show the scatter plot of the voltage sags, represented as dots, recorded in the considered system during the year 2015 before time aggregation and after time aggregation. Figures 3.10 and 3.11 show the scatter plot of the voltage sags, represented as dots, recorded in the considered system during the year 2016 before time aggregation and after time aggregation. Figures 3.12 and 3.13 show the scatter plot of the voltage sags, represented as dots, recorded in the considered system during the year 2017 before time aggregation and after time aggregation.

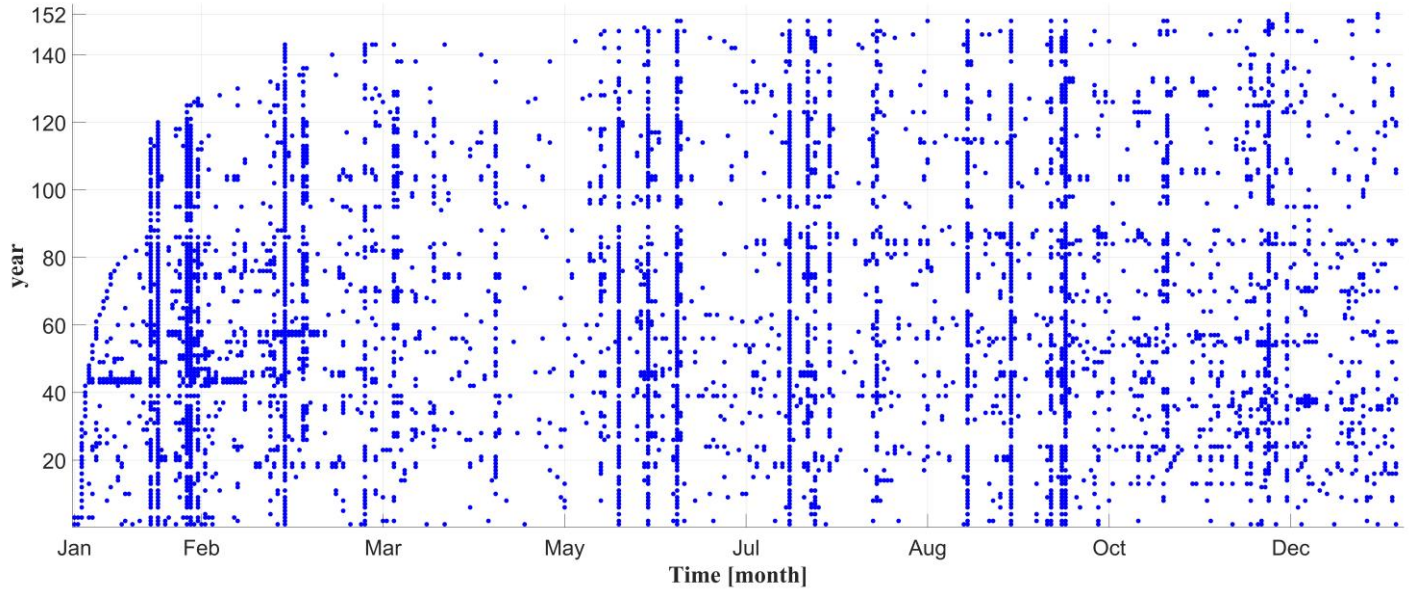

Figure 3.8 Scatter plot of voltage sags(dots) recorded at the system during the year 2015 before time aggregation.

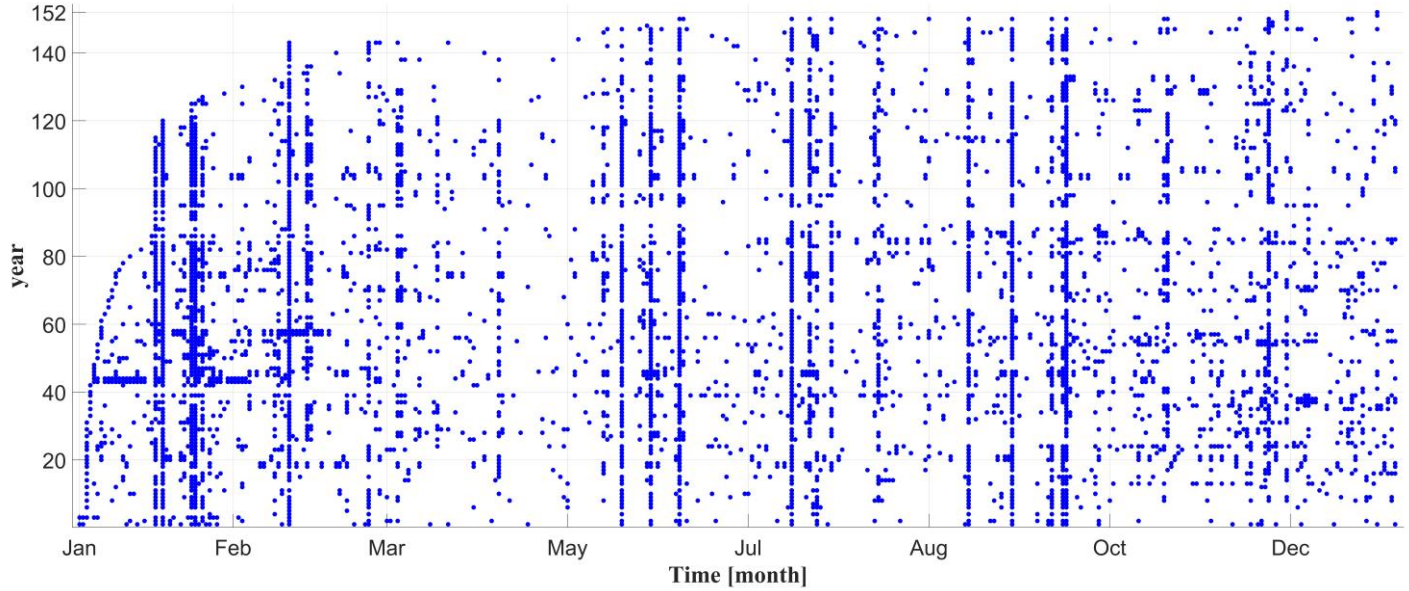

Figure 3.9 Scatter plot of voltage sags(dots) recorded at the system during the year 2015 after time aggregation.

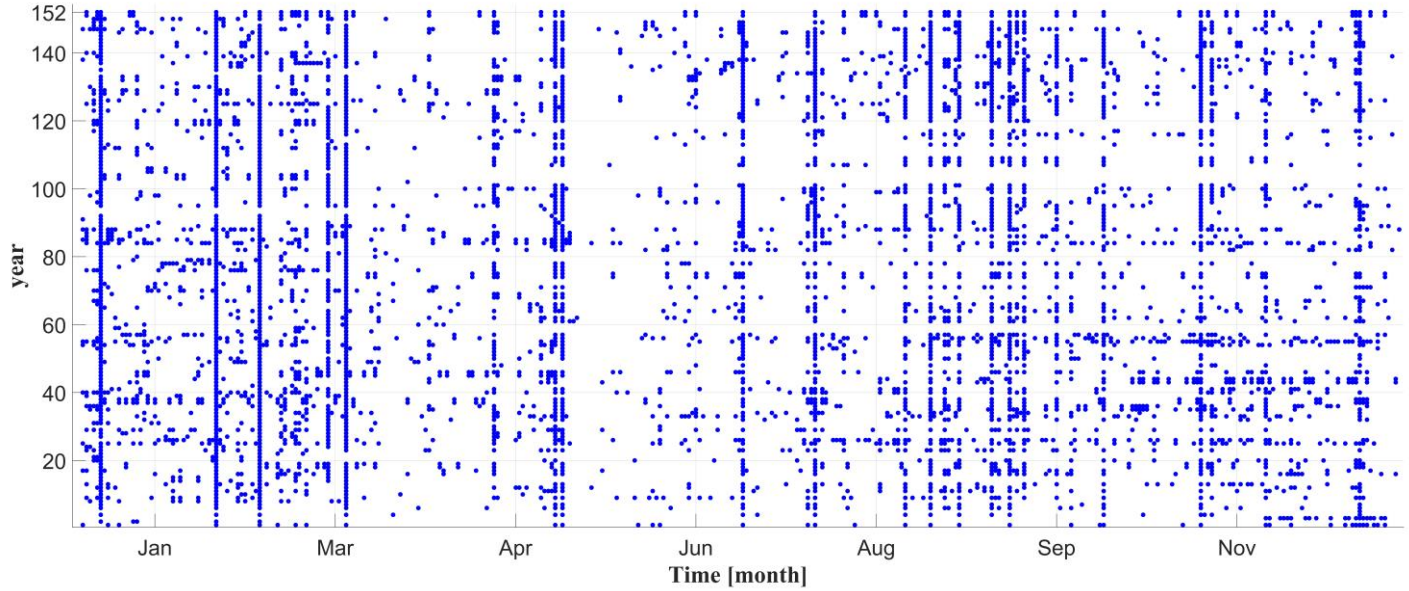

Figure 3.10 Scatter plot of voltage sags(dots) recorded at the system during the year 2016 before time aggregation.

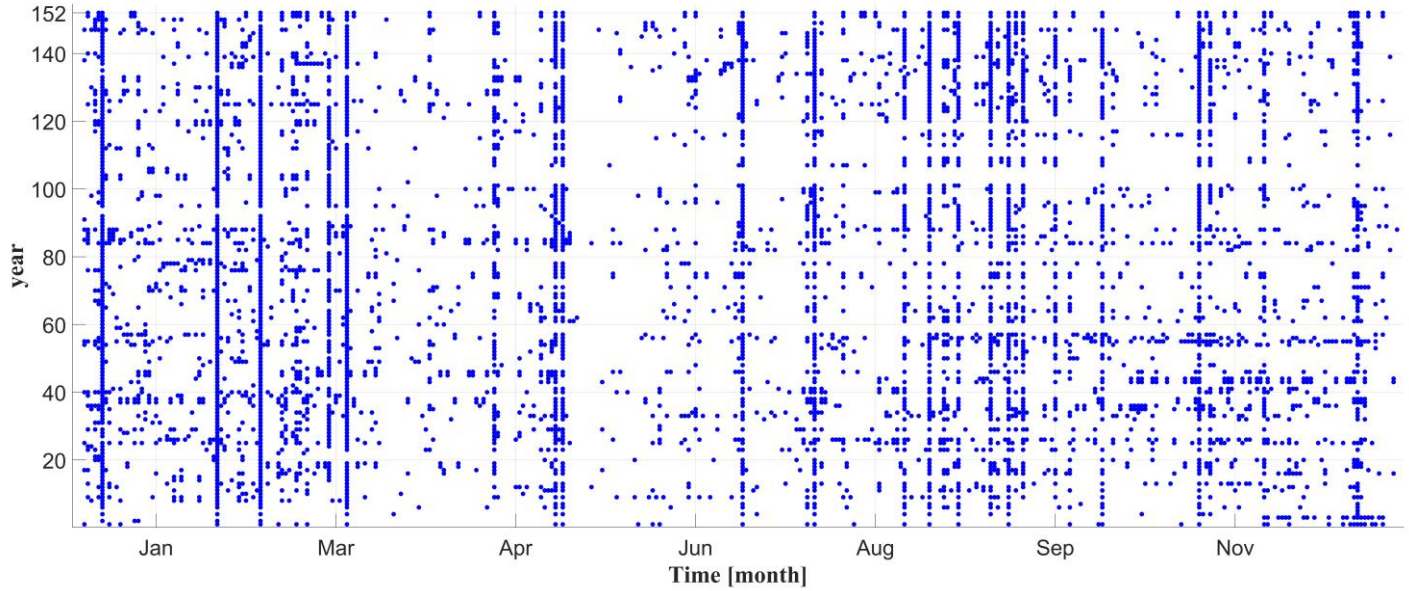

Figure 3.11 Scatter plot of voltage sags(dots) recorded at the system during the year 2016 after time aggregation.

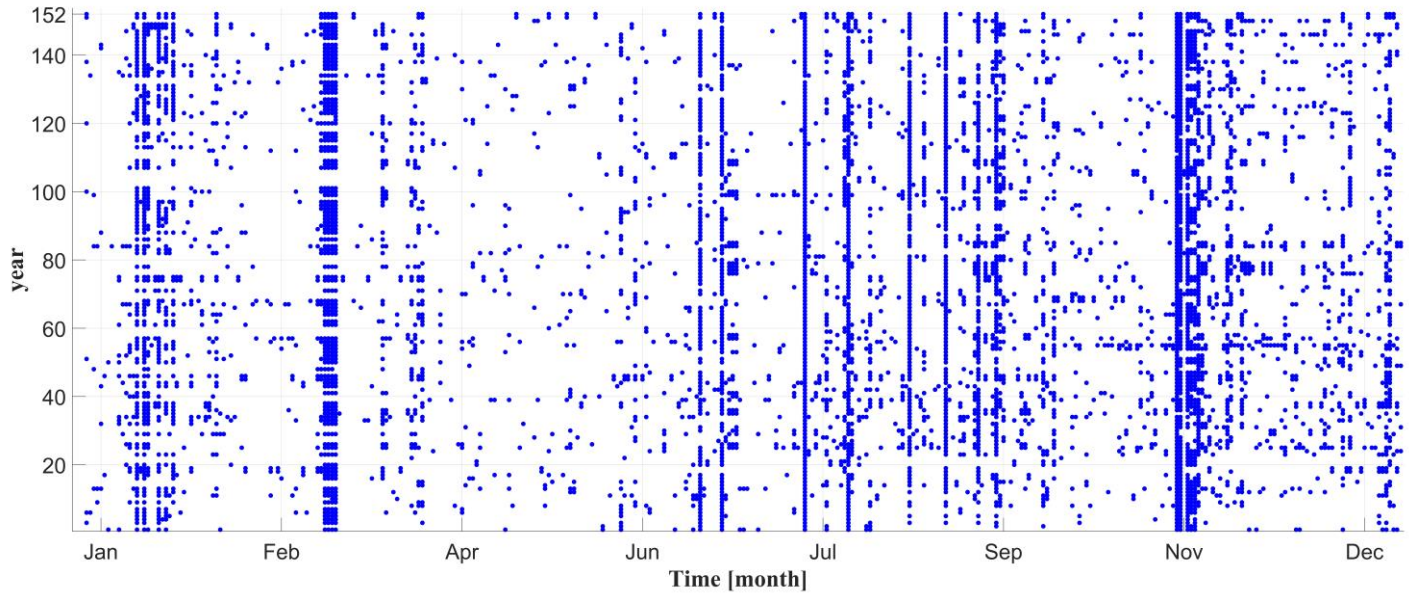

Figure 3.12 Scatter plot of voltage sags(dots) recorded at the system during the year 2017 before time aggregation.

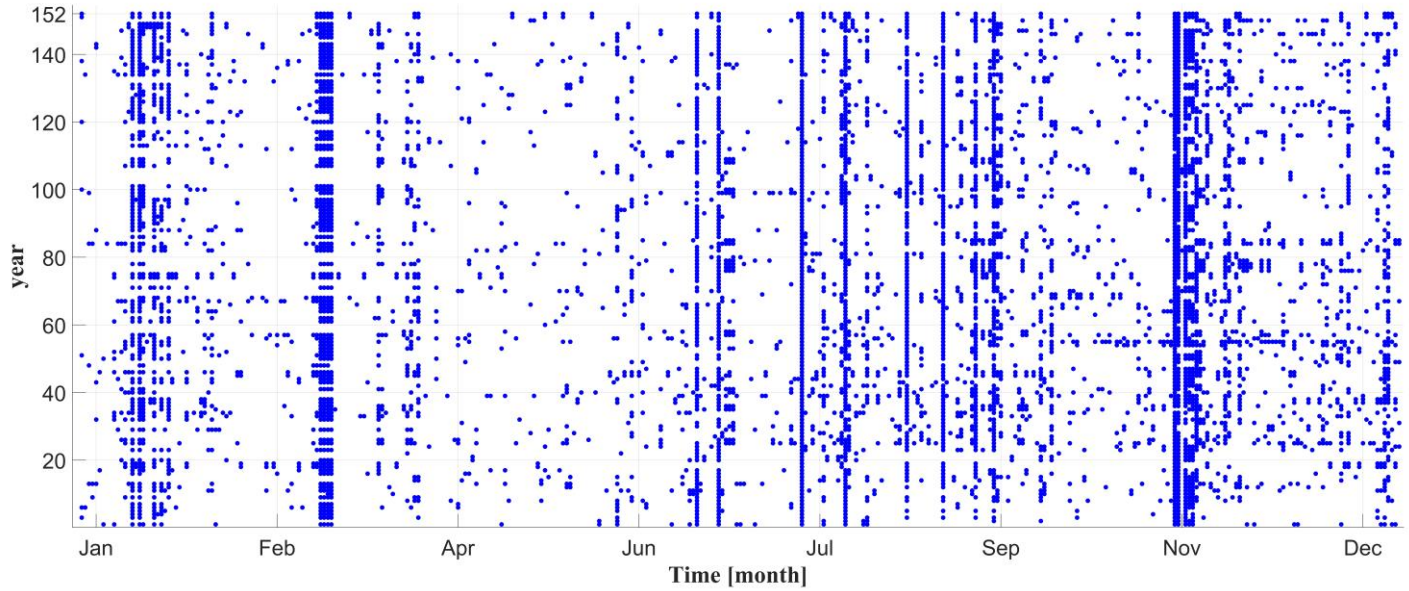

Figure 3.13 Scatter plot of voltage sags(dots) recorded at the system during the year 2017 after time aggregation.

Time aggregation doesn't jeopardize relevant information on data and after this procedure the events that belong to the category of clusters could be caused only by severe weather events and other natural causes.

Table 3.2 reported the comparison between the number of voltage sags measured in four years of measurements in the considered system before and after time aggregation.

Table 3.2 Number of voltage sags measured in 4 years of measurement before and after time aggregation.

Year of measurement	Before Time Aggregation	After Time Aggregation
2015	12371	10877
2016	9633	8559
2017	17107	14699
2018	19664	16697

Before time aggregation, in the first three years of measurements, 39111 voltage sags were measured and after time aggregation 34135 voltage sags were available to further analysis. In summary, the adopted time aggregation allowed to reduce data size without affect data statistics.

3.2 Proposal of new Intermittent Indices

A new site index called $TFIX_k\Delta T$ was introduced in this thesis work. It measured how many groups that contain X voltage sags were registered at a busbar k with a time between each consecutive voltage sag not greater than the time threshold, ΔT. Figure 3.14 shows the procedure for the computation of $TFIX_k\Delta T$ at site k for every assigned value of ΔT.

To give an example of the results obtainable by $TFIX_k\Delta T$, let's consider Table 3.3, which shows 12 voltage sags that were measured at a site k in January 2017. Table 3.3 reports the sequential number for every sag, the time of its occurrence, i.e., the year, month, day, hour, minute, and second it started, and its residual voltage.

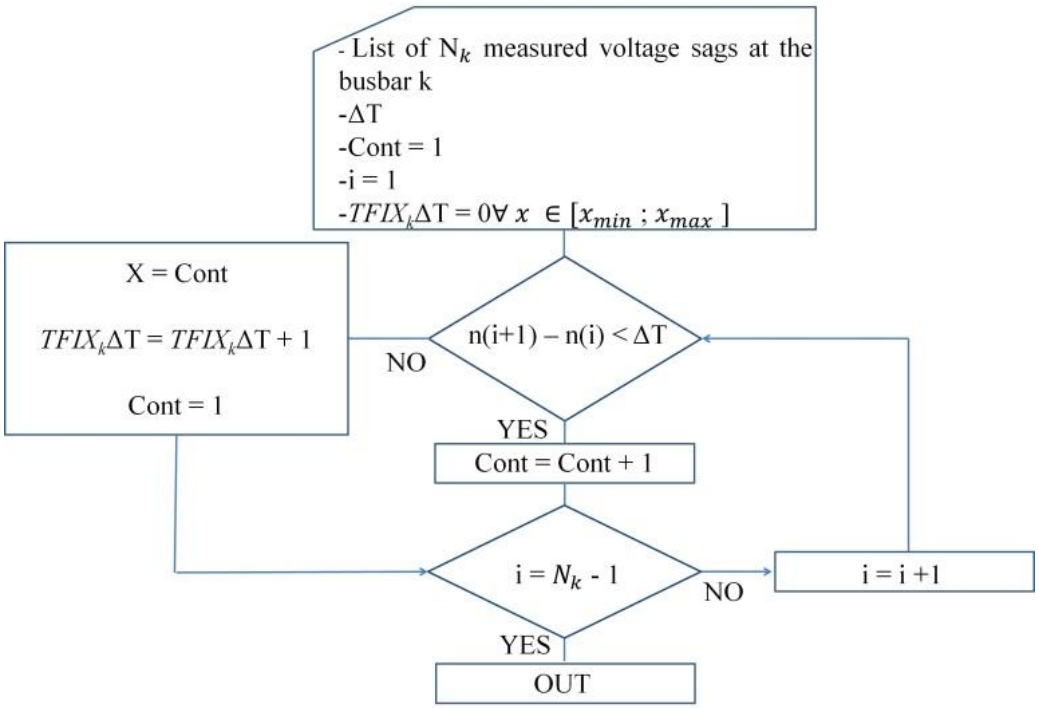

Figure 3.14 Flow-chart for computing TFIXkΔT

Table 3.3 List of measured voltage sags at a site k.

Sag sequential number	Time of occurrence [gg/mm/aaaa - hh:mm:ss]	Residual voltage [%]
1	01/01/2017 - 10:10:20	70
2	01/01/2017 - 10:10:50	60
3	01/01/2017 - 10:11:10	50
4	01/01/2017 - 11:10:50	70
5	01/01/2017 - 12:08:20	80
6	02/01/2017 - 08:10:10	65
7	02/01/2017 - 09:10:05	70
8	02/01/2017 - 09:50:20	80
9	02/01/2017 - 10:50:05	40
10	02/01/2017 - 11:45:45	50
11	05/01/2017 – 13:01:00	30
12	31/01/2017 – 02:10:00	40

From Table 3.3, for ΔT = 1800 s, we have $TFI3_k1800$ = 1; it means that site *k* registered 1 group of 3 voltage sags, which occurred successively with a time distance between them not greater than 1800 s (sags from #1 to #3). Increasing ΔT to 3,600 s, we have $TFI5_k3600$ = 2, which means that site *k* registered 2 groups of 5 voltage sags that occurred successively with the times between the sags being not

greater than 3600 s (sags from #1 to #5, and from #6 to #10). Increasing the value of ΔT from 1800 s to 3600 s, the index $TFIX_k3600$ also counts the group ascertained by $TFIX_k1800$; in fact, the group of sags from sag #1 to sag #5 contains the sags from #1 to #3 ascertained by $TFIX_k1800$. The 11th and 12th sags are not grouped, and they are rare voltage sags.

The intermittence index $TFIX_k\Delta T$ was used to detect the group of intermittent sags in every site. The groups were identified in every site, *k*, by computing the value of $TFIX_k\Delta T$ with ΔT ranging from ΔT_{min} to ΔT_{max}. After the groups were found in every site, *k*, $TFIX_k\Delta T$ allowed to remove them from the available data and consider only rare voltage sags. For this purpose, in every node, *k*, the time limit between the sag, ΔT, i.e., $\Delta TLimit_k$, below which the voltage sags in that site had to be considered to be grouped in clusters, was introduced. In [12], the use of the *1-hour* filter corresponded to $\Delta TLimit_k$ = 1 hour at any site *k*, as mentioned in the Introduction. This filter was effective for describing the statistics of the registered data [12].

The time limit, $\Delta TLimit_k$, was determined by observing the variation of $TFIX_k\Delta T$ for all of the groups of sags that were ascertained versus the increasing value of ΔT. At every site, when we find the maximum value of ΔT, i.e. $\Delta TLimit_k$, above which $TFIX_k\Delta T$ does not increase for any value of *X*, we conclude that no additional groups occurred above $\Delta TLimit_k$.

As a theoretical example, consider a site, *k*, for which the values of $TFIX_k\Delta T$ were computed with ΔT ranging from 3600 s (1 hour) to 36000 s (10 hours) following the procedure of Figure 3.18. Table II shows the values of $TFIX_k\Delta T$.

Table 3.4 indicates that site *k* registered several voltage sags grouped in clusters. In particular, $TFI3_k3600$ = 2 means that 2 clusters of 3 sags were registered, and they occurred successively with the times between them not greater than 3600 s (1 hour); $TFI3_k7200$ = 3 means that 3 clusters of 3 sags were registered, and they occurred successively with the time between them being not greater than 7200 s (2 hours); and so on.

Table 3.4 Values of $TFIX_k\Delta T$ (Theoretical example)

X **[# of grouped sags]**	***ΔT*** **Time between successive sags**	**Name of the intermittent index**	***$TFIX_k\Delta T$*** **[# of groups with *X* sags]**
3	*3,600 s (1 h)*	*$TFI3_k$ 3600*	*2*
3	*7,200 s (2 h)*	*$TFI3_k$7200*	*3*
3	*10800 s (3 h)*	*$TFI3_k$10800*	*4*
4	*14400 s (4 h)*	*$TFI4_k$14400*	*4*
4	*18,000 s (5 h)*	*$TFI4_k$18000*	*5*
4	*21,600 s (6 h)*	*$TFI4_k$21600*	*5*
4	*25,200 s (7 h)*	*$TFI4_k$25200*	*5*
4	*28,800 s (8 h)*	*$TFI4_k$28800*	*5*
4	*32,400 s (9 h)*	*$TFI4_k$32400*	*5*
4	*36,000 s (10 h)*	*$TFI4_k$36000*	*5*

It is evident from Table 3.4 that, for any value of *X*, $TFIX_k\Delta T$ does not increase for ΔT values greater than 18000 s (5 hours). In other words, the last clusters we found are those that corresponded to $TFI4_k18000 = 5$; they were 5 clusters of 4 sags that occurred successively with the time between them being not greater than 18000 s (5 hours). In this theoretical example, this implies that the searched value of $\Delta TLimit_k$ is equal to 18000 s (5 hours) since $TFIX_k\Delta T$ did not increase for values of ΔT greater than 18000 s, so there were no additional clusters.

In real cases, the trend of $TFIX_k\Delta T$ can be different from the theoretical example of Table 3.4. In addition, few groups, even groups with only two sags, can be detected in correspondence of a large value of ΔT, which occurred after a long series of ΔT with constant values of $TFIX_k\Delta T$ for any value of *X*. This additional group is, indeed, a kind of outlier since it has data points that lie an abnormal distance from other groups in the sample of the measured sags. The choice of the value of $\Delta TLimit_k$ being equal to 36000 s (10 hours) would be statistically incorrect in view of the forecast. This abnormal presence could be a singularity which probably did not recur in a future year.

To facilitate the search of $\Delta TLimit_k$ in real cases, a new index $TNS_k\Delta T$ was introduced from the index $TFIX_k\Delta T$ by the following equation:

$$TNS_k\Delta T = \sum_{Xmin}^{Xmax} TFIX_k\Delta T \times X. \tag{3.1}$$

In Equation (1), X_{min} and X_{max} are the minimum and maximum numbers, respectively, of the voltage sags that belong to that cluster. X_{min} was selected to be equal to 2 and X_{max} was 100. $TNS_k\Delta T$ provides the sum of all the multiple sags ascertained as a cluster by the index $TFIX_k\Delta T$. It measured the total number of voltage sags at site *k*, and they were grouped in all of the clusters as ascertained by varying ΔT in $TFIX_k\Delta T$. For the theoretical example of Table 3.4, Table 3.5 shows the values of $TNS_k\Delta T$, and Figure 3.18 shows the corresponding plot of $TNS_k\Delta T$ versus ΔT.

Table 3.5 Values of TNSkΔT that correspond to the values of Table 3.15 (Theoretical example)

ΔT Time between successive sags	**Name of the TNS_k**	**Value of $TNS_k\Delta T$ [# of grouped sags in ΔT]**
3600 s (1 h)	*TNS_k3600*	6
7200 s (2 h)	*TNS_k7200*	9
10800 s (3 h)	*TNS_k10800*	12
14400 s (4 h)	*TNS_k14400*	16
18000 s (5 h)	*TNS_k18000*	20
21600 s (6 h)	*TNS_k21600*	20
25200 s (7 h)	*TNS_k25600*	20
28800 s (8 h)	*TNS_k28800*	20
32400 s (9 h)	*TNS_k32400*	20
36000 s (10 h)	*TNS_k36000*	20

The trend of $TNS_k\Delta T$ versus ΔT in Figure 3.15 makes it easy to detect the limit value of ΔT, $\Delta TLimit_k$, above which there are not additional clusters. In the theoretical example, Figure 3.15 confirms that $TNS_k\Delta T$ is strictly constant from ΔT equal to 18000 s (5 hours), therefore the value of $\Delta TLimit_k$ is easily detectable, i.e., it is 18000 s (5 hours).

In most of the actual cases, however, the trend of $TNS_k\Delta T$ is like that in Figure 3.16, which is an example of a plot of the index obtained from measured voltage sags at an actual site, *k.*

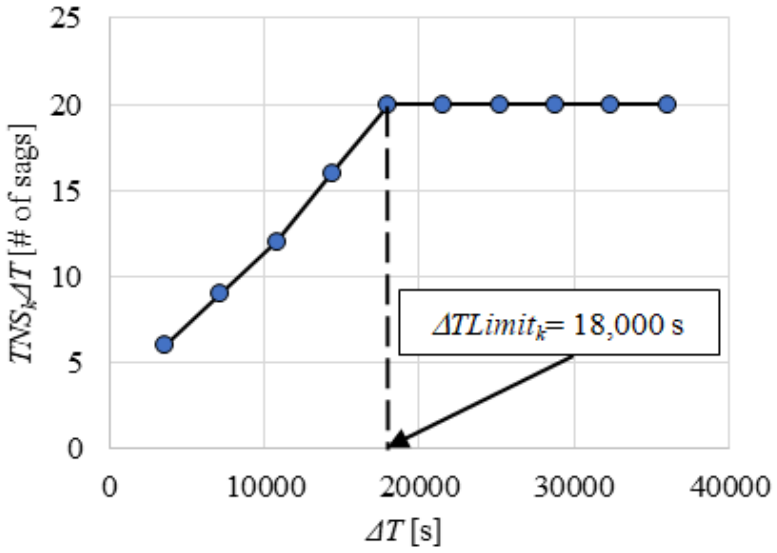

Figure 3.15 Plot of TNSkΔT versus ΔT corresponding to the values of Table 3.16, Theoretical example

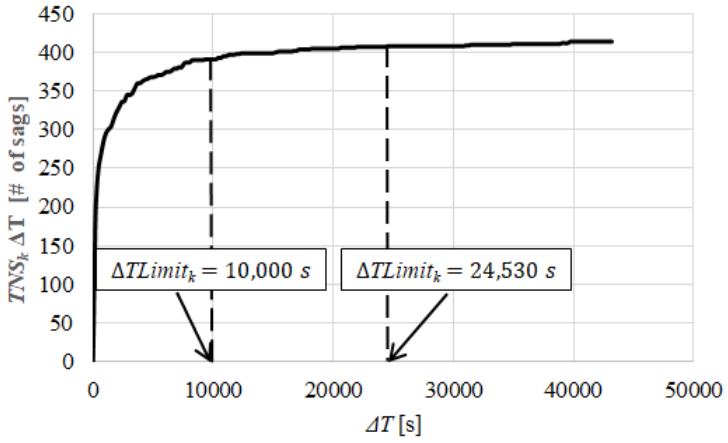

Figure 3.16 Example plot of TNSkΔT versus ΔT computed at an actual site k with measured voltage sags with two possible values of $\Delta TLimit_k$

Figure 3.16 indicates that $TNS_k\Delta T$ had a significant increase for low values of ΔT, but from ΔT values around 10000 s (about 3 hours), the index had a slight increase, but it was not strictly constant. This trend emerged in most of the actual cases. In Figure 3.20, exactly from 24530 s (about 7 hours), the total number of sags grouped in the cluster does not vary significantly from 408. The maximum value of $TNS_k\Delta T$ is 414 in correspondence of ΔT equal to 40000 s (about 11 hours). This means that, when the value of ΔT is increased by about 60%, only a few additional clusters were present (2 clusters of 3 sags) with a total increase of $TNS_k\Delta T$, which is less than 2% from the value of 408 at 24530 s (about 7 hours) to the maximum value of 414 at

40000 s (11 hours). In this case, as in all of the actual cases in which $TNS_k\Delta T$ was not strictly constant, the choice of $\Delta TLimit_k$ is equal to 24,530 s (about 7 hours) rather than the value that corresponds to the maximum value, i.e., $TNS_k\Delta T$ (about 11 hours), and it involves neglecting a few sags grouped in a cluster (6 sags out of 414 total grouped sags). The error linked to this choice is less than 2%.

For a given maximum threshold around the maximum value of $TNS_k\Delta T$, it is possible to select the value of $\Delta TLimit_k$ that guarantees the detection of all the sags grouped in clusters unless a percentage matches the set threshold. Therefore, first, the maximum value of $TNS_k\Delta T$ was addressed and after the value of $\Delta TLimit_k$-%, which corresponded to a maximum percentage threshold of variability of $TNS_k\Delta T$ around its maximum value we selected.

Figure 3.17 shows three possibilities, i.e., $\Delta TLimit_k$-5%, $\Delta TLimit_k$-1%, and $\Delta TLimit_k$. $\Delta TLimit_k$-5% and $\Delta TLimit_k$-1%, correspond to the maximum variability thresholds of $TNS_k\Delta T$ applied to the maximum value of $TNS_k\Delta T$ equal to 5% and 1%, respectively. $\Delta TLimit_k$ corresponds to the maximum value of $TNS_k\Delta T$.

In Figure 3.20, we can ascertain the following points related to different choices:

i) applying the threshold of 5%: the point is (10420s, 403), i.e., 403 sags grouped in clusters with an inter-distance between the sags of about 3 hours.

ii) applying the threshold of 1%, the point is (31043 s, 420), i.e. 420 sags grouped in clusters with an inter-distance between the sags of about 9 hours.

iii) use the maximum value of $TNS_k\Delta$T: the point is (39726 s, 424), i.e., the maximum number of sags grouped in clusters is exactly 424 with a time between the sags of about 11 hours.

When the number of sags ascertained in the three cases listed above are compared, it is evident that, from case i) to case iii), only 21 additional sags are grouped, but the time limit, $\Delta TLimit_k$, to detect and remove these few additional grouped sags increases from about 3 hours to about 11 hours. As discussed previously, the largest part of the grouped sags already can be detected by accepting a threshold of 5% using the $\Delta TLimit_k$-5%, i.e., 10420 s (about 3 hours) or a threshold of 1% using the $\Delta TLimit_k$-1% (about 9 hours).

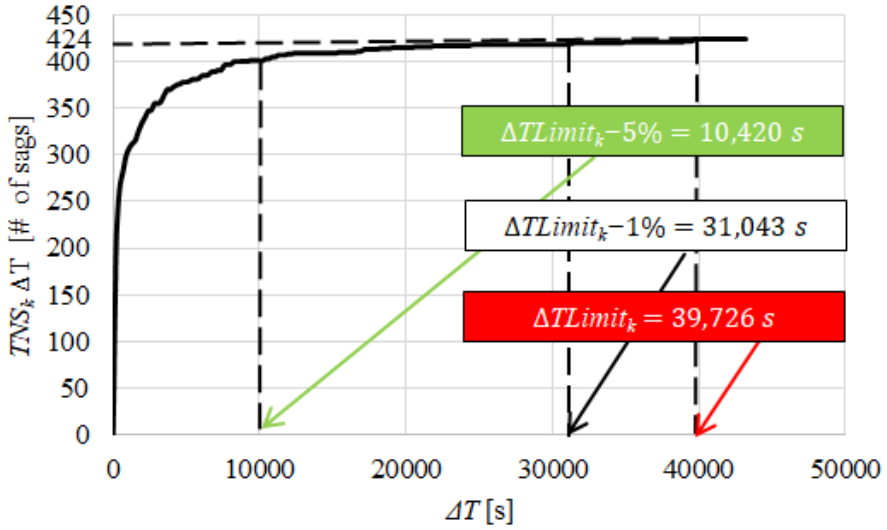

Figure 3.17 Plot of TNSkΔT versus ΔT with the values of ΔTLimitk intercepted as a function of the thresholds on the variation of TNSkΔT

3.3 Numerical Results

The indices $TFIX_k\Delta T$ and $TNS_k\Delta T$ were used to ascertain and filter the clusters of voltage sags from the field. $TFIX_k\Delta T$ was computed with ΔT ranging from ΔT= 1,800 s (0.5 hour) to ΔT= 21600 s (6 hours). To give an example of the results, we show some of the most interesting intermediate results that were obtained at site #39 and #92.

Table 3.6 shows the intermittent indices computed in the site #39 of the considered system during the year 2015. The intermittent indices give an initial screening of the presence of clusters, but by varying ΔT. From the results of Table 3.4 it is possible to see that a cluster of 16 voltage sags was measured for ΔT from 1800 s to 3600 s. From 7200 s to 14400 s an additional cluster of 16 voltage sags was measured and finally from 18000 s to 21600 s a cluster of 16 voltage sags disappeared and an additional cluster of 17 voltage sags was measured.

Table 3.6 List of intermittent indices measured at the site #39 for voltage sags measured in 2015 for ΔT ranging from 1800s to 21600s.

ΔT	**1800 s** **0.5 h**	**3600 s** **1 h**	**7200 s** **2 h**	**10800 s** **3 h**	**14400 s** **4 h**	**18000 s** **5 h**	**21600 s** **6 h**
$TFI2_{39}\Delta T$	17	16	19	13	13	12	9
$TFI3_{39}\Delta T$	9	5	4	8	8	7	6
$TFI4_{39}\Delta T$	2	5	3	2	2	2	2
$TFI5_{39}\Delta T$	4	2	1	1		1	2
$TFI6_{39}\Delta T$	2	4	3	1	2	2	2
$TFI7_{39}\Delta T$			2	3	3	3	2
$TFI8_{39}\Delta T$	1	3	1	1	1	1	1
$TFI9_{39}\Delta T$	1	1	3	4	4	3	3
$TFI10_{39}\Delta T$			1			1	2
$TFI11_{39}\Delta T$				1	1	1	1
$TFI12_{39}\Delta T$							
$TFI13_{39}\Delta T$				1	1	1	
$TFI14_{39}\Delta T$							
$TFI15_{39}\Delta T$	2	2	1	1	1	1	2
$TFI16_{39}\Delta T$	**1**	**1**	**2**	**2**	**2**	**1**	**1**
$TFI17_{39}\Delta T$						**1**	**1**
$TFI18_{39}\Delta T$							
$TFI19_{39}\Delta T$	1	1	1	1	1	1	1

Table 3.7 shows the intermittent indices computed in the site #39 of the considered system during the year 2016. During this year, for *ΔT* from 14400 s to 21600 s, a slight variation of the clusters is evident; in particular for *ΔT*=21600 s an additional cluster of 2 voltage sags was measured. For this reason, the index $TFI2_{39}14400=1$ increased to 2 ($TFI2_{39}21600=2$).

Table 3.7 List of intermittent indices measured at the site #39 for voltage sags measured in 2016 for ΔT ranging from 1800 s to 21600 s.

ΔT	**1800 s** **0.5 h**	**3600 s** **1 h**	**7200 s** **2 h**	**10800 s** **3 h**	**14400 s** **4 h**	**18000 s** **5 h**	**21600 s** **6 h**
$TFI2_{39}\Delta T$	3	1	1	1	1	1	**2**
$TFI3_{39}\Delta T$		2	1				
$TFI4_{39}\Delta T$			1	1	1	1	1
$TFI5_{39}\Delta T$	1	1	1	2	1	1	1
$TFI6_{39}\Delta T$	1				1	1	1
$TFI7_{39}\Delta T$		1	1	1	1	1	1

Table 3.8 shows the intermittent indices computed in the site #39 of the considered system during the year 2017. During this year, for ΔT= 14400 s to ΔT =21600 s, it is possible to notice no variation of the clusters.

Table 3.8 List of intermittent indices measured at the site #39 for voltage sags measured in 2017 for ΔT ranging from 1800 s to 21600 s.

ΔT	**1800 s** **0.5 h**	**3600 s** **1 h**	**7200 s** **2 h**	**10800 s** **3 h**	**14400 s** **4 h**	**18000 s** **5 h**	**21600 s** **6 h**
$TFI2_{39}\Delta T$	6	9	7	11	**10**	**10**	**10**
$TFI3_{39}\Delta T$	2	2	3	4	**5**	**5**	**5**
$TFI4_{39}\Delta T$	4	5	5	5	**5**	**5**	**5**
$TFI5_{39}\Delta T$			1	1	**1**	**1**	**1**
$TFI6_{39}\Delta T$	2	2	2	1	**1**	**1**	**1**
$TFI7_{39}\Delta T$				1	**1**	**1**	**1**
$TFI8_{39}\Delta T$	1	1	1	1	**1**	**1**	**1**
$TFI9_{39}\Delta T$							
$TFI10_{39}\Delta T$							
$TFI11_{39}\Delta T$							
$TFI12_{39}\Delta T$							
$TFI13_{39}\Delta T$	1	1	1	1	**1**	**1**	**1**
$TFI14_{39}\Delta T$	1	1	1	1	**1**	**1**	**1**
$TFI15_{39}\Delta T$							
$TFI16_{39}\Delta T$							
$TFI17_{39}\Delta T$							
$TFI18_{39}\Delta T$							
$TFI19_{39}\Delta T$							
$TFI20_{39}\Delta T$	1	1	1	1	**1**	**1**	**1**

Table 3.9 shows the intermittent indices computed in the site #39 of the considered system during the year 2018. During this year, from ΔT= 18000 s to ΔT =21600 s, it is possible to notice a considered variation of clusters because additional groups of 23 and 22 voltage sags were recorded.

Table 3.9 List of intermittent indices measured at the site #39 for voltage sags measured in 2018 for ΔT ranging from 1800 s to 21600 s.

ΔT	1800 s 0.5 h	3600 s 1 h	7200 s 2 h	10800 s 3 h	14400 s 4 h	18000 s 5 h	21600 s 6 h
$TFI2_{39}\Delta T$	19	15	21	23	19	19	18
$TFI3_{39}\Delta T$	7	7	6	5	8	6	8
$TFI4_{39}\Delta T$	3	4	4	2	2	1	1
$TFI5_{39}\Delta T$		1		2	3	3	2
$TFI6_{39}\Delta T$	1	1	2	3	2	3	2
$TFI7_{39}\Delta T$	3	2	1	1			
$TFI8_{39}\Delta T$	1	1	1	1	1		
$TFI9_{39}\Delta T$		2					
$TFI10_{39}\Delta T$							
$TFI11_{39}\Delta T$	1					1	
$TFI12_{39}\Delta T$		1	2	2	2	2	2
$TFI13_{39}\Delta T$					1	1	1
$TFI14_{39}\Delta T$							
$TFI15_{39}\Delta T$							
$TFI16_{39}\Delta T$							
$TFI17_{39}\Delta T$	1						
$TFI18_{39}\Delta T$							
$TFI19_{39}\Delta T$			1	1	1		
$TFI20_{39}\Delta T$		1	1	1			
$TFI21_{39}\Delta T$					1	1	1
$TFI22_{39}\Delta T$							**1**
$TFI23_{39}\Delta T$						**1**	**1**

During the year 2015, no clusters of sags were recorded in the site #92.

Table 3.10 shows the intermittent indices computed in the site #92 of the considered system during the year 2016.

Table 3.10 List of intermittent indices measured at the site #92 for voltage sags measured in 2016 for ΔT ranging from 1800 s to 21600 s.

ΔT	1800s 0.5h	3600s 1h	7200s 2h	10800s 3h	14400s 4h	18000s 5h	21600s 6h
$TFI2_{92}\Delta T$	2	2	3	3	3	3	3
$TFI3_{92}\Delta T$							
$TFI4_{92}\Delta T$							
$TFI5_{92}\Delta T$	1	2	1	1	1	1	1

Table 3.11 shows the intermittent indices computed in the site #92 of the considered system during the year 2017.

Table 3.11 List of intermittent indices measured at the site #92 for voltage sags measured in 2017 for ΔT ranging from 1800s to 21600 s.

ΔT	1800 s 0.5 h	3600 s 1 h	7200 s 2 h	10800 s 3 h	14400 s 4 h	18000 s 5 h	21600 s 6 h
$TFI2_{92}\Delta T$	4	4	6	6	7	6	4
$TFI3_{92}\Delta T$	1	2	2	3	2	1	1
$TFI4_{92}\Delta T$	1	1	1	1	2	2	3
$TFI5_{92}\Delta T$						1	1

Table 3.12 shows the intermittent indices computed in the site #92 of the considered system during the year 2018.

Table 3.12 List of intermittent indices measured at the site #92 for voltage sags measured in 2018 for ΔT ranging from 1800 s to 21600 s.

ΔT	1800 s 0.5 h	3600 s 1 h	7200 s 2 h	10800 s 3 h	14400 s 4 h	18000 s 5 h	21600 s 6 h
$TFI2_{92}\Delta T$	4	3	3	4	3	3	4
$TFI3_{92}\Delta T$					1	1	1
$TFI4_{92}\Delta T$							
$TFI5_{92}\Delta T$	2	1	1	1	1	1	1
$TFI6_{92}\Delta T$							
$TFI7_{92}\Delta T$		1	1	1	1	1	1

Figure 3.18 is a plot of $TNS_{39}\Delta T$ versus ΔT. It shows that the data at the site were recorded in the three years from 2015 to 2017 with a total number of voltage sags grouped together in the order of hundreds, and the maximum number of sags grouped in clusters, i.e., 381 sags, was detected for ΔT value equal to 21600s (6 hours). Figure 3.18 also shows the value of $\Delta TLimit_{39}$-1% (equal to 17,367 s, i.e. about 4 hours) that was intercepted by the 1% threshold on the variation of $TNS_{39}\Delta T$ around its maximum. $\Delta TLimit_{39}$-1% corresponds to 377.

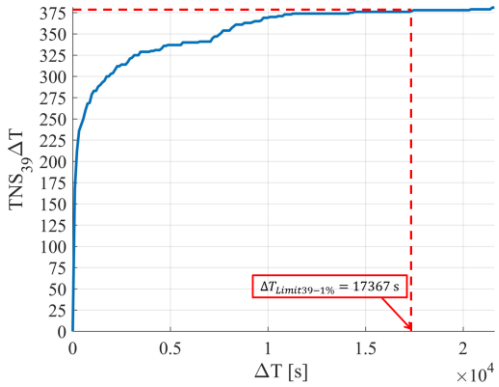

Figure 3.18 Plot of $TNS_{39}\Delta T$ versus ΔT.

Figure 3.19 is a plot of $TNS_{92}\Delta T$ versus ΔT, and it shows that the data at the site were recorded in the three years from 2015 to 2017 with a total number of voltage sags grouped together in the order of hundreds, and the maximum number of sags grouped in clusters, i.e., 37 sags, was detected for ΔT value equal to 14100s (4 hours); Figure 3.19 also shows the value of $\Delta TLimit_{92}$-1% (equal to 11288 s, i.e. about 3 hours) that was intercepted by the 1% threshold on the variation of $TNS_{92}\Delta T$ around its maximum. $\Delta TLimit_{92}$-1% corresponds to 36.

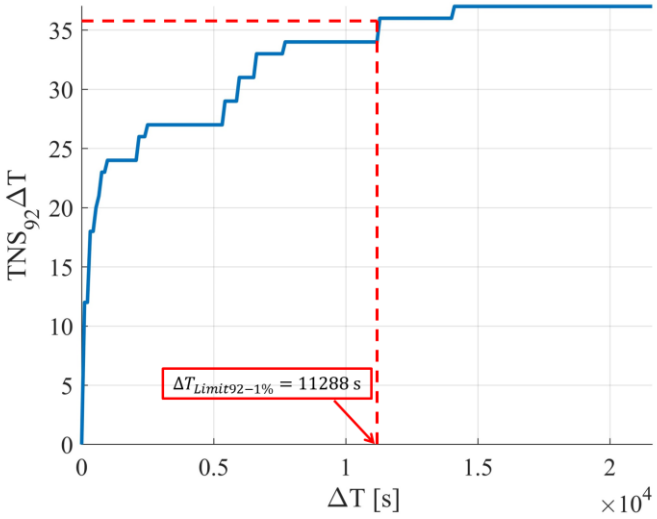

Figure 3.19. Plot of $TNS_{92}\Delta T$ versus ΔT.

Figure 3.20 and Figure 3.21 reported the tale of $TNS\Delta T$ versus ΔT respectively for the site #39 and #92 for voltage sags measured in 2018.

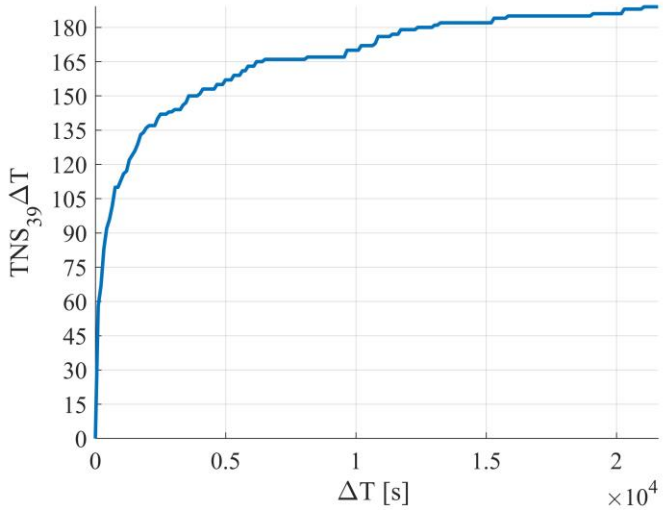

Figure 3.20. Example plot of TNSkΔT versus ΔT computed at the site #39 for voltage sags measured in 2018

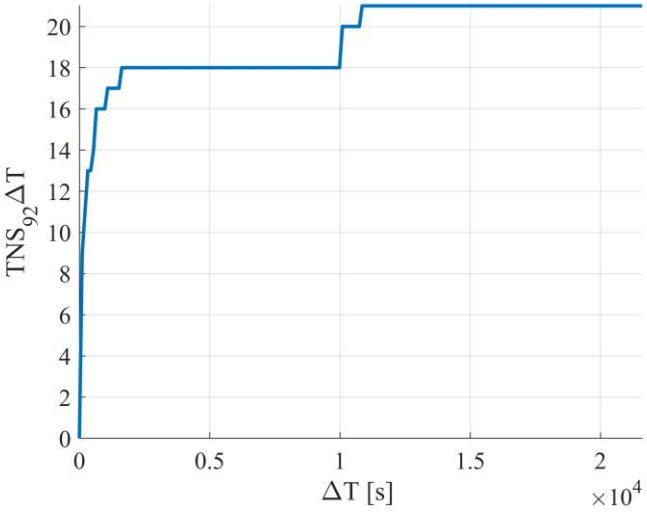

Figure 3.21. Example plot of TNSkΔT versus ΔT computed at the site #92 for voltage sags measured in 2018

CHAPTER 4.

FORECASTING RARE VOLTAGE SAGS

Rare voltage sags meet the conditions of a Poisson process, and they can be used to forecast the performance that can be expected in the future. Clusters must be detected and removed to allow the estimation of the future performance based on a Poisson process. To detect and remove the clusters, the site indices of intermittence proposed in the previous Chapter were applied. The performance of the forecast was evaluated by comparing the results obtained using the proposed indices with the results derived using a time filter equal for every site proposed in literature.

4.1 Introduction

Nowadays, no methodologies for predicting voltage sags are used by network operators to quantify the benefits of the actions proposed to reduce the number of voltage sags. The relevant literature proposed only model-based approaches for estimating the performance of a system in terms of average number expected at the sites of the system. The model-based methods need to know the network topology, the fault rate of lines and busbars, probabilistic model of the fault type, probabilistic model of the fault resistance and the probabilistic model of the fault line location.

The possibility of predicting voltage sags by using measured data has always been considered prohibitive. Using Poisson statistical model for the sags, the forecast of the average number of sags at the nodes with reasonable confidence requires a period of monitoring, i.e., at least tens of years. Recent availability of sags measured at actual systems allowed to re-consider this option, verifying if, and how, measured sags at a site for a reasonable time can be used to forecast the number of sags which will occur at that site.

The first aspect revealed from the measured data is that they are divided in two categories: rare sags and clusters. The rare sags constitute a Poisson process and the time between events follow an exponential probability distribution function. The clusters, instead, introduce a time dependent correlation between events that cannot be described by a Poisson model. The methods needed to forecast the sags must be different for rare sags and for clusters. Consequently, the separation of the rare sags from the cluster is mandatory before performing any prediction of future performance. The intermittent indices, presented in Chapter 3, allow detecting and excluding the clusters, leaving only the rare sags in the database to use for forecasting the number of (rare) sags which will occur at the system sites.

The second aspect revealed from the measured sags concerns the statistical description of the process. Researchers and system operators always described the phenomenon using the variable *yearly frequency of the sags* at a site in terms of number of sags/year. The choice of this statistical variable, however, gives a reduced number of measured data at a site. Every year, only one value can be obtained. In this study, the proposal of [12] was followed and extensively used. The voltage sags are statistically described by a new random variable: the time to next event (*ttne*). This random variable represents the time elapsed between the end of a voltage sag and the start of the next voltage sag. This choice allows a huge increase of the data size for

each measurement year and involved different statistical model to describe the phenomenon. The random variable *ttne,* if all clusters are excluded from the statistical analysis thanks to the intermittent indices, is described by an exponential probability density function.

Graphical tools, like the Quantile-Quantile Plots (QQ), are used to first verify if the filtering was affective to exclude the clusters, and after to estimate the main parameters of the exponential probability density of *ttne* of the remaining rare sags. This procedure is described in this Chapter applied to an Italian Regional electric system constituted by 152 busbars. Using the recorded measurements of three years at the sites of a real Regional electric system, voltage sags without clusters were modelled to forecast the number of sags in the incoming year. The prevision errors are evaluated comparing the forecasted occurrence of the sags with the actual sags that were measured in the fourth year.

4.2 Statistical Models

The first studies on the subject of the forecasting of voltage sags have been conducted at the end of the 90s [57-58], which have considered the forecasting of voltage sags impractical. The main reason is related to the need to have voltage sag measurements available for a number of years that are actually prohibitive for obtaining the prediction with acceptable accuracy.

Table 1 gives a summary of the monitoring times necessary to obtain an assigned accuracy as the frequency of the sags varies [57].

Table 4.1 Monitoring interval required to obtain an assigned accuracy

Event frequency	**50% Accuracy**	**10% Accuracy**	**2% Accuracy**
$\frac{1}{\text{day}}$	2 weeks	1 years	25 years
$\frac{1}{\text{week}}$	4 months	7 years	200 years
$\frac{1}{\text{mese}}$	1 year	30 years	800 years
$\frac{1}{\text{year}}$	16 years	400 years	10000 years

The values reported in Table 4.1 have been calculated by modelling the voltage sags as a probabilistic phenomenon with the characteristics of a Poisson process, i.e. a model of a series of discrete events such that each event is independent from the

one that precedes it. According to this model, the statistical variable number of events, *N*, respects the Poisson probability density function, fdp_N, and the time to the next event *ttne*, respects the exponential fdp_{ttne}; their expressions are reported below.

$$fdp_N = \frac{e^{-\lambda}\lambda^N}{N!} \tag{4.1}$$

$$fdp_{ttne} = \lambda e^{-\lambda * ttne} \tag{4.2}$$

The expected values for the Poisson probability density function and the exponential density function are respectively reported below:

$$E[N] = n\,\lambda \tag{4.3}$$

$$E[ttne] = \frac{1}{\lambda} \tag{4.4}$$

where λ is typically equal to $\frac{N}{year}$ and *n* is the number of years. The values of Table 4.1 are derived from the evaluation of the standard error, i.e. the estimate of the standard deviation of the sample mean. If the objective of the estimation is the mean μ of a population, which is supposed to have a normal distribution with standard deviation equal to σ, starting from a sample *X* of size *n*, the standard error e_S is given by the equation (4.5):

$$e_s = \frac{\sigma}{\sqrt{n}} \tag{4.5}$$

If *n* is adequately high, i.e. the data size is sufficiently large, the central limit theorem can be applied. The sum or the mean of a high number of random independent variables and with the same distribution (as for *ttne* and *N*) is approximately normal. Applying the central limit theorem, a confidence interval of the estimate of the average value $\bar{X}$can be established:

$$\left\{\bar{X} - Z\,\frac{\sigma}{\sqrt{n}};\ \bar{X} + Z\,\frac{\sigma}{\sqrt{n}}\right\} \tag{4.6}$$

where *Z* is the standard score for the assigned confidence level assigned.

The standard score is equal to 1.96 in the case of the assigned confidence level is equal to 95% (estimation error equal to 5%). The error on the mean value is equal to $1.96\,\frac{\sigma}{\mu}$. Considering the random variable *N* following the Poisson distribution, σ and μ can be expressed by the respective values $\sigma = \sqrt{n\,\lambda}$ and $\mu = n\,\lambda$. With such expression, the error ε_μ on the mean value is:

$$\varepsilon_\mu = \frac{1.96}{n}. \tag{4.7}$$

Using the previous relations, the number of samples can be estimated for a defined error ε:

$$n \geq \frac{1.96}{\varepsilon} \tag{4.8}$$

For different values of error, and of corresponding accuracy, the values of Table 4.1 can be obtained in function of the frequency of the sags[4]. For example, considering an error equal to 10%, *n* was equal to 20. Considering an event frequency equal to $\frac{1\ event}{week}$, 4 voltage sags were recorded in a month, and a period of 5 months is required to obtain a data size equal to 20.

The same computation can be performed considering the random variable *ttne* following the exponential distribution function. In such a case, the values of σ and μ are equal to:

$$\mu = \frac{1}{\lambda} \tag{4.9}$$

$$\sigma = \frac{1}{\lambda^2} \tag{4.10}$$

Substituting the expressions (4.9) and (4.10) in (4.8), the following result is obtained:

$$\lambda \geq \frac{1.96}{\varepsilon}. \tag{4.11}$$

[4] The values of the Table 4.1 are computed approximating 1.96 of the relation (4.7) with 2.

Considering an error equal to 10%, λ is equal to 19.6 sags/year; instead considering an error equal to 5% λ is equal to 39.2 sags/year. The conditions obtained for the random variable *ttne* are more favourable than the conditions obtained for the random variable *N*.

As said in the introduction, the choice of the random variable *ttne* instead the random variable *N* allowed a huge increase of the data size for every year of measurement. For example, in Figure 4.1, considering the random variable *N* only 1 value is available, that is 12. Considering the random variable *ttne*, the data size is constituted by 11 values corresponding to the time elapsed between the events.

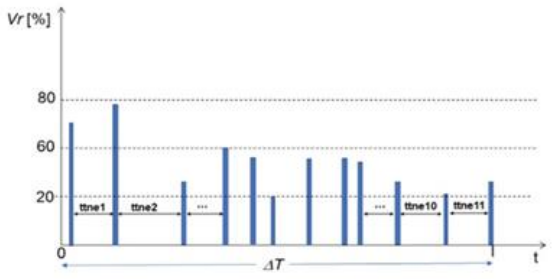

Figure 4.1. Graphical representation of the random variable ttne

For a global analysis of the statistical characteristics of the measured sags, it is useful to model both the rare sags and the clusters to derive the analytical conditions which link sag rate to the probability density function of the time of occurrence of the sags.

Figure 3.1, reported in Chapter 3, showed the stochastic nature of voltage sags. In fact, for different sites belonging to the same system, during three years of measurements, the distribution of voltage sags is completely random. The distribution of measured voltage sags is characterized by large period of absence, followed by period where sags appear grouped.

For each monitored year, *i*, a set of N_i events were recorded. The total amount of events year per year is different. Accordingly, a set of random variable *ttne* were recorded for each year of measurement *Y*. The stochastic process *ttne(n, Y)* is a family of random variables depending by time. For example, in the same site, the value of the random variable *ttne (1,2015)* is different from the value of the random variable *ttne (1,2016).*

Considering the year "*i*" it is possible to define:

- Y_i*:* set of events recorded in the year *i*;

- $N_i \neq N_{i+1}$*:* the number of events change for every year*;*
- $ttne_i\,(n)$*:* time to next event related to the event *n* of the year *i*;
- the process *ttne (n,Y)* is a family of stochastic discrete function.

The probability that the next event happen in time *t* is described by the function *Fe(t)*, which is the probability that the next event occurs in a time less than *t*:

$$Fe(t) = P(ttne(n) \leq t) \tag{4.12}$$

The probability density function is the probability that a random variable is equal to a defined value and it is described by the following relation:

$$fe(ttne) = \frac{dFe(t)}{dt} \tag{4.13}$$

The probability that *ttne (n)* is in the interval ΔT, assuming that there are no events up to time *t*, must be a conditional probability:

$$P(tt(n) \leq t + \Delta T)\,|(tt(n) > t) = \tag{4.14}$$

$$\frac{P(t < tt(n) \leq t + \Delta T)}{P(tt(n) > t)} \tag{4.15}$$

For ΔT tending to zero, from the (14.6) divided by ΔT, the event rate or frequency *Ze(t)* is equal to:

$$Ze(t) = \lim_{\Delta t \to 0} \frac{P(t < tt(n) \leq t + \Delta T)}{\Delta T * P(tt(n) > t)} = \frac{fe(t)}{1 - Fe(t)} \tag{4.16}$$

where:

$$fe(t) = \frac{dFe(t)}{dt} = \frac{P(t<tt(n)\leq t+\Delta T)}{\Delta T} \tag{4.17}$$

$$\frac{1}{1 - Fe(t)} = \lim_{\Delta t \to 0} \frac{1}{P(tt(n) > t)} \tag{4.18}$$

The probability density function *fe(t)* is the event density function, which measures the events in the time unit *t*. This function has the size of events per time

unit. The function *Ze(t)* is defined as the event rate at time *t* subjected to the fact that there are no events until and after the time *t*.

Ze(t) and *fe(t)* are related by a relation considering the variable *N(t)*, that is the event number that have to happen until the end of the monitoring time.

N(t) is a binomial variable characterized by:

- parameter *p= 1 – Fe(t);*
- expected value *n(t) = E(N(t)) = Ni(1-Fe(t)).*

It is possible to derive a relationship between *fe(t)* and the derivative of the expected value *n(t)*:

$$n(t) = Ni\big(1 - Fe(t)\big) \tag{4.19}$$

$$\frac{n(t)}{Ni} = 1 - Fe(t) \tag{4.20}$$

$$Fe(t) = 1 - \frac{n(t)}{Ni} \tag{4.21}$$

Remembering that $fe(t) = \frac{\mathrm{d}Fe(t)}{\mathrm{dt}}$, the following equation is obtained:

$$fe(t) = \frac{d}{dt}\left[1 - \frac{n(t)}{Ni}\right] = \frac{-1}{Ni}\,\frac{dn(t)}{dt}. \tag{4.22}$$

Putting the equation (4.22) in (4.16):

$$Ze(t) = \frac{fe(t)}{1-Fe(t)} = \frac{-1}{Ni}\,\frac{dn(t)}{dt}\,\frac{1}{1-Fe(t)} \tag{4.23}$$

Considering equation (4.19):

$$Ze(t) = -\frac{1}{n(t)}\frac{dn(t)}{dt} = -\frac{d}{dt}ln\big(n(t)\big) \tag{4.24}$$

The expected value n(t) is equal to:

$$\int_0^t Ze\,(t) = -\,ln\big(n(t)\big) \tag{4.25}$$

$$n(t) = Ke^{-\int_0^Y z_e(Y)\,dY} \tag{4.26}$$

where *K* is the integration constant.

Considering the initial conditions for t = 0,

- *n(0) = Ni;*
- *K = Ni*,

the following equation is obtained:

$$n(t) = N_i e^{-\int_0^Y z_e(Y)\,dY} \tag{4.27}$$

Substituting the equation (4.24) in (4.19):

$$Ni\ e^{-\int_0^Y z_e(y)\,dY} = Ni\big(1 - Fe(t)\big) \tag{4.28}$$

If $Ze(t) = \frac{fe(t)}{1-Fe(t)}$, *fe(t)* is equal to:

$$fe(t) = Ze(t)\,\big(1 - Fe(t)\big) \tag{4.29}$$

The correlation between *fe(t)* and *Ze(t)* is obtained:

$$fe(t) = Ze(t)\ e^{-\int_0^Y z_e(y)\,dY} \tag{4.30}$$

It is possible to state that the random variable *ttne* has an exponential probability density function only if the clusters are discarded from the statistical analysis. In such a case, *z(t)* is constant and equal to λ, and consequently it is:

$$fe(ttne) = \lambda\ e^{-\lambda ttne} \tag{4.31}$$

4.3 Proposed Method to Forecast Rare Sags

Figure 4.2 shows the scheme of the proposed method for forecasting the rare voltage sags. The registered data from the field over a period of *N* years were used to forecast the sags in the successive year.

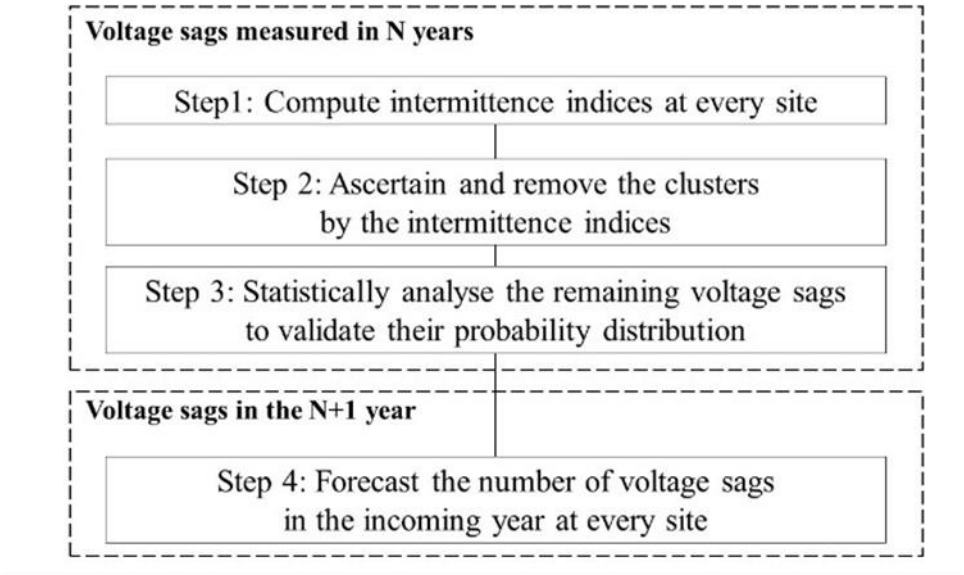

Figure 4.2 Flow chart of the proposed method

There are two separate blocks, which are included in rectangles with the dashed lines. In the first block, the statistical analysis of the measured voltage sags in *N* years is performed. In the second block, the statistics derived from these years of measurements were used to forecast the following $(N+1)^{th}$ year. The first block consists of three successive steps, as follows:

- 1^{st} step: Computation of the proposed intermittence indices at every site of the system in the study.
- 2^{nd} step: Site-by-site detection of sags grouped in clusters and subsequent removal in the function of the trend of $TNS_k \Delta T$ around its maximum value. A maximum threshold around the maximum value of $TNS_k \Delta T$ is stated to select the maximum value of the time that elapsed between consecutive sags, below which any sag is considered to have occurred in a cluster.

- 3rd step: Statistical analysis of the sags that are not grouped in clusters, e.g., the rare voltage sags, to verify if they respect the conditions required to be modelled as a Poisson process.

The second block contains the 4th and final step. It is aimed at forecasting the number of sags that will occur in the incoming year, i.e., $(N+1)^{th}$.

The availability of sags registered in the $(N+1)^{st}$ year were used to evaluate the performance of the forecast as a function of the different thresholds applied to the proposed index, $TNS_k\Delta T$, in the 2nd step.

The 1st and 2nd step were presented in the paragraph 4.3.2, the 3rd step was presented in the paragraph 4.3.2 and the final step was presented in the paragraph 4.3.3.

4.3.1 Filtering the Rare Sags by the Intermittent Indices

The indices $TFIX_k\Delta T$ and $TNS_k\Delta T$, presented in the Chapter 3, were used to ascertain the clusters of voltage sags measured during four consecutive years, i.e., 2015 through 2018. The voltage sags of the years 2015-2017 were used to forecast the number of voltage sags measured in 2018.

As stated earlier, the first two steps were aimed at ascertaining and filtering the clusters of voltage sags by using the indices $TFIX_k\Delta T$ and $TNS_k\Delta T$; the values of $TFIX_k\Delta T$ were computed with ΔT ranging from 1,800 s (0.5 hour) to 12,600 s (3.5 hours). To give an example of the results, some of the most interesting intermediate results that were obtained at site #39 and #92 were showed.

Figure 4.3 and Figure 4.4 refer to the *ttne* without any filter, Figure 4.5 and 4.6 refer to *ttne* of the remaining sags after the application of a *1-hour filter*; Figure 4.7 and 4.8 refer to *ttne* of the remaining sags after the application of the $\Delta TLimit_{39}$*-1%* and $\Delta TLimit_{92}$*-1%* filter. Figure 4.10 and Figure 4.11 show the three curves of the cumulative probability of *ttne* together, which already were shown separately in the preceding figures. They are shown together so they can be compared.

For site #39 and #92, it was evident from the scatter plot of Figures 4.3 and 4.4, that several sags were registered with low values of *ttne*; they corresponded to the

red points close to the *y*-axis[5]. This also was proved by the high value of probability (about 65%) of the lowest values of *ttne* in the curve of the cumulative probability (top of Figure 4.4). This means that about 65% of all of the *ttne* had the lowest values.

For the site #39, Figures 4.6 and 4.8, showed the effect of applying the filters. The *1-hour* filter still left residual sags with low values of *ttne* (red points close to the *y*-axis in the scatter plot, i.e., Figure 4.5). This was reflected in an initial value of probability of about 20% (curve in the top of Figure 4.5), which was lower than that of the unfiltered sags (curve in the top of Figure 4.3). The application of the filter based on the intermittence indices, i.e., the $\Delta TLimit_{39}$-1% filter, improved the efficacy in cleaning the sags with low values of *ttne*, as shown in the scatter plot of Figure 4.8. The initial value of probability decreased appreciably to about 5% for the $\Delta TLimit_k$-1% filter (curve in the top of Figure 4.8).

Eventually, Figure 4.9 showed that the three curves of cumulative probability were modified extensively as they passed from the *ttne* without any filter (curve A) to the *ttne* of the remaining sags after the application of the filters (Curve B refers to the *1-hour* filter, and curve C refers to $\Delta TLimit_k$-1% filter). Table 4.2 shows the percentiles of the three curves. The lowest percentiles, i.e., the $P_{10\%}$, of the three curves are very different; they varied from about 50 s for the unfiltered sags (column A) to about 3 hours for the sags filtered by the *1-hour* filter (column B) to about 17 hours for the sags filtered by $\Delta TLimitk$-1% (column C).

Also, it is evident that 50% of the unfiltered sags (column A) have *ttne* values equal to or less than 0.48 h; instead, 50% of the sags filtered by the *1-hour* filter had *ttne* values greater than 65 h (about 3 days), and 50% of those filtered by $\Delta TLimit_k$-1% had *ttne* values greater than 93 h (about 4 days).

To summarize, these outcomes proved that additional clusters of sags were still present in the sags filtered by the *1-hour* filter; they were identified only using a filter that was linked directly to the measure of the sag intermittence, such as the $\Delta TLimit_k$-1% filter that was linked to the variation of the intermittence index, $TNS_k\Delta T$. The good effect of the $\Delta TLimit_k$-1% filter has resulted in our applying it in all of the sites of the regional system.

5 The values of ttne along the y-axis were not null, but they corresponded to the minimum value of the time aggregation, which was 3 s. It was selected as a function of the actual protection characteristics installed in the analysed MV networks [14]. The scale of the plots did not allow distinguishing 3 s from zero.

For site #92, it was evident from the scatter plot of Figure 4.4, that several sags were registered with low values of *ttne*; they corresponded to the red points close to the *y*-axis. This also was proved by the high value of probability (about 40%) of the lowest values of *ttne* in the curve of the cumulative probability (top of Figure 4.5). This means that about 40% of all of the *ttne* had the lowest values. However, instead site #39, the site #92 presents a minor number of clusters. This means, probably, that the intermittent index necessary to discard clusters for the site #92 will be, in value (second), less than the one used to discard clusters for the site #39.

To verify this issue, Figures 4.11 and 4.12 reported the $TNS_{39}\Delta T$ and $TNS_{92}\Delta T$ measured at the sites #39 and #92 respectively from 2015 to 2017.

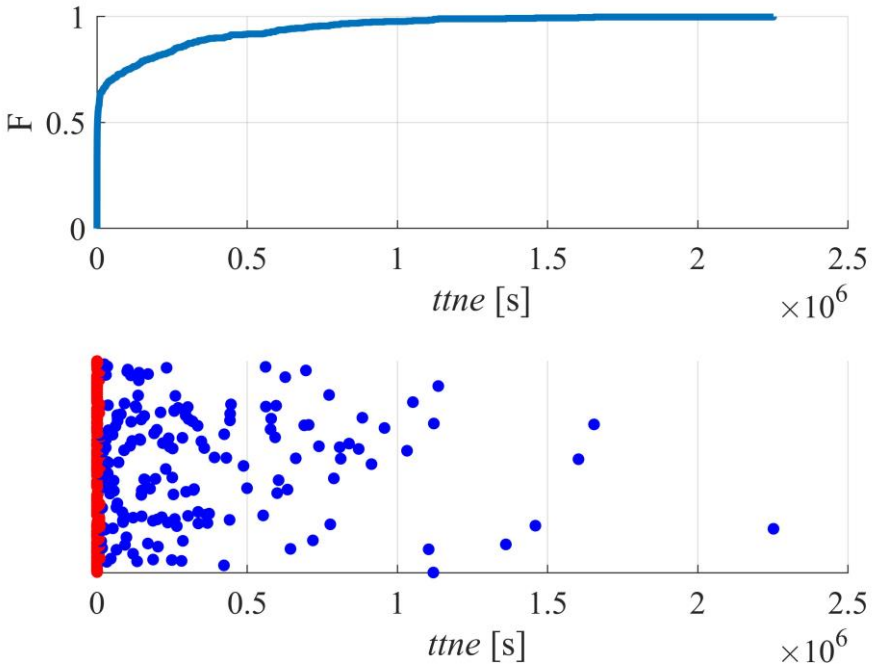

Figure 4.3. Cumulative probability, F, of the ttne at site #39 without the application of filters (top); scatter plot of monitoring data (below)

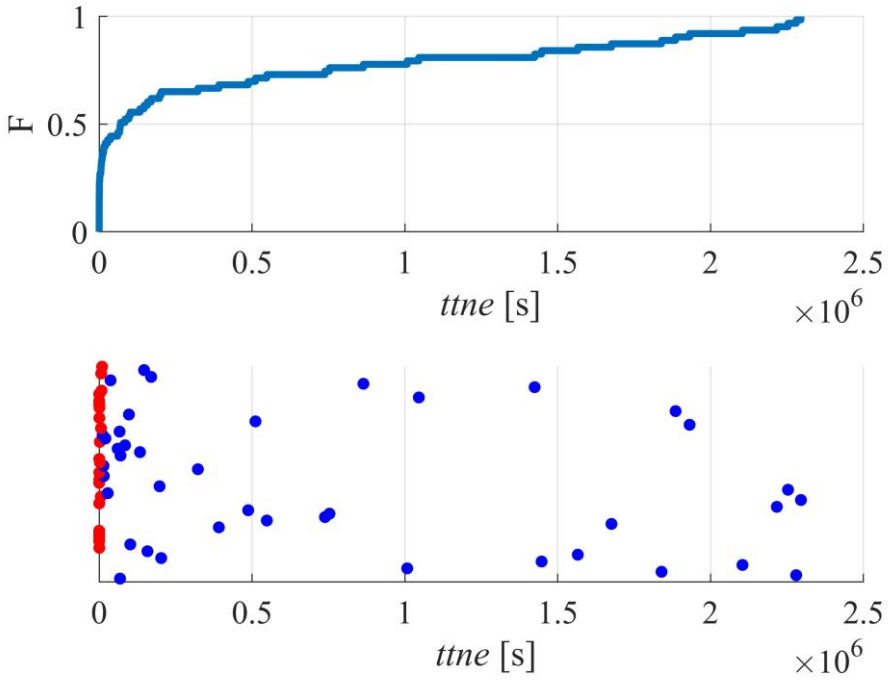

Figure 4.4. Cumulative probability, F, of the ttne at site #92 without the application of filters (top); scatter plot of monitoring data (below)

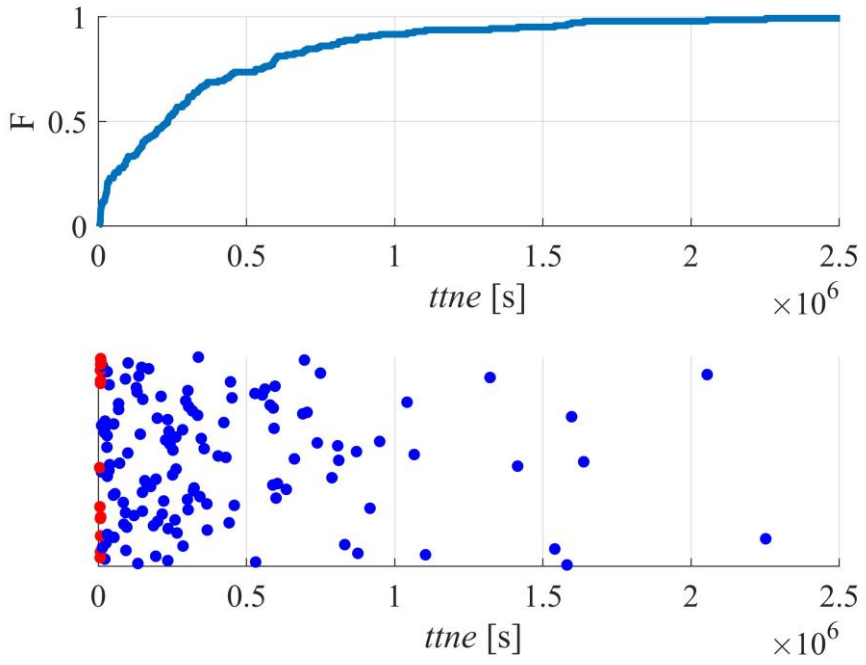

Figure 4.5. Cumulative probability, F, of the ttne at site #39 filtered from the clusters using the 1-hour filter (top). Scatter plot of monitoring data (below).

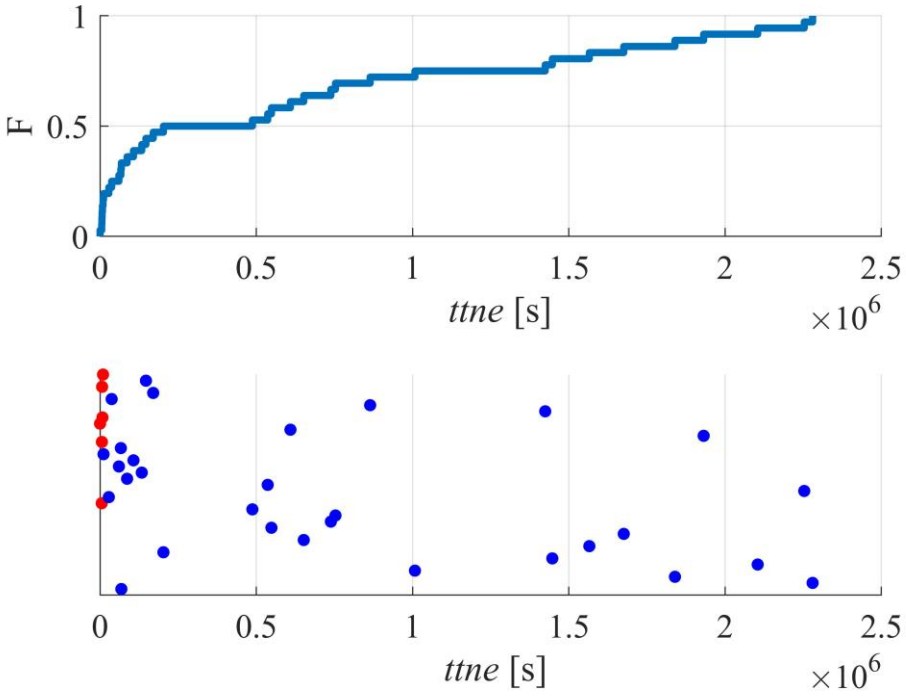

Figure 4.6. Cumulative probability, F, of the ttne at site #92 filtered from the clusters using the 1-hour filter (top). Scatter plot of monitoring data (below).

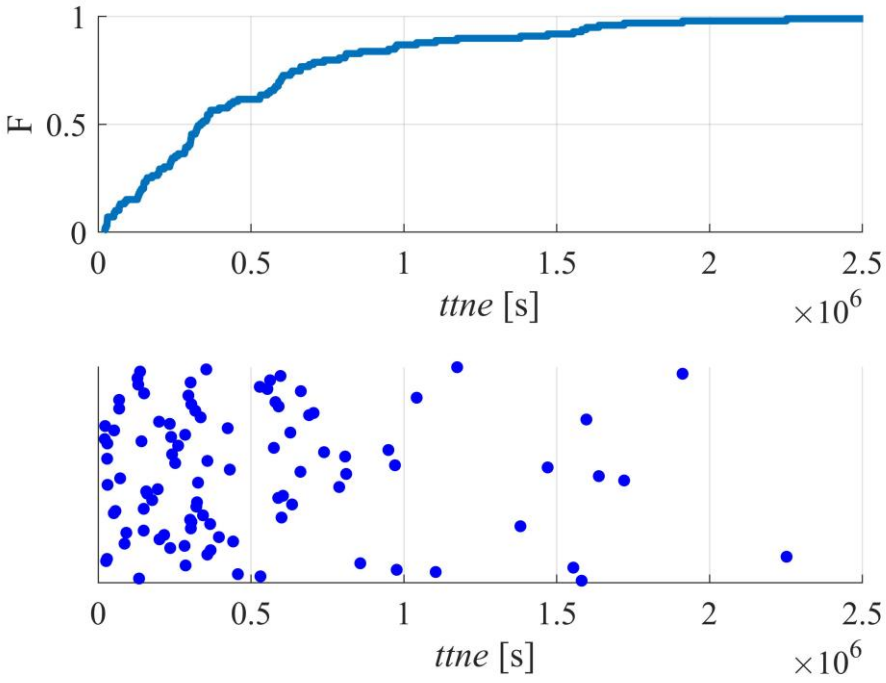

Figure 4.7. Cumulative probability, F, of the ttne at site #39 filtered from the clusters using the ΔTLimitk-1% filter (top); scatter plot of monitoring data (below)

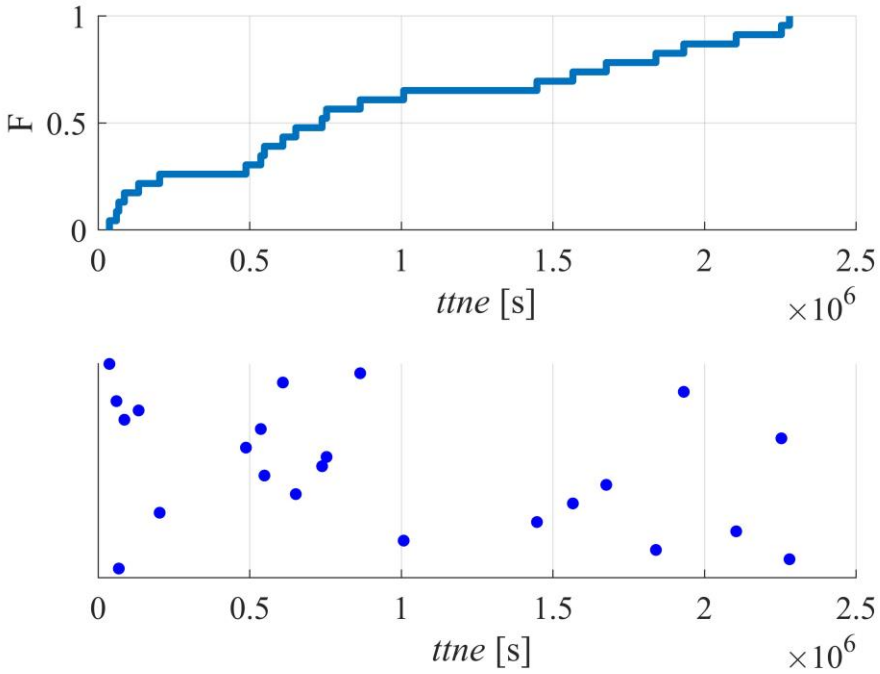

Figure 4.8. Cumulative probability, F, of the ttne at site #92 filtered from the clusters using the ΔTLimitk-1% filter (top); scatter plot of monitoring data (below)

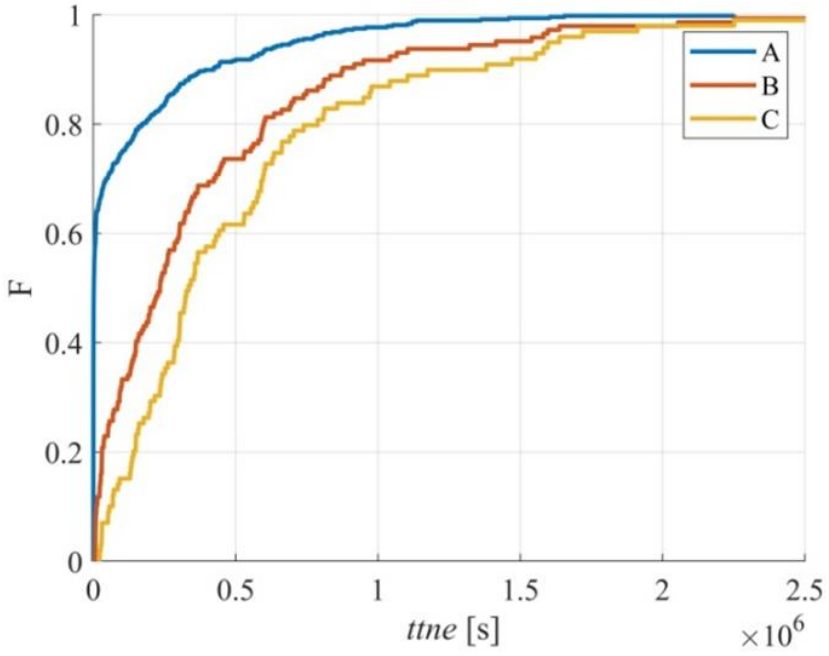

Figure 4.9. Cumulative probability, F, of the ttne at site #39: (A) without the application of filters; (B) with the 1-hour filter; and (C) with the ΔTLimitk-1% filter

Table 4.2 Percentiles of the cumulative probability, F, of the ttne at site #39: (A) without the application of filters; (B) with the 1-hour filter; (C) with the ΔTLimitk-1% filter

Percentiles	A	B	C
$P_{10\%}$	49.16 s (0.01 h)	1.12×10^4 s (3.11 h)	6.13×10^4 s (17.03 h)
$P_{30\%}$	206.67 s (0.06 h)	9.20×10^4 s (25.56 h)	2.20×10^5 s (61.11 h)
$P_{50\%}$	1.71×10^3 s (0.48 h)	2.34×10^5 s (65.00 h)	3.35×10^5 s (93.06 h)
$P_{70\%}$	4.60×10^4 s (12.78 h)	4.26×10^5 s (118.33 h)	5.95×10^5 s (165.28 h)
$P_{90\%}$	4.23×10^5 s (117.50 h)	8.80×10^5 s (244.44 h)	1.30×10^6 s (361.11 h)

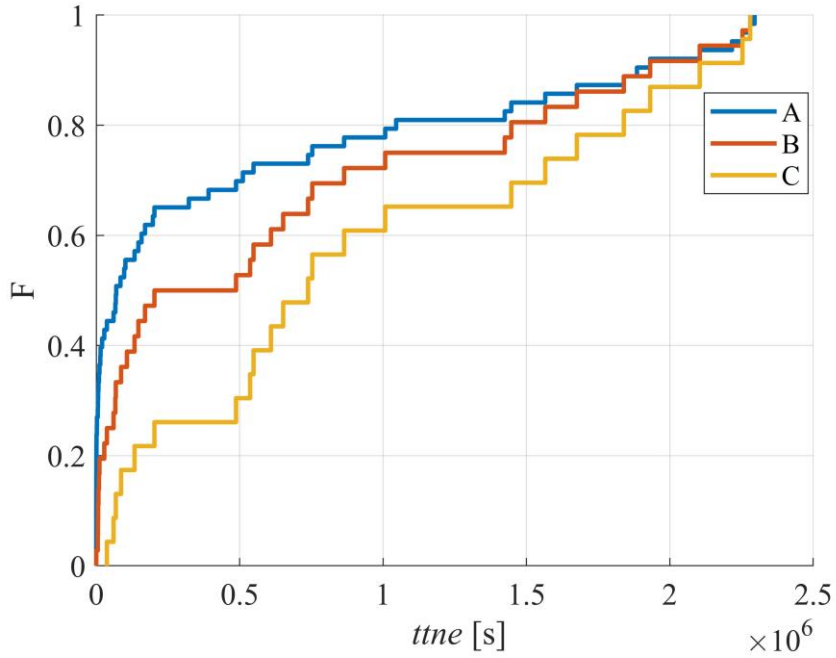

Figure 4.10. Cumulative probability, F, of the ttne at site #92: (A) without the application of filters; (B) with the 1-hour filter; and (C) with the ΔTLimitk-1% filter

Table 4.3 Percentiles of the cumulative probability, F, of the ttne at site #92: (A) without the application of filters; (B) with the 1-hour filter; (C) with the ΔTLimitk-1% filter

Percentiles	A	B	C
$P_{10\%}$	78.68 s (0.02 h)	6.70×10^3 s (1.86 h)	6.66×10^4 s (18.5 h)
$P_{30\%}$	6.21×10^3 s (1.73 h)	6.71×10^4 s (18.64 h)	5.07×10^5 s (140.83 h)
$P_{50\%}$	6.98×10^4 s (19.39 h)	3.45×10^5 s (95.83 h)	7.39×10^5 s (205.27 h)
$P_{70\%}$	5.02×10^5 s (139.44 h)	8.31×10^5 s (230.8 3h)	1.52×10^6 s (422.22 h)
$P_{90\%}$	1.89×10^6 s (525.00 h)	1.92×10^6 s (533.33 h)	2.13×10^6 s (591.67 h)

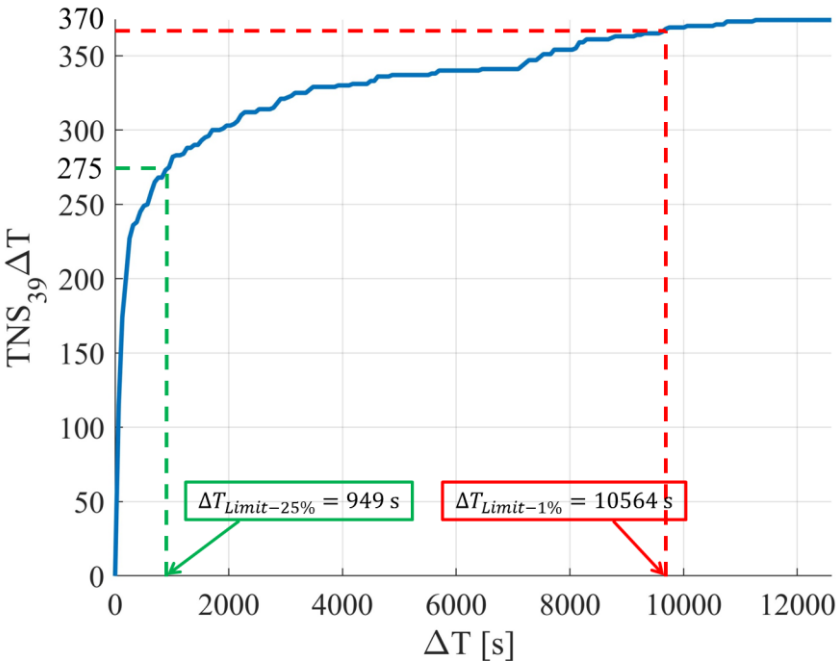

Figure 4.11. Plot of $TNS_{39}\Delta T$ versus ΔT computed at the site #39 for voltage sags measured from 2015 to 2017

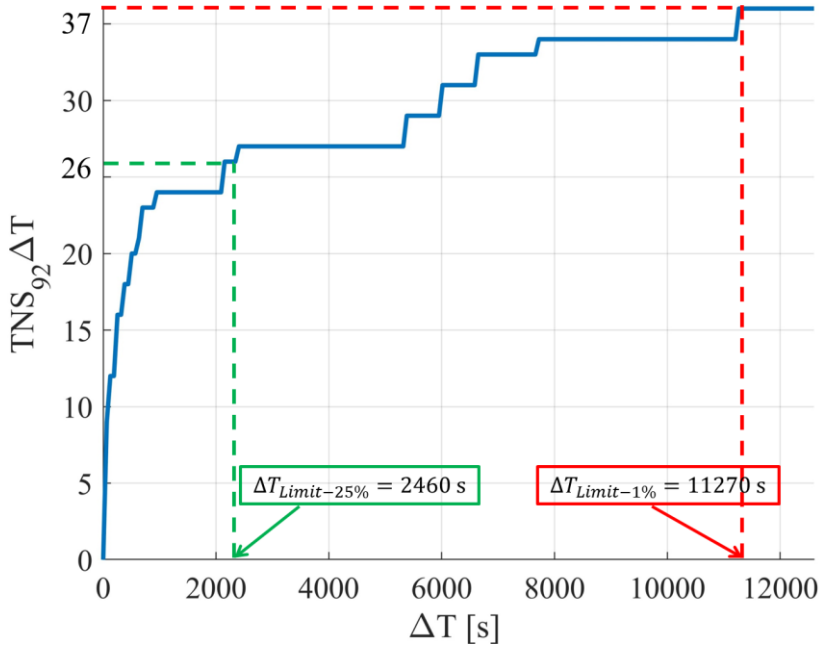

Figure 4.12. Plot of $TNS_{92}\Delta T$ versus ΔT computed at the site #92 for voltage sags measured from 2015 to 2017

The value $\Delta TLimit_{92}1\%$ discard from the statistical analysis no voltage sags because from 11270 seconds the maximum percentage threshold of variability of $TNS_{92}\Delta T$ around its maximum value (37) is equal to 1%. The value $\Delta TLimit_{39}1\%$ discard from the statistical analysis 4 voltage sags because from 10564 seconds the maximum percentage threshold of variability of $TNS_{92}\Delta T$ around its maximum value (374) is equal to 1%. The value $\Delta TLimit_{39}1\%$ measured at the site #39 is comparable to the value $\Delta TLimit_{92}1\%$ measured at the site #92. This is due to the small number of voltage sags recorded at the site #92 from 2015 to 2016. Although the comparable value of $\Delta TLimit_k1\%$, the number of discarded sags is different. The value $\Delta TLimit_{92}25\%$ discard from the statistical analysis 11 voltage sags because from 2460 seconds the maximum percentage threshold of variability of $TNS_{92}\Delta T$ around its maximum value (37) is equal to 25%. The value $\Delta TLimit_{39}25\%$ discard from the statistical analysis 95 voltage sags because from 949 seconds the maximum percentage threshold of variability of $TNS_{25}\Delta T$ around its maximum value(374) is equal to 25%.

From this analysis it is evident that the threshold $\Delta TLimit_k1\%$ applied for low values of $TNS_k\Delta T$ could cause an incorrect detection of clusters. The maximum value of ΔT (12600 s) for low value of voltage sags recorded in three years could be inadequate. Also, a maximum value of ΔT tuned in according of the maximum number of sags measured during the measurement years could improve the clusters detection. Future studies will consider artificial intelligence algorithms capable of learning from historical data similar trends to those of the site #92

After this procedure, the voltage sags, which time between events was greater than 2.59×10^6 s, were discarded from the statistical analysis in according to [12]. These *ttne* values were considered outliers because they could be due to incorrect registration or data measurement failure.

After the detection of the clusters, they were removed from all of the voltage sags; the remaining voltage sags, which were referred to as rare voltage sags, were validated and used to forecast the performance of the system in the year 2018. The objective of this validation step was to verify the validity of the assumption of the statistical variable *ttne* distributed following the exponential *pdf* by means of global features, like the percentiles. The objective was not to identify the specific *pdf*, which best fitted with data. This also was motivated by the fact that, in the case of positive validation, the only searched parameter was the estimate of the constant event rate, λ, of expression (4.31). Several graphical techniques were available for this type of

validation. As also was done in [12], the theoretical quantile-quantile plots, referred to as Q-Q plots, was implemented.

4.3.2 Graphical Methods to Validate the Statistical Assumption

Q-Q Plot is one of the graphical tools used to make distributional analyses between an empirical distribution derived from a dataset and a theoretical distribution. It is based on the plotting of the quantiles of an empirical distribution derived from a dataset against the corresponding quantiles of the theoretical distribution. The two main analyses allowed by the Q-Q Plots are the distributional comparisons between the two distributions [12], and the estimation of one distribution parameter of the theoretical distribution [13-15]. This second target was used in this study. The Q-Q Plots allowed to compare the empirical distribution, obtained from the monitoring data, with a theoretical distribution [59]. The Q–Q Plot used the values of the quantiles of the two probability distributions in comparison by representing in a plot the quantiles of one distribution against the quantiles of the other distribution. If the two distributions are related linearly, the points in the Q–Q Plot will lie approximately on a line with a grade of correlation measurable by the correlation factor, *r*.

The quantiles of the theoretical exponential distribution of *ttne* against the quantiles of the measured *ttne* are plotted. Given the wide range of the values of the measured *ttne*, a cubic-square transformation was needed, and this introduced the auxiliary variable, y_i, for every value of $ttne_i$:

$$y_i = \sqrt[3]{ttne_i} \tag{4.32}$$

The searched parameter, λ, of distribution (4.31) was the slope *m* of the straight line where the points in the Q-Q Plots lay:

$$\lambda^{-1} = m^3 \tag{4.33}$$

where m is estimated by the least square's method.

Figure 4.13 shows the Q-Q Plots of the data registered for the substation at busbar #39. The Q-Q Plots of *ttne* related to the voltage sags filtered with a 1-hour filter (Figure 4.14) and with the $\Delta TLimit_k$-*1%* filter (Figure 4.15) were considered.

Figure 4.16 shows the Q-Q plots of the data registered for the substation at busbar #92. The Q-Q Plots of *ttne* related to the voltage sags filtered with a 1-hour filter (Figure 4.17) and with the $\Delta TLimit_k$-*1%* filter (Figure 4.18) were considered.

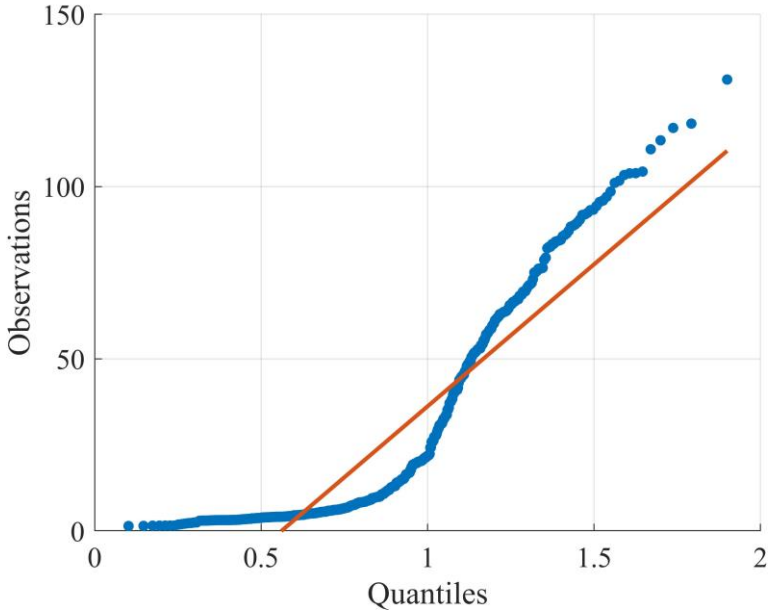

Figure 4.13. Exponential distribution Q-Q Plots with cubic square transformation for the site #39: no filter

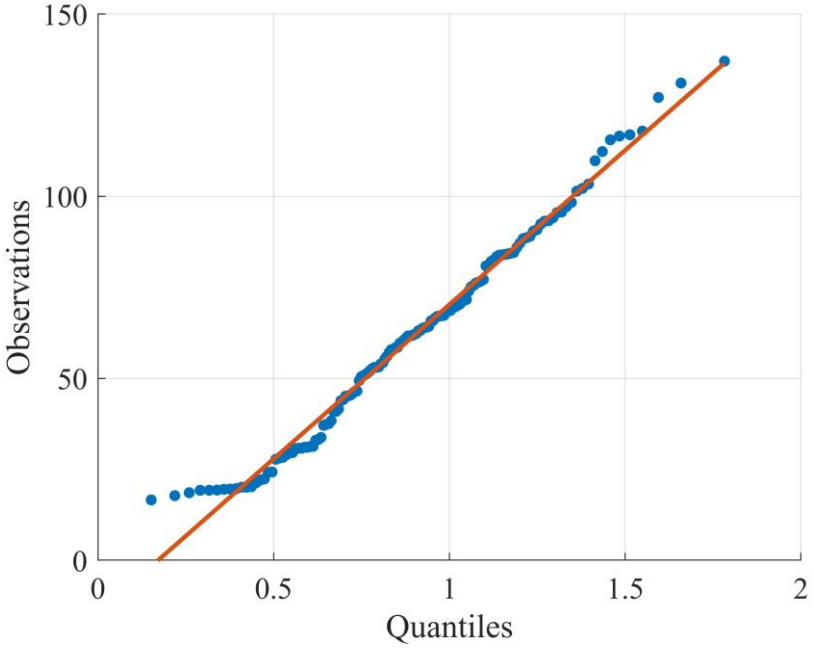

Figure 4.14. Exponential distribution Q-Q Plots with cubic square transformation for the site #39: 1h filter

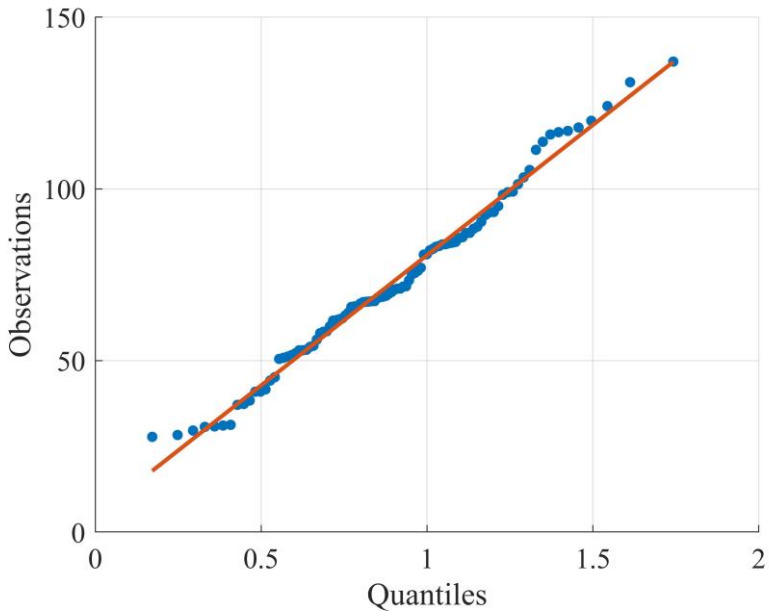

Figure 4.15. Exponential distribution Q-Q Plots with cubic square transformation for the site #39: ΔTLimitk-1% filter

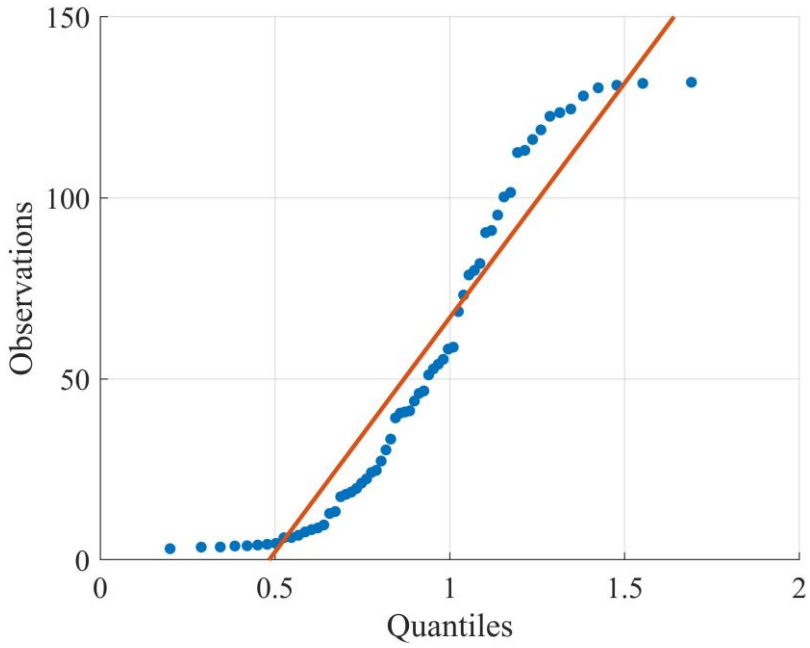

Figure 4.16. Exponential distribution Q-Q Plots with cubic square transformation for the site #92: no filter

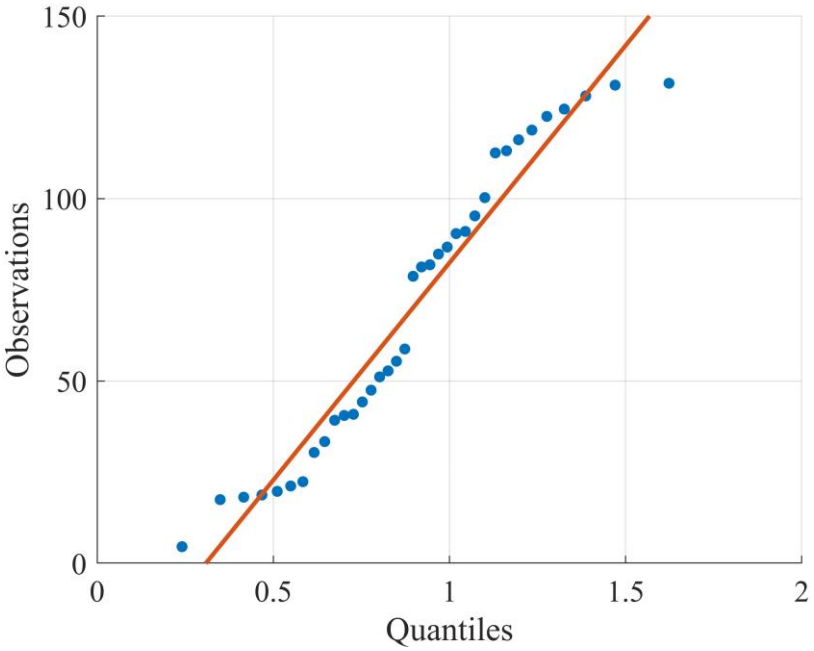

Figure 4.17. Exponential distribution Q-Q Plots with cubic square transformation for the site #92: 1h filter

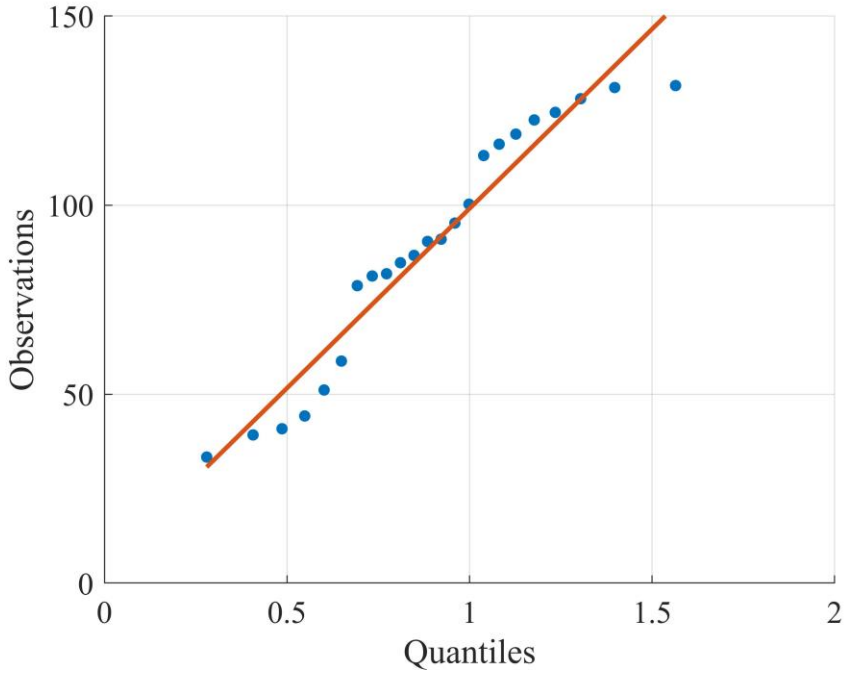

Figure 4.18. Exponential distribution Q-Q Plots with cubic square transformation for the site #92: ΔTLimitk-1% filter

The numerical results of the estimation of the mean value of *ttne*, i.e., λ^{-1}, and the correlation factor *r* are reported in Table 4.4.

Table 4.4 Numerical results after filtering and validation steps, of the ttne at site #39 and #92: without the application of filters; with the 1-hour filter; with the ΔTLimitk-1% filter

Site	**Filter**	**Without clusters**	λ^{-1} $[s^{-1}]$	***r***	***m [°]***	**Y=0**	**X=0**
	No Filter	478	5.60×10^5	0.91	70.00	0.56	-46.22
#39	1 *hour*	148	6.08×10^5	0.99	52.83	0.17	-14.46
	$\Delta TLimit_{39}$*-1%*	108	4.36×10^5	1.00	43.73	0.06	4.86
	No Filter	72	2.17×10^6	0.95	71.29	0.48	-62.53
#92	1 *hour*	47	1.69×10^5	0.97	63.58	0.30	-36.73
	$\Delta TLimit_{92}$*-1%*	36	8.56×10^5	0.96	48.00	0.04	4.14

In according to the obtained results of Figure 4.11 and Figure 4.12, from site #39 and #92, 370 and 26 voltage sags were discarded by $\Delta TLimit_k$*-1%* filter respectively. From the results in Table 4.3, in fact, only 108 and 36 voltage sags were considered rare sags by the intermittent index.

It was interesting to note that the results with the 1-*hour* filter and with the $\Delta TLimit_k$-*1%* filter were quite different. The 1-*hour* filter left additional clusters in the rare voltage sags for the site #39, which are the points on the left tail of the curves in Figure 4.14. This caused an increased slope, *m*, of the straight line, which, in turn, caused an increase in the value of λ^{-1} in Table 4.3. In Table 4.3 are reported also the x-axis intercepted of the straight line (*Y=0*) and the y-axis intercepted of the straight line (*X=0*).

It is interesting to note that for the site #39, in correspondence of the $\Delta TLimit_{39}$-*1%* filter:

- the values of the x-axis intercepted, and y-axis intercepted of the straight line are close to zero;
- the value of *m* is close to 45°;
- the value of *r* is equal to 1.

These information's suggest a perfect correlation between the straight line and the observations.

For the site #92, the filter $\Delta TLimit_k$-*1%* discards from the statistical analysis too much data and 34 observations are not sufficient to perform a forecast in according to the previous theoretical considerations in paragraph 4.2.

4.3.3 Computation of Forecasted Number of Sags at Each Node

The forecasted mean number of voltage sags, N_f, was derived easily from the following equation [12]:

$$N_f = \lambda * Y \tag{4.34}$$

where λ is the sag rate in number of sags per second, and *Y* is the period of observation of one year expressed in seconds (31.5 ×106 s).

The voltage sags measured in 2018 first were filtered by the same filters applied to the sags measured in 2015-2017. As described previously, the first filters that were used were *1-hour* and $\Delta TLimit_k$-*1%* filters. The number of voltage sags that occurred in 2018 was compared with the value of N_f calculated by relation (4.34).

As an example, Table 4.5 shows the first results of the forecasting activity for the sites of example #39 and #92, where the forecast error, ε_F, was computed as the

absolute value of the difference between the number of forecasted sags in 2018 and the number of measured sags in 2018, in percentage of the measured sags in 2018.

Table 4.5 Numerical results after filtering and validation steps, of the ttne at site #39 and #92: without the application of filters; with the 1-hour filter; with the ΔTLimitk-1% filter

Site	Filter	N_f	Measured in 2018	$\varepsilon_{F\,[\%]}$
#39	No Filter	56	249	78
	1 *hour*	52	101	50
	$\Delta TLimit_{39}$-1%	72	76	5
#92	No Filter	14	34	59
	1 *hour*	18	18	0
	$\Delta TLimit_{92}$-1%	36	15	140

For the site #39, the performance of the forecasting using the $\Delta TLimit_{39}$-1% filter, is very good in according to the theoretical considerations of the previous paragraph (4.2) and the literature [58]. For the site #92, the performance of the forecasting using the $\Delta TLimit_{92}$-1% filter, is not acceptable because the number of observations is insufficient for obtaining good forecast performance. The 1 *hour* filter gives excellent forecasting performance for the site #92.

4.4 Numerical Results

The forecasting performances of the proposed model were verified on an entire regional electric system constituted by 83 HV/MV substations and 152 MV busbars that represents the measurements point of the voltage sags. The average forecast error for the entire system was measured by the index of error, i.e., Symmetrical Medium Absolute Percentage Error (*SMAPE*); it was defined by the following expression:

$$SMAPE = \frac{100}{K}\sum_{k=1}^{K}\frac{\left|N_{f,k} - N_k\right|}{\frac{|N_k| + \left|N_{f,k}\right|}{2}}. \tag{4.35}$$

In Eq. (38), N_k is the true value of the number of sags measured in 2018 at the site k, $N_{f,k}$ is the forecasted number of voltage sags at the same site k, and K is the total number of sites where voltage sags were measured. For the whole system, the value of *SMAPE* was 24.6% in the case of the application of the $\Delta TLimit_k$-1%, and it was 35.9 % in the case of the application of the *1-hour* filter. Table 4.6 shows the percentiles of ε_F after the application of the $\Delta TLimit_k$-1% filter.

Table 4.6 Percentiles of ε_F of the Sites of the Regional System using 1-hour filter and $\Delta TLimit_k$-1%

Percentile [%]	***1-hour* filter [%]**	***$\Delta TLimit_k$-1%* [%]**
$P_{5\%}$	8.9	1.7
$P_{10\%}$	14.3	2.2
$P_{25\%}$	27.2	6.7
$P_{50\%}$	36.8	21.0
$P_{75\%}$	45.0	38.0
$P_{90\%}$	55.2	56.9

Table 4.4shows that, in 75% of the sites, ε_F passed from about 45% with *1-hour* filter to 38% with $\Delta TLimit_k$-1%, only the extreme values of ε_F ($P_{90\%}$) increased from 55.2% with *1-hour* filter to 56.9 % with $\Delta TLimit_k$-1%.

The first results obtained on the entire system, even if the forecast was generally improved with respect to the one obtained by *1-hour* filter, were not yet completely satisfactory. Consequently, we performed a parametric analysis of forecast for every site by differing the threshold of variation of $TNS_k\Delta T$ from 1% up to 25%. In particular, at every site of the regional system, the clusters of the sags measured from 2015 to 2017 were filtered and removed by imposing all the thresholds from 1% to 25% to the variation of $TNS_k\Delta T$; for each value of the threshold, the rare sags in the year 2018 were forecasted.

Therefore, at each site, multiple forecast results were obtained, each corresponding to different values of $\Delta TLimit_k$-%. Among these solutions, that one that presented the minimum value of ε_F were considered for successive evaluations. Figures 19 and 20 present some of the main results. In particular, Figure 4.19 shows, for every value of $\Delta TLimit_k$-%, how many sites reported the minimum value of ε_F. Figure 4.19 shows that more than 70 sites presented the minimum ε_F with the threshold equal to 1%, but the remaining sites gave the minimum ε_F in correspondence of higher value of the threshold up to 25%. Further, Figure 4.20 indicates that more than 100 sites (117 sites) presented the minimum ε_F lower than 15.5%, and that only in few sites the minimum ε_F reached higher values up to about 62%.

The number of sites with minimum ε_F from 31% to 46.5% was 9, and only for 1 site the minimum error ε_F was between 46.5% and 62%. Table 4.7 gives the percentiles of ε_F computed using the forecasted number of sags with the minimum ε_F. It is evident that in 75% of the sites, the forecast presented ε_F values less than 13%, and only the extreme value of percentile ($P_{90\%}$) reached about 27%. The value

of *SMAPE* was 9.6%. Further parametric analyses were performed for the same regional system to forecast the number of voltage sags in the year 2017. We considered both the sags measured from 2014 to 2016 and the sags measured from 2015 to 2016 to evaluate if a time window of two years could be sufficient for the forecast.

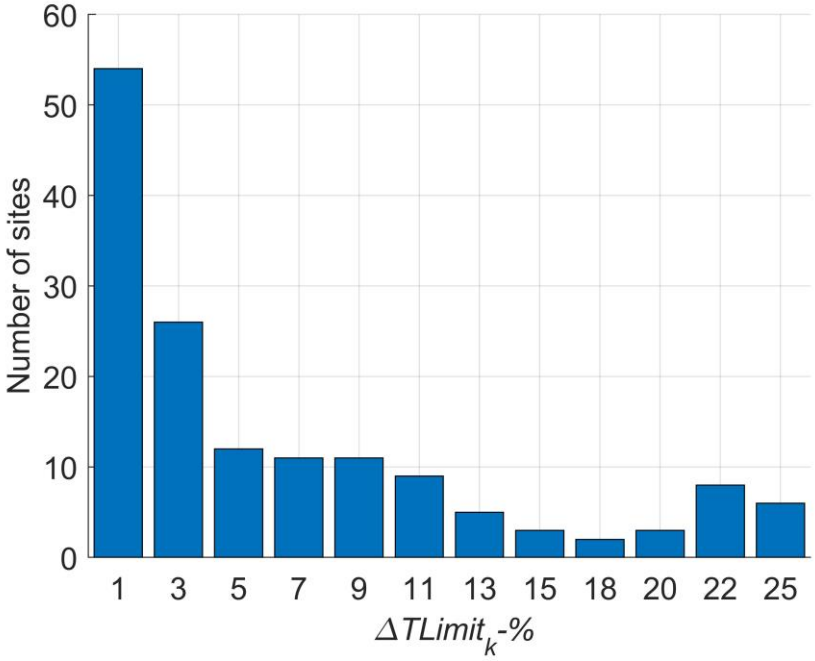

Figure 4.19 Distribution of the sites that had the minimum value of ε_F in correspondence of the threshold $\Delta TLimit_k$-% – Forecast for the year 2018.

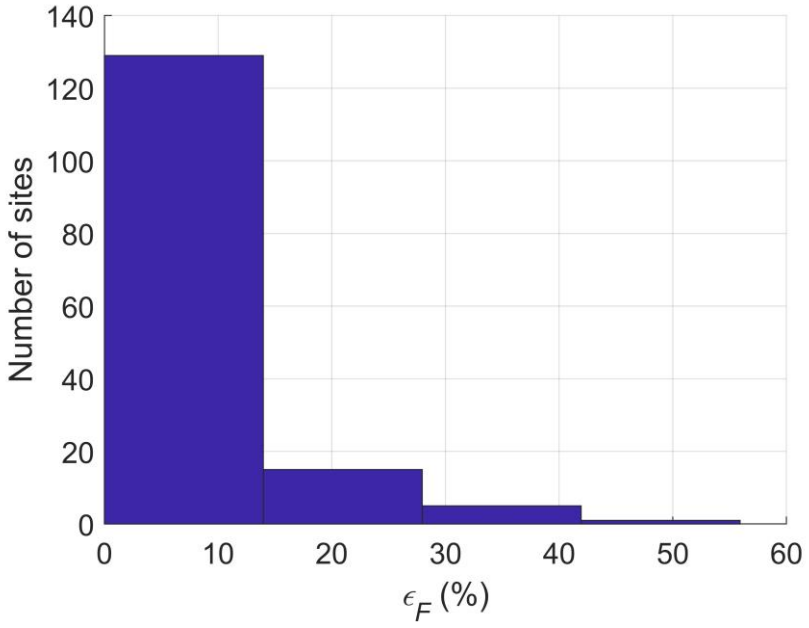

Figure 4.20 Distribution of the minimum ε_F along the sites of the system – Forecast for the year 2018.

Table 4.7 Percentiles of the Minimum ε_F of the Sites of the Regional System – Forecast for the year 2018

Percentile	**ε_F [%]**
$P_{5\%}$	0.0
$P_{10\%}$	0.0
$P_{25\%}$	2.2
$P_{50\%}$	4.6
$P_{75\%}$	12.9
$P_{90\%}$	27.3

In both the cases, clusters were filtered and removed by imposing all the thresholds from 1% to 25% to the variation of $TNS_k \Delta T$; for each value of the threshold, the rare sags in the year 2017 were forecasted, and the forecast error ε_F was computed. Analogously to Table 4.7, Table 4.8 shows the percentiles of ε_F computed using the forecasted number of sags with the minimum ε_F, and the corresponding value of *SMAPE*. Table 4.8 proves that also for a different year of forecast, the results are quite good and close to those of 2018 (Table 4.7). The best performance of the forecast was obtained using three years of measurements with an appreciable reduction of *SMAPE* and of the percentiles of minimum ε_F. Figure 4.21 shows the distribution of the minimum ε_F along the sites for two different windows

of time. It is interesting to note that the use of two years of measurements does not change the number of sites with the minimum ε_F of lowest value but affects the distribution of the minimum ε_F with largest value. In the case of two years of measurements used to forecast the performance in the year 2017 (Figure 4.21a)) the minimum ε_F reached the unacceptable value of 80%, instead when three years of measurements were used (Figure 4.21b)), the minimum ε_F did not overcome the value of 50%.

The results of the parametric studies showed that the forecast was not prohibitive and had acceptable errors when only three years of measurements were used. The values of the minimum ε_F and the *SMAPE* are acceptable since they prove that the forecast gives the appropriate order of magnitude of the number of sags that will occur at most of the sites in the incoming year (117 sites over 152 for the forecast of 2018).

Table 4.8 Percentiles of the Minimum ε_F and SMAPE of the Sites of the Regional System for two different time window – Forecast for the year 2017

Percentile [%]	**Time window**	
	2015-2016	***2014-2015-2016***
	ε_F [%]	**ε_F [%]**
$P_{5\%}$	0.0	0.0
$P_{10\%}$	0.0	0.0
$P_{25\%}$	2.5	1.9
$P_{50\%}$	4.5	4.1
$P_{75\%}$	8.9	8.6
$P_{90\%}$	24.7	15.6
SMAPE	8.6	6.6

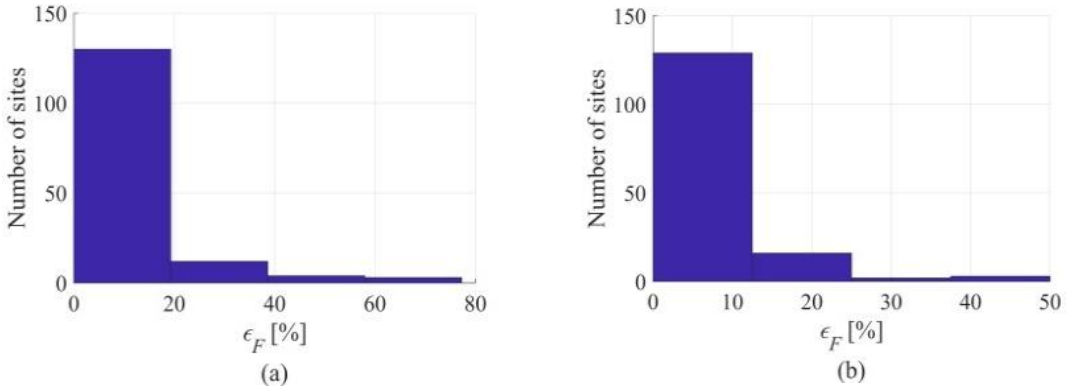

Figure 4.21 Distribution of the minimum ε_F along the sites of the system – Forecast for the year 2017; a) sags measured from 2015 to 2016; b) sags measured from 2014 to 2016.

CHAPTER 5.

FORECASTING VOLTAGE SAGS COMPREHENSIVE OF CLUSTERS

The Gamma distribution was proposed for modelling the whole sags, which also include the clusters. Different techniques for assessing the parameters of the Gamma distribution are presented and applied to forecast the number of sags expected at selected sites and the entire system in the year successive to those when the sags were measured. The outcomes of the forecast are compared with the sags effectively occurred in those sites, using different criteria for evaluating the forecast error. The not completely satisfactory results on all the system suggested to deep analyse in few sites the rare sags separately from the sags comprehensive of clusters. The intermittence indices proved to be an effective tool to discriminate the forecast model to use.

5.1 Introduction

The presence of the sag clusters makes the sag frequency dependent on the time. The sags, which contain both rare sags and sag clusters, present the features of a stochastic process. They do not have the characteristics of memoryless events and, consequently, cannot be modelled as a Poisson process. As stated in the previous Chapters, to make successful forecast, filtering the sag clusters out from all the measured sags is crucial

In this thesis, a first approach aimed to predict all the sags, which contain both rare sags and sag clusters is proposed. The statistical model of such time-dependent events must respect the stochastic nature of the phenomenon. It is possible by means of the Gamma distribution of *ttne*. This model was first proposed in [12] to describe the recorded data but not for forecast purposes.

Modelling a process by the Gamma distribution requires to select two parameters, that is the shape parameter α, and the scale parameter β. Analytical and graphical methods to establish the values of α and β, which statistically describe the random variable *ttne* with minimum error were analysed in order to evaluate if there is an estimation method that furnishes the best forecast performance. The proposed model to forecast the voltage sags comprehensive of clusters was validated using the sags recorded from 1st January 2015 to 31st December 2017 with the specific target to forecast the expected number of voltage sags in 2018. The sags were recorded at the regional electric system, whose main characteristics were described extensively in the previous Chapters. The availability of the sags really occurred in the year 2018 allowed to evaluate the errors of the forecast.

5.2 Statistical Models

The sags belonging to clusters do not have the statistical characteristics of a Poisson process since they are events related to each other, often they have a common origin, for example an adverse atmospheric phenomenon or fires, and for these reasons, their time independence cannot be assumed. If the statistical analysis is conducted on the measured sags, the only way to apply the exponential distribution

is to filter and remove the clusters of sags, leaving only the rare sags in the data to be analysed, as done in the previous Chapter. Without applying these filters, a stochastic model of voltage sag occurrences is required to describe their random appearance in the time, with large periods of absences, when only rare sags occur, and others when sags appear as clusters. To model all the recorded sags, the assumption of constant sag rate is not valid, and the distribution of the random variable *ttne* is given by:

$$f_s\big(ttne, \lambda(t)\big) = \lambda(t) e^{\left[-\int_o^{ttne} \lambda(\xi)\, d\xi\right]}. \tag{5.1}$$

where $\lambda(t)$ is the sag rate variable with the time.

Figure 5.1 shows the probability density function (*pdf*), of *ttne* of the voltage sags recorded at the site of example #38. It is evident a thickening of the *ttne* values in the first class. The first class of the histograms in Figure 5.1 is linked to the presence of clusters of sags. For successive classes, there is a decay of the *pdf* values.

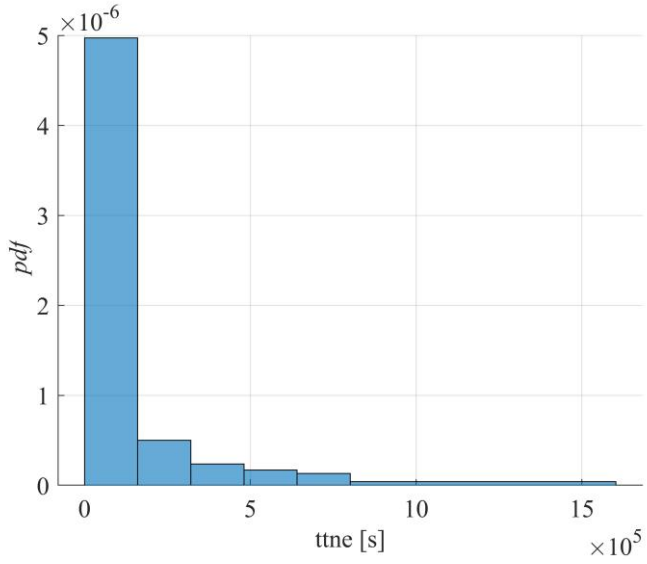

Figure 5.1 Histogram of density of probability of the random variable ttne measured in the site #39.

Figure 5.2 shows the empirical cumulative density function (*ecdf*) corresponding to the *pdf* of Figure 5.1; the plot of Figure 5.2 (b) is zoomed in the low range of *ttne.*

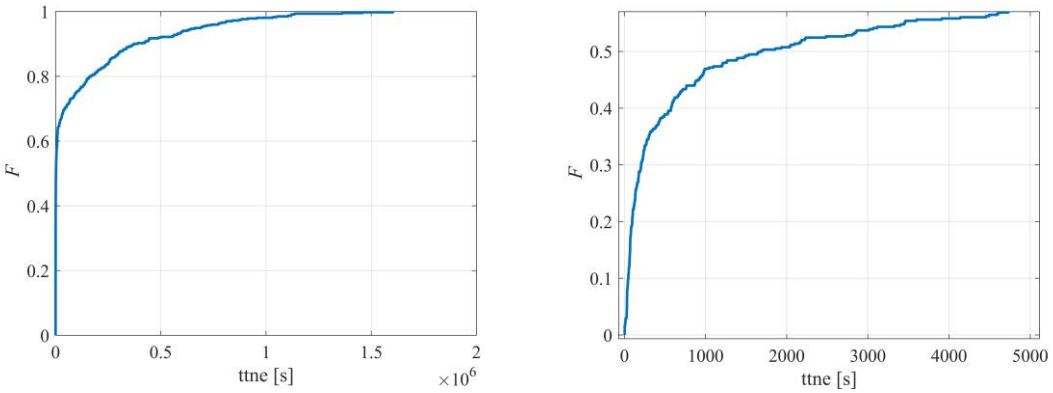

(a) (b)

Figure 5.2 Empirical cumulative density functions of the random variable ttne for the site #39; (a): complete plot; (b) plot zoomed in the range [0,5000] s.

From Figure 5.2(a), it is evident that the values of *ttne* range from 3 s to 1.6×10^6 s (444 hours), but Figure 5.2 (b) revealed that the greatest probability, up to 60%, is already reached by *ttne* less than 5×10^3s (1.4 hours), leaving the remaining 40% to the *ttne* up to 1.6×10^6 s. This feature of the recorded data, evident also for other sites beside site #39, proved that the sag rate is not constant, if all the sags have to be statistically modelled.

Figure 5.3 shows the probability density function (*pdf*), of *ttne* of the voltage sags recorded at the site of example #92.

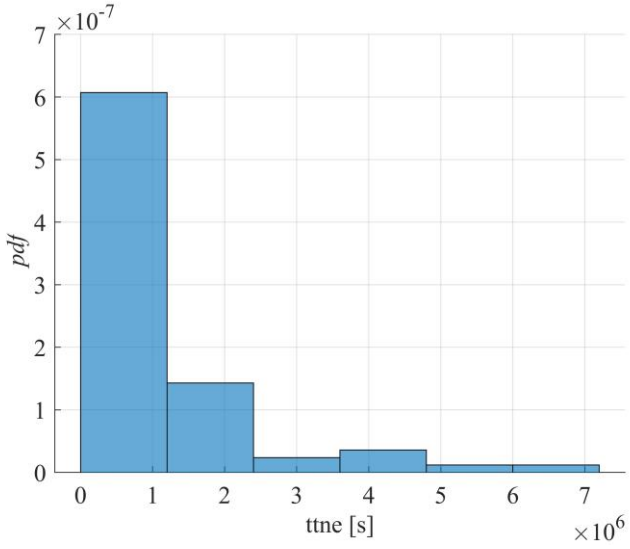

Figure 5.3 Histogram of density of probability of the random variable ttne measured in the site #92.

Figure 5.2 shows the empirical cumulative density function (*ecdf*) corresponding to the *pdf* of Figure 5.1; the plot of Figure 5.2 (b) is zoomed in the low range of *ttne.*

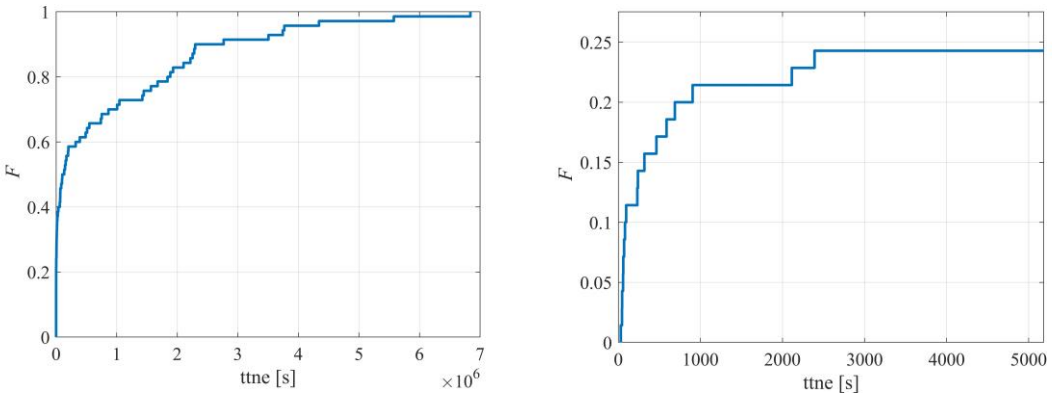

(a) (b)

Figure 5.4 Empirical cumulative density functions of the random variable ttne for the site #92; (a): complete plot; (b) plot zoomed in the range [0,5000] s.

From Figure 5.4(a), it is evident that the values of *ttne* range from 3 s to 7×10^6 s (1944 hours), but Figure 5.4 (b) revealed the probability that the values of *ttne* measured in the site #92 are less than 5000 s is equal to 25%. This feature of the recorded data demonstrated that a minor number of clusters were measured in this site instead in the site #39.

As proposed in [12], the random variable *ttne* of all the sags, both rare and clusters, can be described by the Gamma distribution as:

$$pdf(ttne, \alpha, \beta) = \frac{\beta^{\alpha} ttne^{\alpha-1} e^{-\beta ttne}}{\Gamma(\alpha)} \tag{5.2}$$

where α and β are the shape and the scale parameters, respectively.
The corresponding *cdf* is given by:

$$cdf(ttne, \alpha, \beta) = \int \frac{ttne^{\alpha-1}}{\beta^{\alpha}\,\Gamma(\alpha)} exp\left(-\frac{ttne}{\beta}\right) dttne \tag{5.3}$$

$$= \frac{\gamma(\alpha, \beta, ttne)}{\Gamma(\alpha)}$$

where γ (α, β, *ttne*) is the incomplete Gamma function and $\Gamma(\alpha)$ is the Gamma function. The mean value of the Gamma distribution is equal to:

$$E[X] = \frac{\alpha}{\beta} \tag{5.4}$$

For β = 1, and for different values of the shape parameter α, Figure 5.5 shows the theoretical plots of the *pdf* and of the *cdf* of the Gamma distribution of a generic

random variable t in seconds. Figure 5.5 shows that, for a given value of β, the variation of α implies completely different waveshapes of the Gamma *pdf* and *cdf*.

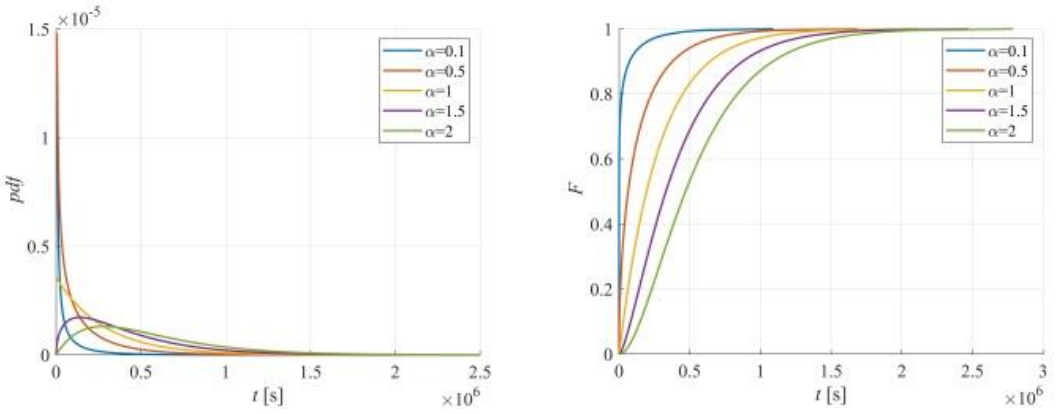

(a) (b)

Figure 5.5 Theoretical probability density distribution (a), and cumulative distribution (b) of the Gamma distribution of a generic variable t in seconds.

For α from 0.1 to 0.5, the *pdf* in Figure 5.5 (a) presents a thickening of observations close to zero, as derived by the empirical distribution of all the measured sags at the site #39 showed in Figure 5.2. For α equal to 1, the Gamma *cdf* is equal to the exponential *cdf* with mean parameter λ equal to the scale parameter β of the Gamma distribution.

Table 5.1 shows different percentiles of the theoretical Gamma *cdf* of a random variable *t*, with β =1 and α ranging from 0.1 to 2.

Table 5.1 Percentile Values of the Gamma Distribution with β=1 and α ranging from 0.1 to 2.

Percentile		**A**				
		0.1	**0.5**	**1**	**1.5**	**2**
$\mathbf{P_{10\%}}$	**[s]**	2.6×10^{-5}	2.4×10^{3}	3.1×10^{4}	8.4×10^{4}	1.5×10^{5}
	[h]	7.2×10^{-9}	0.7	8.6	23.3	41.7
$\mathbf{P_{30\%}}$	**[s]**	4.3	2.8×10^{4}	1.2×10^{5}	2.3×10^{5}	3.4×10^{5}
	[h]	1.2×10^{-3}	7.8	33.3	63.9	94.4
$\mathbf{P_{50\%}}$	**[s]**	303.2	7.3×10^{4}	2.1×10^{5}	3.5×10^{5}	5.0×10^{5}
	[h]	8.4×10^{-2}	20.3	58.3	97.2	138.9
$\mathbf{P_{70\%}}$	**[s]**	6.0×10^{3}	1.6×10^{5}	3.5×10^{5}	5.3×10^{5}	7.0×10^{5}
	[h]	1.7	44.4	97.2	147.2	194.4
$\mathbf{P_{90\%}}$	**[s]**	7.3×10^{4}	3.8×10^{5}	6.4×10^{5}	8.7×10^{5}	1.1×10^{6}
	[h]	20.3	105.6	177.8	241.7	305.6

For α equal to 0.1, 10% of *t* is less than 2.6×10^{-5}, i.e. very close to zero, and 70% of the values are not greater than 1.7 h. As the shape parameter α increases, the 10th

percentile increases too. For α equal to 2, 10% of t is less than about 42 h, and 70% of the values are not greater than 194.4 h.

In conclusion, the use of Gamma distribution requires the correct estimation of the parameters α and β, as shown in the successive paragraph.

5.3 Proposed Method

Figure 5.6 shows the scheme of the proposed method for forecasting voltage sags comprehensive of clusters. The registered data from the field over a period of N years were used to forecast the sags in the successive year.

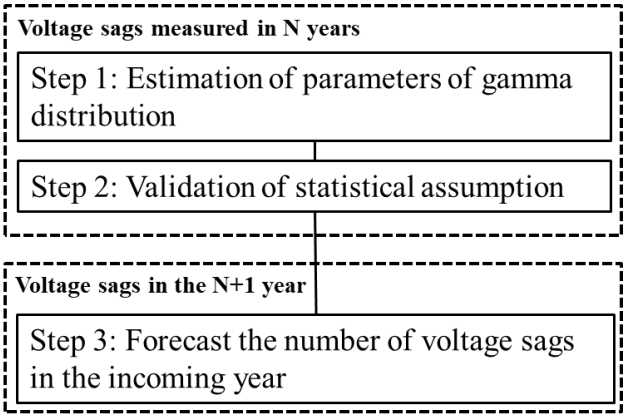

Figure 5.6 Flow chart of the proposed method

There are two separate blocks, which are included in rectangles with the dashed lines. In the first block, the estimation of the parameters of the Gamma distribution and the successive validation of statistical assumption is performed. In the second block, the statistics derived from the years of measurements were used to forecast the following $(N+1)^{th}$ year.

The 1st and 2nd step were presented in the paragraph 5.3.1 and 5.3.2 respectively. The 3rd step was presented in the paragraph 5.3.3.

5.3.1 Estimation of the Parameters of Gamma Distribution

Modeling *ttne* of all the measured sags by the Gamma distribution requires to establish the two parameters α and β. Different techniques are available for the optimal selection of statistical parameters of an assumed *pdf* [60-63].

In this thesis both analytical and graphical methods were considered:

- Maximum Likelihood Estimation;
- Hill Climbing Algorithm;
- QQ Plot.

The Maximum Likelihood Estimation (*MLE*) is a very popular technique used for determining the parameters of a distribution chosen to describe observed data. The obtained parameters by *MLE* can be successively optimized in function of an analytical criterium or applying a graphical method, as done in this paper.

In the following, we first show the application of *MLE* to the case of Gamma distribution, and after we describe two methods, one analytical and one graphical, which we used to optimize the parameters obtained by *MLE*. These methods are the Hill Climbing Algorithm (*HCA*) and the Quantile-Quantile plot (*Q-Q plot*), respectively.

- ***Maximum Likelihood Estimation***

The searched values of the parameters α and β are found such that they maximise the likelihood that the process described by the *pdf* produced the data that were observed.

Let:

- $\bar{x}_i = (x_{i,1}, x_{i,2}, \ldots, x_{i,N})$ be the vector of the N observations at the site i of the random variable x_i;
- f_0 be the *pdf* which describes the observations and depends on the parameters included in the vector $\bar{\Theta}$;
- $\boldsymbol{\Theta}$ be the space of all the possible values of the vector $\bar{\Theta}$, i.e. $\bar{\Theta} \in \boldsymbol{\Theta}$.

The application of *MLE* implies that f_0 belongs to the family of Gamma distributions obtainable by different values of the parameters α and β, which are the components of the vector $\bar{\Theta}$.

The likelihood function $L(\overline{x_i};\ \overline{\Theta})$ is the product of the individual *pdf* of all the *N* samples of the random variables, assumed independent, that is:

$$L(\overline{x_i};\ \overline{\Theta}) = \prod_{k=1}^{N} F_0(\ \overline{x_i}\ , \overline{\Theta}). \tag{5.5}$$

For the case of Gamma distribution, the likelihood function is equal to:

$$L(\overline{x_i};\ \overline{\Theta}) = L\ (\overline{x_i};\ \alpha, \beta\ ) = \prod_{k=1}^{N} \frac{\beta^{\alpha} e^{-\beta x_{i,k}}\ {x_{i,k}}^{\alpha-1}}{\Gamma(\alpha)}. \tag{5.6}$$

The Log-likelihood function, $l\ (\overline{x_i};\ \overline{\Theta})$, is the natural logarithm of $L(\overline{x_i};\ \overline{\Theta})$, i.e.:

$$l\ (\overline{x_i};\ \overline{\Theta}) =\ \ln L(\overline{x_i};\ \overline{\Theta})\ . \tag{5.7}$$

Putting equation (5.6) in (5.7), the Log-likelihood function for the Gamma distribution with shape parameter α and scale parameter β, $l\ (\overline{x_i};\ \alpha, \beta)$, is defined as:

$$l\ (\overline{x_i};\ \alpha, \beta) =\ \ln \prod_{k=1}^{N} \frac{\beta^{\alpha} e^{-\beta x_{i,k}}\ {x_{i,k}}^{\alpha-1}}{\Gamma(\alpha)}. \tag{5.8}$$

Applying the logarithm properties and after some simplifications, the final expression $l\ (\overline{x_i};\ \alpha, \beta)$, is equal to:

$$l\ (\overline{x_i};\ \alpha, \beta) = N\alpha \ln \beta\ -\beta \sum_{k=1}^{N} x_{i,k} + (\alpha\text{-}1) \times \sum_{k=1}^{N} \ln x_{i,k}\ - \text{N} \ln \Gamma(\alpha). \tag{5.9}$$

Maximizing equation (5.9) with respect of the parameters α and β, we can derive the so called *MLE* estimators of the parameters. With this aim, equalling to zero the derivative of $l(\overline{x_i};\ \alpha, \beta)$ in (5.9) with respect to β, the maximum likelihood estimator of the parameter β is:

$$\beta = \frac{N\ \alpha}{\sum_{k=1}^{N} x_{i,k}}. \tag{5.10}$$

Substituting equation (5.10) in (5.9), we obtain:

$$l(\alpha) = N\alpha\ ln\ N\alpha -\ N\alpha\ ln\ \sum_{k=1}^{N} x_{i,k} - N\alpha + \alpha\ \sum_{k=1}^{N} ln\ (\ x_{i,k}) - \sum_{k=1}^{N} ln(x_{i,k})\ \ - N ln\big(\Gamma(\alpha)\big). \tag{5.11}$$

Equalling to zero the derivative of *l(α)* with respect to α:

$$\frac{\partial l}{\partial \alpha} = N ln\, N\alpha + N\alpha\, \frac{1}{\alpha} - N\, ln\left(\sum_{k=1}^{N} x_{i,k}\right) - N + \sum_{k=1}^{N} ln\,(x_{i,k}) - \quad (5.12)$$

$$N\psi(\alpha) = 0$$

where $\psi(\alpha) = \frac{\Gamma(\alpha)'}{\Gamma(\alpha)}$ is the Digamma function. After some simplifications on (5.12), we obtain:

$$\ln N\alpha - \psi(\alpha) = \ln \sum_{k=1}^{N} x_{i,k} - \frac{\sum_{k=1}^{N} ln\,(x_{i,k})}{N}. \quad (5.13)$$

Equation (5.13) gives the optimal value of α in implicit form, which can be solved by a numerical method.

- ***Hill Climbing Algorithm (HCA)***

HCA is an iterative algorithm which starts with an arbitrary solution and, in accordance with a function to be maximized or minimized, attempts to find a better solution by making an incremental change to the parameters. The optimal value of the parameters is found by using a test function [63]. In the case of this study, the arbitrary solution of start is given by the *cdf* of the Gamma distribution with α and β obtained by *MLE*, and the test function is the Chi Squared Test (*CS*). Let observations be divided into *M* bins:

- *F* is the theoretical *cdf*;
- $O_{i,1}, O_{i,2}, \ldots, O_{i,N}$ are the *N* observed values of each bins,
- the χ^2 value is equal to:

$$\chi^2 = \sum_{K=1}^{M} \left(\frac{\sum_{i=1}^{N} O_{i,K} - \sum_{i=1}^{N} EV_{i,K})^2}{\sum_{i=1}^{N} EV_{i,K}} \right) \quad (5.14)$$

where EV_K are the expected values for each bin computed as:

$$EV_K = F(b) \times N - F(a) \times N \quad (5.15)$$

where N is the data size, a is the start value of the k^{th} bin and b is the end value of the k^{th} bin, (b-a) is the length of the k^{th} bin, $F(a)$ and $F(b)$ are the values of the *cdf* of the Gamma distribution computed in a and b, respectively.

The searched optimal values of the parameters α and β are those corresponding to the minimum value of χ^2.

- ***Quantile-Quantile plots (Q-Q Plots)***

The theoretical distribution was the Gamma distribution with α obtained by *MLE*, and we used the *Q-Q Plot* to estimate the value of β. To this aim, the values of the quantiles of the data Q_d are equal to:

$$Q_d = \sqrt[3]{ttne} \tag{5.16}$$

and the quantiles of the theoretical distribution Q_t are equal to:

$$Q_t = (F^{-1})^{\frac{1}{3}} \tag{5.17}$$

where F^{-1} is the inverse *cdf* of the standard Gamma function with $\beta = 1$ and α estimated with *MLE*.

The searched value of the parameter β of the Gamma distribution, is equal to the slope of the regression line:

$$\beta = m^3 \tag{5.18}$$

Table 2 shows the results for three sites of example obtained applying the three different methods above recalled, that is: α and β estimated by *MLE*, α and β estimated by *HCA*; α estimated by *MLE* and β estimated by *Q-Q plot*.

Table 5.2 Parameters of the CDF of the Gamma Function Estimated by MLE, HCA and Q-Q plot.

Gamma distribution #	**Site #**	$E[ttne]$ **[s]**	α	β **[s^{-1}]**
Parameters estimated by *MLE*	39	1.14×10^5	0.20	1.78×10^{-6}
	92	8.84×10^5	0.25	2.81×10^{-7}
Parameters estimated by *HCA*	39	1.25×10^5	0.22	1.78×10^{-6}
	92	1.17×10^6	0.27	2.34×10^{-7}
Parameters estimated by *Q-Q Plot*	39	1.28×10^5	0.20	1.58×10^{-6}
	92	9.58×10^5	0.25	2.59×10^{-7}

From Table 5.2, it is evident that the shape parameter changes from *MLE* to *HCA* for all the sites, instead the scale parameter appreciably changes for the site #39 using the *Q-Q plot*. These changes of the parameters provided different values of the expected value of the Gamma distribution computed by relation (5.4).

Figures 5.7a and 5.7b present, for the site #39 and #92, the histogram of the *pdf* of the measured *ttne* (blue bars) and the *pdfs* with parameters estimated by *MLE (yellow curve)*, by *HCA (red curve)*, and by *Q-Q plot (green curve)*.

Figures 5.8a and 5.8b present, for the site #39 and #92, the *cdf* of the measured *ttne* (blue curve) and the *cdfs* with parameters estimated by *MLE* (red curve), by *HCA* (green curve), and by *Q-Q plot* (blue curve).

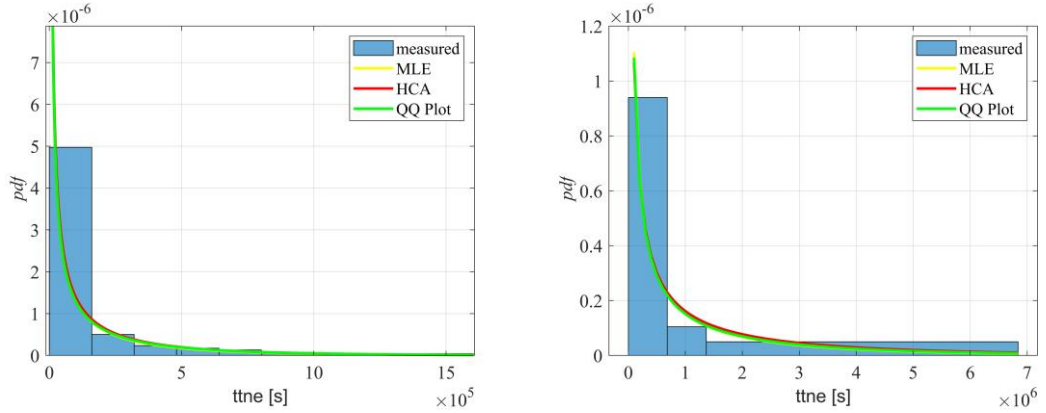

a) b)

Figure 5.7 Histogram of the probability density function (blue bars) and gamma pdfs with parameters estimated by MLE (yellow curve), by HCA (red curve), and by Q-Q Plot (green curve) – Site #39 and #92

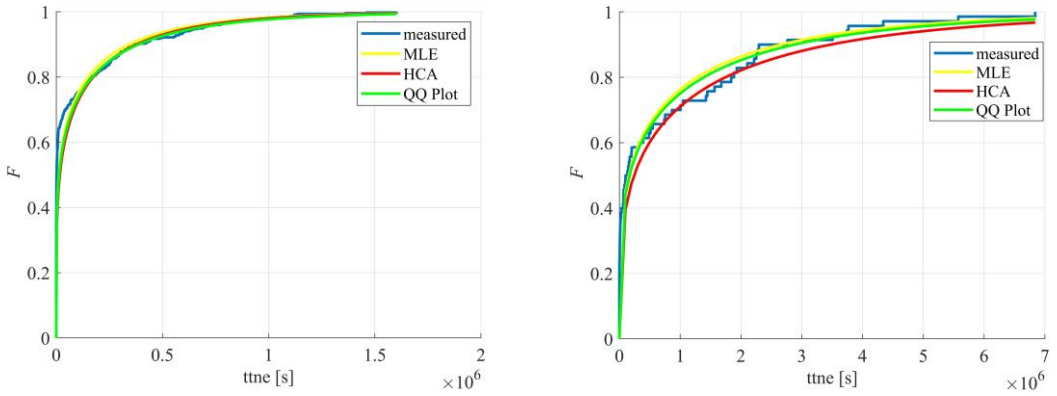

a) b)

Figure 5.8 cdf of the measured ttne (blue curve) and the cdfs with parameters estimated by MLE (yellow curve), by HCA (red curve), and by Q-Q Plot (green curve) – Site #39 and #92

From the curves in Figures 5.7 and 5.8, all the estimation methods provided very similar plots, analogous results have been obtained for the other sites of the system (#39 and #92) considered as example.

Therefore, it was mandatory to perform a numerical quantification of the goodness of the assumed fit of the data to the Gamma distribution.

5.3.2 Validation of Statistical Assumptions

Three statistical tools, the R^2-test, the Root Mean Squared Error (*RMSE* test), and Chi-Squared test (χ^2 test) were considered to perform a numerical quantification of the goodness of the assumed fit of the data to the Gamma distribution

The R^2-test is based on the computation of R^2 by the relation:

$$R^2 = \frac{\sum_{i=1}^{N}\left(F_{t,i} - F_{mean}\right)^2}{\sum_{i=1}^{N}\left(F_{t,i} - F_{mean}\right)^2 + \sum_{i=1}^{N}\left(F_i - F_{t,i}\right)^2} \tag{5.19}$$

where $F_{mean} = \frac{1}{N}\sum_{i=1}^{N} F_{t,i}$, $F_{t,i}$ are the values of the *cdf* of the Gamma distribution and F_i are the values of the *ecdf*.

The *RMSE* test provides a term-by-term comparison of the actual deviation between observed probabilities and theoretical probabilities; *RMSE* is computed by the relation:

$$\mathrm{RMSE} = \left[\frac{1}{\mathrm{N}}\sum_{\mathrm{i}=1}^{\mathrm{N}}\left(\mathrm{F_i} - \mathrm{F_{t,i}}\right)\right]^2 \tag{5.20}$$

Finally, the χ^2 test is based on the computation of χ^2 already described by relation (5.14). Table 5.3 presents the results obtained applying these three tools on the Gamma distribution of *ttne* of the sags measured at sites #39 and #92 having the parameters estimated by *MLE*, *HCA*, and *Q-Q plot*.

Table 5.3 Statistical Errors of the CDF of the Gamma Function Estimated by MLE, HCA, and Q-Q Plot

Gamma distribution	Site #	χ^2 *test*	R^2 *test*	*RMSE test*
Parameters estimated by *MLE*	39	3.59	0.92	1.87
	92	3.38	0.98	0.35
Parameters estimated by *HCA*	39	2.03	0.88	2.30
	92	1.31	0.95	0.57
Parameters estimated by *Q-Q Plot*	39	2.68	0.91	1.98
	92	2.51	0.98	0.98

Table 5.3 evidenced that the χ^2 test for the *MLE* method has the highest value for all the three sites considered, instead the R^2 test gives the best value for the site #92, for any method, and for the site #39, for the method *MLE*. *RMSE* test, finally, gives the lowest value for the site #92 for any method. Summarising, the fit of the data to the Gamma distribution presented an adequate goodness for all the methods used to estimate the α and β parameters.

5.3.3 Computation of Forecasted Number of Sags at Each Node

The final goal was to forecast the mean number of events per year at each site k, $N_{f,k}$. We obtained this value by correlating the average sag rate at the site k, $1/E[ttne_k]$, with the duration of one year, P, by the relation:

$$N_{f,k} = P / E[ttne_k] \tag{5.21}$$

where the average sag rate is expressed in number of sags per seconds and P is expressed in seconds (31.5×10^6 s).

$E[ttne_k]$ in (5.21) is the expected value of the Gamma function given by (5.4). For every method presented to estimate the parameters of the Gamma distribution, i.e. *MLE*, *HCA*, and *Q-Q plot*, we have a different value of $E[ttne_k]$ and, then a different value of forecasted $N_{f,k}$.

Thanks to the availability of the voltage sags really measured in 2018, we were able to quantify the error of the forecast in each of the considered sites. Let $N_{m,k}$ be the number of voltage sags measured at the site k in the year 2018 and $N_{f,k}$ be the number of sags forecasted at the same site k the relation (5.21) using the sags

measured in the preceding three years (2015, 2016, 2017). The error of the forecast at each site *k*, $\varepsilon_{f,k}$, was computed as the percentage value of the difference between $N_{f,k}$ and $N_{m,k}$, in per unit of $N_{m,k}$. For the considered sites #39 and #92, Table 5.4 shows the results of the forecast and the computed values of the error $\varepsilon_{f,k}$ for the three presented methods (*MLE*, *HCA*, *Q-Q plot*) used to estimate the parameters of the Gamma distribution.

Table 5.4 Forecasted Sags, Measured Sags, and Forecast Error Using the Gamma Function with Parameters Estimated by MLE, HCA, and Q-Q plot.

Gamma distribution	**Site #**	$N_{f,k}$	$N_{m,k}$	$\varepsilon_{f,k}$
Parameters estimated by *MLE*	39	277	249	11.2%
	92	36	32	12.5%
Parameters estimated by *HCA*	39	252	249	1.2%
	92	27	32	15.6%
Parameters estimated by *Q-Q plot*	39	246	249	1.2%
	92	33	32	3.1%

The forecast error of all the sags comprehensive of the clusters ranges from 1% to a maximum value lightly greater than 10%. This performance of the forecast is really close to the one obtained for the forecast of the rare sags.

For the considered sites of example, the different methods used to estimate the parameters of the Gamma distribution are effective to provide the range of the mean number of events per year with acceptable errors. However, we cannot ascertain the method, among *MLE*, *HCA* and *Q-Q plot*, which gives the best performance of forecast in all the sites. For the site #39, *Q-Q plot* and *HCA* give the minimum forecast error value, instead the minimum forecast error is obtained by *QQ-Plot* for the site #92.

5.4 Numerical Results

The same regional system presented in the previous Chapter was considered. The system has 83 HV/MV Substations with 152 MV busbars that represents the points of measurement of the voltage sags, that is the sites of interest for the forecast study. The available data start from 1 January 2015 to 31 December 2018. The main

characteristics of the measured data were extensively reported in the previous Chapter.

It should be noted that only 107 of the 152 sites were considered. In fact, 20 sites were not considered because they presented unregistered sags for a long period in the years 2015-2017 (from about six months to one year), and further 25 sites had 2 consecutive months of lack of measurements in the year 2018.

The total sags recorded in the years 2015-2017 were statistically analysed to ascertain the parameters α and β at each of the 107 sites, using the techniques shown in the paragraph 5.3.1. The Gamma distribution, characterised by these values of α and β, was used to forecast the expected number of total sags by (5.21). Since the total sags measured in the year 2018 were available, the forecast error $\varepsilon_{f,k}$ as the absolute value of the difference between the number of forecasted sags in 2018 at each site k and the number of measured sags in 2018 at that site k, in percentage of the measured sags in 2018 was computed. Table 5.5 shows the percentiles and the mean value of the forecast error $\varepsilon_{f,k}$ along the sites.

From Table 5.5 it is evident that the MLE method has the lowest mean value error and, for this method, only 25% of the sites, presented $\varepsilon_{f,k}$ values less than 9%. The other techniques, namely HCA and QQ Plot, show performances slightly worse than MLE.

Table 5.5 Percentiles and Mean Value of the Forecast Error of an Actual Regional System for the Year 2018

Method	***MLE***	***HCA***	***QQ Plot***
Percentile		$\varepsilon_{f,k}$ **[%]**	
$P_{5\%}$	2.3	1.4	3.3
$P_{10\%}$	4.3	3.1	4.9
$P_{25\%}$	8.3	10.0	10.7
$P_{50\%}$	18.1	21.3	22.0
$P_{75\%}$	30.7	35.7	34.1
$P_{90\%}$	53.8	47.8	49.4
Mean Value	22.7	24.1	24.3

These results are not completely satisfactory. Consequently, some selected sites were considered, and compared the forecast sags comprehensive clusters, conducted as described in the previous paragraph, with that of rare sags, conducted as described in Chapter 4.

The basic idea was to verify if the forecast of rare sags showed acceptable errors and, consequently, the bad performance of the forecast of the total sags was mainly linked to the presence of the clusters. To this aim, three sites of example, that is #19, #37, and #52 were considered.

The total number of measured sags in the years 2015 - 2017 was 323 for site #19, 617 for site #37, and 208 for site #52.

Tables 5.5 and 5.6 show the results of the forecast at these sites for the total sags and for rare sags, respectively. In particular, the expected number of total sags, $N_{f,k}$, the number of measured total sags, $N_{m,k}$, and the computed values of the error $\varepsilon_{f,k}$. For the total sags, the outcomes refer to the three presented techniques (*MLE*, *HCA*, *QQ Plot*).

It is interesting to evidence that the forecast at a given site is quite different comparing the results of total sags (Table 5.6) and rare sags (Table 5.7).

Table 5.6 - Forecasted Total Sags, Measured Sags, and Forecast Error at Selected Sites Using the Gamma Function with Parameters Estimated by MLE, HCA, and QQ Plot.

Gamma distribution	**Site #**	$N_{f,k}$	$N_{m,k}$	$\varepsilon_{f,k}$
Parameters estimated by *MLE*	19	121	133	9.0
	37	246	206	19.4
	52	87	61	42.3
Parameters estimated by *HCA*	19	121	133	9.0
	37	224	206	**8.7**
	52	80	61	31.1
Parameters estimated by *Q-Q plot*	19	109	133	18.0
	37	233	206	13.1
	52	78	61	27.9

Table 5.7 - Forecasted Rare Sags, Measured Sags, and Forecast Error at Selected Sites Using the Poisson Function.

Site #	$\mathbf{N_{f,k}}$	$N_{m,k}$	$\varepsilon_{f,k}$ **[%]**
19	50	50	**0.0**
37	47	64	26.6
52	37	36	**2.8**

At site #19, the forecast of rare sags is particularly good ($\varepsilon_{f,19}$ =0.0 %), and the best forecast of total sags is acceptable, too ($\varepsilon_{f,19}$ less than 10% for MLE and HCA). At site #37, instead, the forecast of rare sags shows a bad performance ($\varepsilon_{f,37}$ = 26.6 %), but the total sags can be forecasted with an error equal to 8.7%. An opposite case refers to site #52, for which the forecast of rare sags is very good ($\varepsilon_{f,52}$ = 2.8 %), instead the forecast of the total sags presents an error always greater than 30%. To better analyse these results, the intermittence indices introduced in Chapter 3 were used. Figures 5.9, 5.10 and 5.11 show the plots of the index $TNS_k\Delta T$ versus the ΔT for the three selected sites (k= 19, 37, 52); Figures 5.12, 5.13 and 5.14 also show the zooms around low values of ΔT. From Figures 5.15 and 5.17, it is evident that the good forecast of rare sags (for the sites #19 and #52) corresponds to a plot of $TNS_k\Delta T$ characterized by discontinuous steps at the initial values of ΔT (see in particular the zooms in Figure 5.12 ad Figure 5.14. These steps prove a reduced number of clusters. The number of sags belonging to a cluster remains constant for an appreciable range of ΔT (see for example Figure 5.14)). In such cases, the Poisson model is adequate to describe and forecast the sags measured at these sites. This corresponds to reduced value of forecast error. On the other hand, $TNS_k\Delta T$ for site #37 shows a large increase of values for the first low values of ΔT (see Figure 5.10)) and the zoom in Figure 5.13)). This feature reveals that at site #37, several clusters were measured. Consequently, the Poisson model is not adequate to describe the measured sag, and the proper model is the stochastic model obtainable by the Gamma distribution.

As a further tool of analysis, the cumulative distribution function (*cdf*) of the rare sags measured at the three sites of example during the year 2018 were derived. Each *cdf* of the sags measured during the year 2018, named empirical *cdf*, was compared with the theoretical *cdf* obtained using the parameters computed with the techniques presented in this Chapter; Figures. 5.15, 5.16, and 5.17 show these plots.

It is evident that the empirical *cdfs* of rare sags of the sites #19 and #52 are very close to the theoretical *cdfs*. On these sites, we remind that the forecast of rare sags was really good. Instead, at site #37, the empirical *cdf* is appreciably far from the theoretical one. At site #37, the forecast of rare sags was really bad in some way confirming that the sags measured in site #37 were characterized by a large number of clusters, as also confirmed by the plot of $TNS_k\Delta T$.

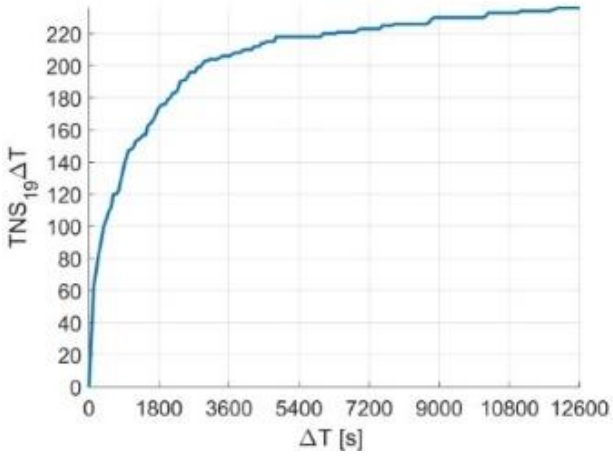

Figure 5.9. Plots of the index $TNS_k\Delta T$ versus the ΔT for site #19

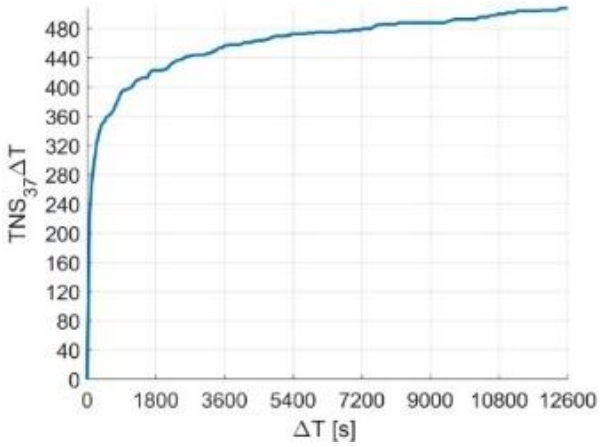

Figure 5.10 Plots of the index $TNS_k\Delta T$ versus the ΔT for site #37

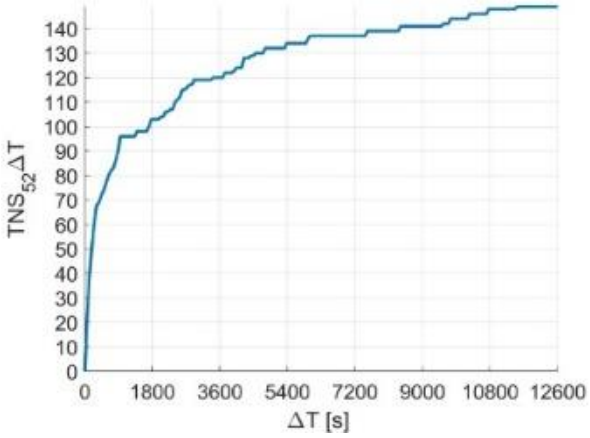

Figure 5.11 Plots of the index $TNS_k\Delta T$ versus the ΔT for site #52

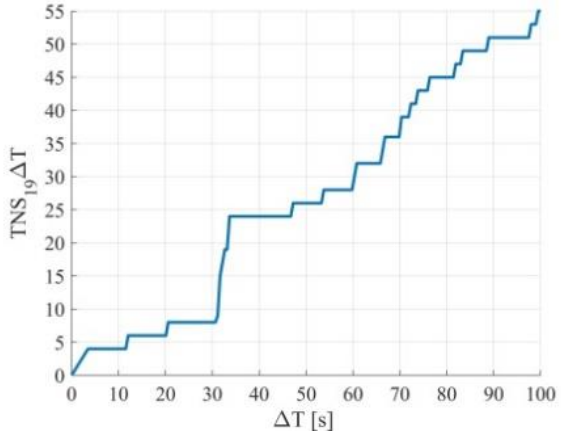

Figure 5.12 Plots of the zoom of index $TNS_k\Delta T$ versus the ΔT for site #19

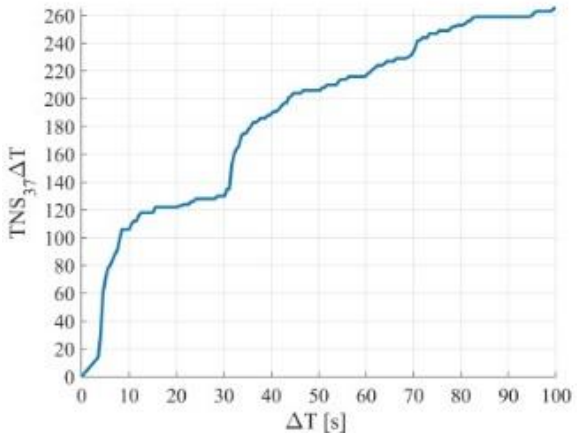

Figure 5.13 Plots of the zoom of index $TNS_k\Delta T$ versus the ΔT for site #37

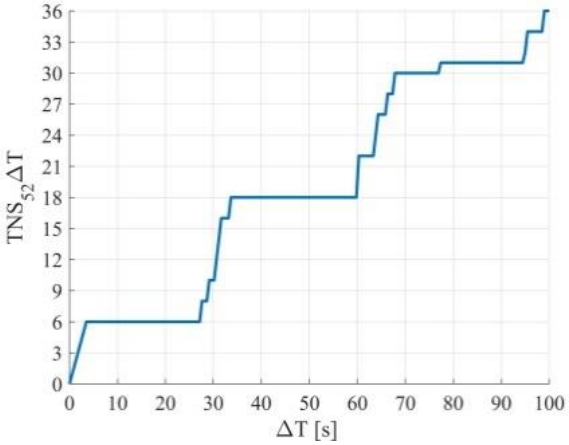

Figure 5.14 Plots of the zoom of index $TNS_k\Delta T$ versus the ΔT for site #52

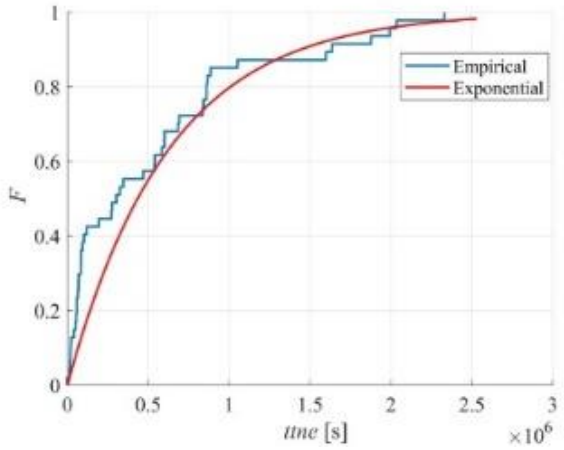

Figure 5.15 Empirical and theoretical cdf of site #19 – Rare sags

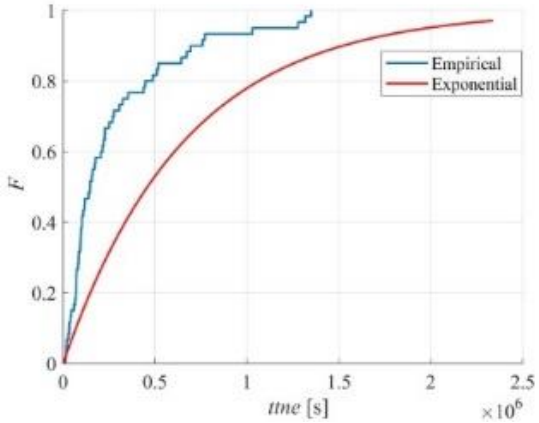

Figure 5.16 Empirical and theoretical cdf of site #37 – Rare sags

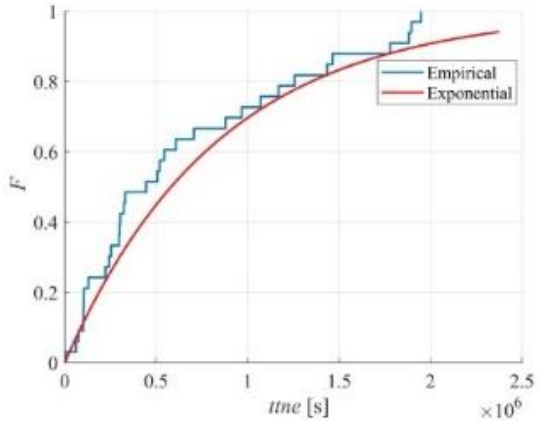

Figure 5.17 Empirical and theoretical cdf of site #52 – Rare sags

CONCLUSIONS

In the thesis, data driven methods were adopted to analyse the measured sags at actual systems for four years. The collaboration with E-Distribuzione allowed the use of voltage sags measured at actual MV distribution systems. Two problems were faced: the assessment of the origin of the sags and the forecast of the sags which will occur in the next year at the sites of the system. To assess the origin of a voltage sag measured at the MV busbar of a HV/MV station means to detect the part of the system, which is an interconnected system between HV and MV by the HV/MV stations, where the fault originating that voltage sag occurred. The study started from two methods already applied by the Italian TSO and DSOs. These methods, proposed, and after modified, by the Italian energy Authority ARERA, use only the residual voltages and the times of occurrence of the sags. The objective of the study presented in this thesis was to compare the methods, analyse the effect of their application in modern distribution systems characterised by GD units, OLTC, and to study some particular cases revealed from the measurements on field. The possibility of the propagation of sags originated in MV system to HV system is one of the most interesting. In summary, the main outcomes of the study are:

- the methods applied in Italian regulation could be affected by the presence of GD and the different position of the OLTC, giving false attribution of the origin;
- a fault in MV network could cause two different voltage sags measured in the MV busbars of the same HV/MV station when the MV busbar switch is in open position;
- the correlation between MV voltage sags assigned to MV by the methods applied in Italian regulation and the intervention of MV protection systems is weak for the studied regional system;
- the different positions of the MV busbar switch could affect the results of the methods applied in Italian regulation for ascertaining the origin of voltage sags;
- MV voltage sags originated in the MV network could move toward the HV/MV transformer and could be registered in the HV Network if the P_{cc} value of the HV network is low and the fault is close to the MV busbar;

- the reclosing cycles of the protection systems of the MV lines while improving the supply continuity can affect the voltage quality; in the case of a permanent fault, up to four voltage sags can occur at the MV busbar where the protected line is connected.

Regarding the forecast, the thesis presents the first studies in literature aimed to predict the number of voltage sags which will occur at the sites of a system. The literature was only focused on model-based approaches which estimate the average performance of a system derived from historical data. The forecast was considered inapplicable since too many years of measurements were needed to obtain acceptable accuracy. The change of the statistical variable describing the phenomenon of the voltage sags, *ttne* rather than *N*, the proposal of indices to detect and discharge the clusters of sags allowed forecasting the rare voltage sags. The study also faced the problem to forecast all the voltage sags comprehensive of clusters. The phenomenon presents the characteristics of a stochastic process, that is the statistical characterization is dependent on the time, and requires different modelling. The first results were not very satisfactory, but a path of studies is traced in the thesis. In summary, the main outcomes are:

- the use of the random variable *ttne* allowed a huge increase of the data set and allowed to perform a forecast analysis using only three years of measurements;
- the forecast errors of our analysis effected on three years of measurements are comparable with those of literature that requires measurements over tens of years;
- the forecasting of the rare voltage using field data of a few years with acceptable errors was not prohibitive;
- filtering of the clusters is crucial in view of the forecast;
- the choice of the threshold to be applied to the variation of the intermittence index, $TNS_k \Delta T$, at any site *k* was the most critical aspect of the statistical analyses of the data;
- future studies should consider artificial intelligence techniques for the choice of the optimal value of the filter thresholds to improve the performance of the forecast;
- the forecasting of the rare voltage comprehensive of clusters using field data of a few years nowadays provide unacceptable results in terms of forecast errors if compared with those provided by the forecasting of rare voltage;

- further studies are needed to validate if the intermittence indices could guide the forecast, performing a prior analysis of the measured sags.

REFERENCES

[1] Voltage characteristics of electricity supplied by public electricity networks, EN 50160, July 2015.

[2] A.R. Di Fazio, V. Duraccio, P.Varilone, P. Verde, Voltage Sags in an Actual Automotive Industry: Analysisand Solutions, Electric Power Systems Research, vol. 110, pp. 25-30, 2014.

[3] Joint Working Group Cigre/Cired C4.107: Economic Framework for Power Quality, Report 467, Cigré, 2011.

[4] M. Didden, R. Belmans, W.D.Haeseleer, Cost-benefit Analysis of Voltage Sag Mitigation Methods in FiberExtrusion Plants, Eur. Trans. Electr. Power, vol. 13, n. 2, pp. 73–78, 2003.

[5] G. Carbone, M. Ceccarelli, C. Fabrizi, P. Varilone, P. Verde, (2019, Apr.), Effects of Voltage Dips on Robotic Grasping. Robotics.8(28), pp.1-13.

[6] Directive 2009/72/EC of the European Parliament and of the Council of 13 July 2009 concerning common rules for the internal market in electricity and repealing Directive 2003/54/EC ("3rd Package")].

[7] AEEGSI, Resolution. 198/2011, www.autorita.energia.it.

[8] ARERA, Resolution 23 Dicembre 2019 566/2019/R/EEL, https://www.arera.it/it/docs/19/566-19.htm.

[9] CEI EN 61000-4-30:2015, Electromagnetic compatibility (EMC), 2017, my.ceinorme.it/index.html?locale=it#detailsId=bsi_30354293.

[10] C. Noce, M. De Santis, P. Varilone and P. Verde, "Comparison of Methods Using only Voltage Measurements for Detecting the Origin of Voltage Sags in the Modern Distribution Networks," 2018 18th International Conference on Harmonics and Quality of Power (ICHQP), Ljubljana, 2018, pp. 1-6.

[11] C. Noce, M. De Santis, L. Di Stasio, P. Varilone, P. Verde, "Detecting the Origin of the Voltage Sags Measured in the Smart Grids", 7° International Conference on Clean Electrical Power "Renewable Energy Resources Impact", Otranto (LE), Italy, 2-4 July 2019.

[12] A. d. Santos, T. Rosa and M. T. Correia de Barros. (2019, April). Stochastic Characterization of Voltage Sag Occurrence Based on Field Data. IEEE Transactions on Power Delivery. 34 (2), pp. 496-504.

[13] C. Noce, L. Di Stasio, P. Varilone, P. Verde and M. De Santis. (2020, Sept.), On the Forecast of the Voltage Sags: First Stages of Analysis on Real Systems. Presented at 55th International Universities Power Engineering Conference (UPEC), Torino, Italy, pp. 1-6.

[14] De Santis M, Di Stasio L, Noce C, Verde P, Varilone P. Initial Results of an Extensive, Long-Term Study of the Forecasting of Voltage Sags. Energies.

2021; 14(5):1264. https://doi.org/10.3390/en14051264. [15] Joint Working Group Cigre/Cired C4.107: Economic Framework for Power Quality, Report 467, Cigré, 2011.

[15] M. De Santis, L. Di Stasio, C. Noce, P. Verde and P. Varilone, "Indices of Intermittence to Improve the Forecasting of the Voltage Sags Measured in Real Systems," in IEEE Transactions on Power Delivery, 2021, doi: 10.1109/TPWRD.2021.3082280.

[16] Leonardo Di Stasio, Paola Verde, Pietro Varilone, Michele De Santis, Christian Noce, "Stochastic Model to Forecast the Voltage Sags in Real Power Systems", AEIT International Conference 2021.

[17] CEI EN IEC 61000-4-1 Electromagnetic compatibility (EMC) Part 4-11: Testing and measurement techniques - Voltage dips, short interruptions and voltage variations immunity tests for equipment with input current up to 16 A per phase.

[18] CEI EN IEC 61000-4-34:2005 Electromagnetic compatibility (EMC) - Part 4-34: Testing and measurement techniques - Voltage dips, short interruptions and voltage variations immunity tests for equipment with input current more than 16 A per phase.

[19] Quality of Electricity Supply: Initial Benchmarking on Actual Levels, Standards and Regulatory Strategies", April 2001.

[20] ["3rd CEER Benchmarking Report on Quality of Electricity Supply 2005", December 2005, Ref. C05-QOS-01-03.

[21] Guidelines of good practice on the implementation and use of voltage quality monitoring systems for regulatory purposes. CEER and ECRB, December 2012

[22] Incentives Schemes for Regulating Distribution System Operators, including for innovation, CEER, Brussels, 2018.

[23] Iniziative per il monitoraggio della qualità della tensione sulle reti di distribuzione dell'energia elettrica,06 Aprile 2005.

[24] Sistema di monitoraggio nazionale della qualità della tensione alle semisbarre MT di cabina primaria: formato dei dati e individuazione dell'origine dei buchi di tensione per la trasmissione all'Autorità e la rendicontazione/visualizzazione dal sito web MonNaLiSA, Liliana Tenti, Riccardo Gian Maria Chiumeo, Dicembre 2017.

[25] Chiumeo, R.; De Nigris, M.; Garbero, L.; Gandolfi, C.; Tenti, L.; Carpaneto, E. Implementation of a New Method for an Improved Voltage Dips Evaluation by the Italian Power Quality Monitoring System in Presence of VT Saturation Effects. Renew. Energy Power Qual. J. 2010, 1, 519–522.

[26] ARERA Resolution 483/2014/R/eel, 9 Ottobre 2014.

[27] Delibera ARERA, 524/2020/R/eel, 09 dicembre 2020.

[28] A. Kazemi, A. Mohamed, H. Shareef, H. Zayandehroodi, Review of voltage sagsource identification methods for power quality diagnosis, Przegla˘n DElektrotechniczny 8 (2013) 143–149.

[29] R.C. Leborgne, D. Karlsson, Voltage sag source location based on voltage measurements only, J. Electr. Power Qual. Util. XIV (1) (2008) 25–30.

[30] J.U.A. Seon, et al., A new approach to determine the direction and cause ofvoltage sag, J. Electr. Eng. Technol. 3 (3) (2008) 300–307.
[31] Dong-Jun Won, Seung-Il Moon, Topological locating of power quality eventsource, J. Electr. Eng. Technol. 1 (2) (2006) 170–176.
[32] G.W. Chang, J.-P. Chao, H.M. Huang, C.-I. Chen, S.-Y. Chu, On tracking thesource location of voltage sags and utility shunt capacitor switching transients, IEEE Trans. Power Deliv. 23 (4) (2008).
[33] M. De Santis, C. Noce, P. Varilone, P. Verde, Analysis of the origin of measured voltage sags in interconnected networks, ELSEVIER.
[34] Yongduanl, X., X. Bing Yin, and F. Zuren, "Average and Instantaneous reactive power of non- sinusoidal circuit based on Hilbert transformation", Automation of Electric power system, 28 (2004), No.35-39.].
[35] W. Kanokbannakorn , T. Saengsuwan, S. Sirisukprasert, "Unbalanced voltage sag source location identification based on superimposed quantities and negative sequence", Electrical Engineering/Electronics, Computer, Telecommunications and Information Technology (ECTI-CON), 2011 8th International Conference, 17-19 May 2011 Page(s): 617 – 620.35
[36] Hussain Shareef, Azah Mohamed, Ahmad Asrul Ibrahim, "Identification of voltage sag source location using S and TT transformed disturbance power", J. Cent. South Univ. (2013) 20: 83−97.
[37] Zhang Xuemeng, XU Yong-hai, "Analysis of voltage sag source location based on wavelet-multiresolution method", Asia-Pacific power and energy engineering conference, 2010, pp. 1-4.
[38] Zhenguo Shao, JinPing Peng, Jian Kang, "Locating Voltage Sag Source with Impedance Measurement", 2010 International Conference on Power System Technology.
[39] Seon-Ju Ahn, Dong-Jun Won, Il-Yop Chung, Seung-Il Moon, "Determination of the Relative Location of Voltage Sag Source According to Event Cause", Power Engineering Society General Meeting, 6-10 June 2004, Page(s):620 - 625 Vol.1.
[40] Won, D.-J. and Moon;Seung-II, "Topological Locating of Power Quality Event Source", Journal of Electrical Engineering & Technology, 1 (2006), No.2, 170.].
[41] Bin Wang, Wilsun Xu, Zhencun Pan, "Voltage Sag State Estimation for Power Distribution Systems", IEEE Transactions on Power Systems, vol. 20, no. 2, may 2005.].
[42] G. W. Chang, J. P. Chao, S. Y. Chu, C. Y. Chen, "A New Procedure for Tracking the Source Location of Voltage Sags", Power Engineering Society General Meeting, 24-28 June 2007,pages 1 – 4.].
[43] A. Kazemi, A. Mohamed, H. Shareef, H. Raihi, "Accurate voltage sag-source location technique for power systems using GACp and multivariable regression methods", Electrical Power and Energy Systems 56 (2014) 97–109.
[44] Kazemi, A. and A. Mohamed, "A New Approach for Location Voltage Sag Source in a Power System by Using Regression Coefficients", in Regional

Engineering Postgraduate Conference (EPC). Malaysia - UKM, 2010. 374-381.

[45] Kazemi, A., A. Mohamed, and H. Shareef, “A New Method for Determining Voltage Sag Source Locations by Using Multivariable Regression Coefficients”, Journal of Applied Sciences, 11 (2011), No.15, 2734- 2743.

[46] Kazemi, A., A. Mohamed, and H. Shareef, “Tracking the Voltage Sag Source Location Using Multivariable Regression Model”, International Review of electrical Engineering (IREE), 6 (2011), No.4, 1853-1861.

[47] L. Alfieri; G. Carpinelli; A. Bracale ; P. Caramia ; A. R. Di Fazio, Impact of Photovoltaic Generators on the Three Phase Short Circuit Operating Conditions, 2018 IEEE International Conference on Environment and Electrical Engineering and 2018 IEEE Industrial and Commercial Power Systems Europe (EEEIC / I&CPS Europe), 2018, pages 1-7.

[48] A. Bracale, P. Caramia, G. Carpinelli, A. R. Di Fazio, Modeling the Three-Phase Short-Circuit Contribution of Photovoltaic Systems in Balanced Power Systems, International Journal of Electrical Power & Energy Systems, Volume 93, December 2017, Pages 204-215.

[49] A. Yazdani et al., "Modeling Guidelines and a Benchmark for Power System Simulation Studies of Three-Phase Single-Stage Photovoltaic Systems," in IEEE Transactions on Power Delivery, vol. 26, no. 2, pp. 1247-1264, April 2011.

[50] Regola tecnica di riferimento per la connessione di Utenti attivi e passivi alle reti AT ed MT delle imprese distributrici di energia elettrica, CEI 0-16, 2014, www.ceinorme.it/it/norme-cei-0-16-e-0-21.html (in Italian).

[51] IEEE Recommended Practice for the Design of Reliable Industrial and Commercial Power Systems," in IEEE Std 493-, vol., no., pp.1-383, 25 June 2007, doi: 10.1109/IEEESTD.2007.380668.

[52] Gong, X.; Yu, Y.;Wang, B.; Ye, F.; Zhou, N. A severity assessment method for multiple voltage sag. In Proceedings of the 2017 IEEE 3rd Information Technology and Mechatronics Engineering Conference (ITOEC), Chongqing, China, 3–5 October 2017;pp. 135–140.

[53] IEEE Guide for Voltage Sag Indices. In IEEE Std 1564–2014; IEEE: Piscataway, NJ, USA, 2014; pp. 1–59.

[54] Liu, H.; Zeng, Q.; Liu, S.; Wu, Z.; Li, L.; Ma, R. Voltage sag analysis based on cluster analysis and correlation analysis. In IOPConference Series: Materials Science and Engineering, Proceedings of the 2020 The 6th International Conference on Electrical Engineering,Control and Robotics, Xiamen, China, 10–12 January 2020; IOP Publishing: Bristol, UK, 2020; Volume 853, p. 12018.

[55] L. Conrad, K. Little and C. Grigg, "Predicting and preventing problems associated with remote fault-clearing voltage dips," in IEEE Transactions on Industry Applications, vol. 27, no. 1, pp. 167-172, Jan.-Feb. 1991, doi: 10.1109/28.67549.

[56] M. H. J. Bollen, "Reliability analysis of industrial power systems taking into account voltage sags," Conference Record of the 1993 IEEE Industry

Applications Conference Twenty-Eighth IAS Annual Meeting, 1993, pp. 1461-1468 vol.2, doi: 10.1109/IAS.1993.299191.

[57] M. R. Qader, M. H. J. Bollen and R. N. Allan, "Stochastic prediction of voltage sags in a large transmission system," in IEEE Transactions on Industry Applications, vol. 35, no. 1, pp. 152-162, Jan.-Feb. 1999, doi: 10.1109/28.740859.

[58] M. R. Qader, M. H. J. Bollen and R. N. Allan, "Stochastic prediction of voltage sags in a large transmission system," 1998 IEEE Industrial and Commercial Power Systems Technical Conference. Conference Record. Papers Presented at the 1998 Annual Meeting (Cat. No.98CH36202), Edmonton, Alta., Canada, 1998, pp. 8-18, doi: 10.1109/ICPS.1998.692526.

[59] J. M. Chambers, W. S. Cleveland, B. Kleiner, and P. A. Tukey. (1983). Assessing Distributional Assumptions about Data. in Graphical Methods for Data Analysis, Belmont, CA, USA, pp. 191–242.

[60] Kadry, Seifedine, Stochastic Methods for Estimation and Problem Solving in Engineering. Editor IGI Global, 2018. https://doi.org/10.4018/978-1-5225-5045-7.

[61] Richard J. Rossi, Mathematical Statistics: An Introduction to Likelihood Based Inference. Wiley 2018, https://doi.org/10.1002/9781118771075 .

[62] Peter Olofsson, Mikael Andersson, Probability, Statistics, and Stochastic Processes. 2nd Edition, Wiley, 2012, https://doi.org/10.1002/9781118231296.

[63] Z. Klaić, D. Šljivac and Z. Baus "Probability Density Functions of Voltage Sags Measured Indices," Journal of Electrical Engineering, vol.62, no.6, 2011, pp.335-341. https://doi.org/10.2478/v10187-011-0053-8.